Taxonomy of the symbiotic dinoflagellates, transcriptomic analyses of Calvin cycle genes in mixotrophic and heterotrophic dinoflagellates, and an improved real-time PCR method to quantify a red tide dinoflagellate

공생성 와편모류 종들에 대한 분류, 혼합영양성 및 종속영양성 와편모류들의 광합성유전자 전사체 분석, 적조유발 와편모류의 정량화를 위한 RT-PCR 방법의 개선

2017년 2월

서울대학교 대학원

지구환경과학부 해양학전공

이 승 연

Taxonomy of the symbiotic dinoflagellates, transcriptomic analyses of Calvin cycle genes in mixotrophic and heterotrophic dinoflagellates, and an improved real-time PCR method to quantify a red tide dinoflagellate

공생성 와편모류 종들에 대한 분류, 혼합영양성 및 종속영양성 와편모류들의 광합성유전자 전사체 분석, 적조유발 와편모류의 정량화를 위한 RT-PCR 방법의 개선

지도교수 정 해 진

이 논문을 이학박사학위논문으로 제출함
2017년 2월

서울대학교 대학원
지구환경과학부 해양학 전공
이 승 연

이승연의 박사학위논문을 인준함
2016년 12월

위 원 장 _____ (인)

부 위 원 장 _____ (인)

위 원 _____ (인)

위 원 _____ (인)

위 원 _____ (인)

Abstract

Taxonomy of the symbiotic dinoflagellates, transcriptomic analyses of Calvin cycle genes in mixotrophic and heterotrophic dinoflagellates, and an improved real-time PCR method to quantify a red tide dinoflagellate

Sung Yeon Lee

Oceanography

School of Earth and Environmental Sciences

College of Natural Sciences

Seoul National University

Dinoflagellates are ubiquitous protists and live in marine environments as diverse forms. Although they often cause red tides or harmful algal blooms, they also play such important roles in marine food webs as prey, predator, endosymbiont, and parasite. However, in studying taxonomy, genetics and quantification of some dinoflagellate species, there have been some difficulties and problems in identifying species, quantifying their abundances, and understanding their molecular genetic characteristics. To solve the difficulties in exploring the taxonomy, the trophic mode associated molecular genetic characteristics, and improved qPCR based quantification of small dinoflagellates and mixotrophic protists, this study focused on 1) discovering and distinguishing symbiotic species by molecular and morphological method to set up their morphological standard, 2) comparing the genetic status

with the trophic mode of dinoflagellates by analyzing the expressed genes through transcriptome analysis, and 3) developing a fast and accurate method to detect red-tide organisms.

Among the dinoflagellate species, the genus *Symbiodinium* forms symbiosis with a broad diversities of host species such as corals, jellyfish, sea anemones or giant clams. Especially they provide organic photosynthases to host species, mostly coral, and in return, corals provide other nutrients to *symbiodinium*. Thus, they are crucial components for survivals of corals and for building tropical reef ecosystems. However, despite their ecological and economic importance in marine ecosystems, the taxonomy of *Symbiodinium* remains limited due to their small size and fragile surface, which has been causing the difficulties in identification of these species for several decade. Especially, type species of genus *Symbiodinium* have been described to have incomplete morphology, although the morphological and molecular characteristics of type species plays as a overall standard for species belonging to the genus. These incomplete morphological standards have ended with multiple synonyms for a single species. Thus, here, I completed the morphological characterization of *Symbiodinium microadriaticum*, the type species, and also established a new *Symbiodinium* species which is symbiotic to the giant clam (Tridanidae), to name it as *Symbiodinium tridacnidorum* sp. nov.. Furthermore, I clarified the unreported morphological characteristics of two clade B *Symbiodinium, Symbiodinium minutum* and *Symbiodinium psygmorphilum*, to complete their plate formula.

The dinoflagellate are known to have three different trophic modes; autotrophic, heterotrophic and mixotrophic. Due to these characteristics, dinoflagellates plays diverse roles in marine food webs as prey and predators. However, the difference in molecular genetic characteristics

between mixotrophic and heterotrophic dinoflagellates have not been reported so far. Thus, molecular genetic characteristics of mixotrophic and heterotrophic dinoflagellates should be compared to trace evolutionary routes of trophic modes in dinoflagellates. I explored the transcriptome of two closely related dinoflagllates which have high similarity in their morphology, ribosomal DNA, and edible prey species, but have different trophic modes in order to discover any parallellism between the gene expression and the trophic modes. When I compared the expressed gene sets of the mixotrophic dinoflagellate *Paragymnodinium shiwhaense* and the heterotrophic dinoflagllate *Gyrodiniellum shiwhaense* by analyzing their transcriptome, the expressed genes exhibited huge dissimilarities, although there were many similar expressed genes, especially in the gene groups related to photosynthesis. Furthermore, based on this comparison analysis, I proved that the mixotrophic dinoflagllate may have more genes that play diverse functional characteristics in genetic level than the heterotropic dinoflagellates because the former must conduct both photosynthesis and phagotrophy in contrast to the latter performing phagotrophy only.

Every summer, Korea suffers from harmful algal blooms (HABs) caused by red tide dinoflagellate *Cochlodinium polykrikoides*. Thus, it is important to detect and quantifying their abundances accurately. However, quantifying the harmful dinoflagellate *Cochlodinium polykrikoides* in natural samples is not easy due to similarity in morphologies between *Cochlodinium polykrikoides* and closely related species. Furthermore, qPCR method for *C. polykrikoides* is also not easy due to potential variations in DNA contents among individual cells. Here, I also developed new species-specific primers and probe for detecting all the 3 ribotypes of ichthyotoxic dinoflagellate *Cochlodinium*

polykrikoides, and comparatively evaluated the efficiencies of the 4 different preparation methods used to determine standard curves. Furthermore, to confirm the accuracy of result, the abundance of *C. polykrikoides* in the > 500 samples collected from the coastal South Sea of Korea, in 2014 and 2015, were independently determined using all the 4 methods. Standard curves constructed by by extraction of DNA from each of the serially diluted cultures with different concentrations of cultured *C. polykrikoides* were most accurate followed by the standard curve obtained by extracting DNA from each of serially diluted field sample with different concentrations of *C. polykrikoides*. Thus, this study provided more accurately modified methods to detect dinoflagellate species from natural sea water samples.

The result of this thesis provided complete morphological standard and eventually provided the basis of overall understanding of taxonomy of symbiotic dinoflagellate *Symbiodinium* species. Furthermore, the result of comparative transcriptome analyses of dinoflagellates possessing different trophic modes obtained in this thesis will provide better understanding of genetic influence to the trophic mode of dinoflagellate species. In addition, the improved qPCR methods and a newly developed set of specific primer and probe set resolving the two recently discovered 2 new ribotypes of *Cochlodinium polykrikoides* will facilitate simple and automatic estimation of *C. polykrikoides* abundance.

Keywords: *Symbiodinium, Cochlodinium polykrikoides*, Taxonomy, Mixotrophy, Trophic mode, Transcriptome, Quantitative real-time PCR.

Student Number: 2011-30118

Contents

List of Table

List of Figure

Chapter 1. Overall Introduction

The dinoflagellates are known as ubiquitous protists that are mostly abundant in diverse marine environments (Jeong, 1999; Jeong et al., 2010; Bayer et al., 2012; Lee et al., 2014a; 2014b, 2015a, 2015b; Murray et al., 2016). Mostly, they are known as main species that cause red tide, the discoloration of the sea surface caused by severe microalgal bloom (Heisler et al., 2008; Kudela and Gobler, 2012; Jeong et al., 2015). Their bloom is also known to be critical to economy, ecology and to human health, because it causes massive mortality of fish by clogging gills, or causes food poisoning by its concentration within shells (Jeong et al., 2013; Kang et al., 2013; Kim et al., 2013b; Yoo et al., 2013; Lim et al., 2014). Thus, the accurate and fast way to detect the outbreak of dinoflagellate blooms and method to prevent its harmful effects are one of the key concern to the people in the aquacultural industry, government, and to scientists. Thus, understanding the ecological role of dinoflagellate and distinguishing advantageous and harmful species among these microorganisms are necessary. Especially, the dinoflagellate play an important role in marine food web as prey, predator, or endosymbionts (Jeong, 1999; Jeong et al., 2010; Bayer et al., 2012; Lee et al., 2014a; 2014b, 2015a, 2015b; Murray et al., 2016).

Among these species, the genus *Symbiodinium* contains numerous genetically distinct lineages of dinoflagellates that appear 'morphologically cryptic', however, recent study have proven that the detailed morphological assessments of the visible plate formulae of diverse *Symbiodinium* clade including clade "A" and "E" in their motile phase (mastigote) have differences (Hansen and Daugbjerg, 2009; Jeong et al., 2014a). Furthermore, while there are several formally described species in Clade A and E, many more species described by genetic

characteristics (Freudenthal, 1962; Kevin et al., 1969; McLaughlin and Zhhl, 1966; Taylor, 1974; Loeblich and Sherley, 1979; Trench and Blank, 1987; Trench, 2000; LaJeunesse, 2001; LaJeunesse et al., 2012). However, the morphologies of these species are not much reported due to their fragile surface and small size causing difficulties of analyzing plate formular or shapes (Jeong et al., 2014a; Lee et al., 2014d, 2015b). For example, the *Symbiodinium* species belonging to clade B *Symbiodinium* were established as new species only with genetic characters such as nuclear ribosomal internal transcribed spacers 1 and 2, single copy microsatellite flanker Sym15, mitochondrial cytochrome b, and the chloroplast 23S rRNA gene by LaJeunesse et al. (2012). However, some critical morphological characters of these species, such as plate formula and related diagnoses have not been provided yet. Therefore, closely related phylogenetic lineages within these groups became main concern of this study to examine whether differences in morphology can be used together with genetic and ecological evidence to describe new species.

The ubiquity, diverse roles, and predominating plankton assemblages of dinoflagellates have been thought to be related to their diverse trophic modes (Stoecker, 1999; Sherr and Sherr, 2007); The dinoflagellates are known to have 3 major trophic modes; i.e., exclusive autotrophy, heterotrophy, and mixotrophy (i.e., combination of photosynthesis and heterotrophy). Theoretically, these diverse trophic modes may be related to evolution of dinoflagellates responding to diverse environmental changes in geological scales (Porter, 1988). Furthermore, recent studies have newly reported that the dinoflagellate species that had been thought to be exclusively autotrophic and some newly described species have been revealed to be mixotrophic (Jeong et al., 2012; Lee et al., 2014a, 2014b, 2015a, 2015b). Thus, the dinoflagellate species may have

difference in molecular characterizations between mixotrophic and heterotrophic dinoflagellates should be explored to understand evolution in dinoflagellates.

Red tides by the ichthyotoxic dinoflagellate *Cochlodinium polykrikoides* have caused large scaled mortality of fish and great loss in aquaculture industry in many countries. Especially, Korea suffers severe *C. polykrikoides* red tide every summer, which causes massive mortality of fish by clogging gills (Hallegraeff, 1993; Anderson, 1997; Jeong et al., 2000, 2010, 2013; Park et al., 2009a, 2013a, 2013b; Dyhrman et al., 2006; Moorthi et al., 2006; Kudela and Gobler, 2012; Lee et al., 2013). Thus, detecting and quantifying the abundance of this species are the most critical step in minimizing the loss (Park et al., 2009a, 2013a, 2013b). The quantitative real-time PCR (qPCR) method is a most conventional method to detect dinoflagellate species because of its fast and conveniences. However, when analyzing > 500 samples collected during huge *C. polykrikoides* red tides in South Sea of Korea in 2014, this conventional method and the previously developed specific primer and probe set for *C. polykrikoides* did not give reasonable abundances when compared with cell counting data. Thus improved qPCR methods and a new specific primer and probe set reflecting recent discovery of 2 new ribotypes have to be developed.

For these reasons, the goal of this study focused on 1) taxonomic analysis of small symbiotic dinoflagellate species using molecular and morphological method, and conducting their morphological standard, 2) comparing and exploring the difference in expression of genes between mixotrophic and heterotrophic dinoflagellates to understand evolution in dinoflagellate, and 3) developing quantifying methods of the abundance of the harmful dinoflagellate *Cochlodinium polykrikoides* in natural

samples and develop species-specific primers and probe reflecting 2 new ribotypes.

In chapter 2, based on morphological and genetic comparisons, I recognized and established new symbiotic dinoflagellate *Symbiodinium tridacnidorum* sp. nov., a new Indo-Pacific species. Also, in this chapter, I found differences in nuclear (internal transcribed spacer [ITS] and large subunit rDNA), chloroplast (cp23S) and mitochondrial (cob) gene sequences from cultured and field-collected samples of *Symbiodinium microadriaticum* (*sensu* Trench and Blank, 1987) and *Symbiodinium* sp. associated predominantly with giant clams and Pacific *Cassiopeia* jellyfish [comprising members of the *ITS2 A3* lineage, *sensu* LaJeunesse (2001)]. Amphiesmal plate tabulations were formulated for the strain of *S. microadriaticum* (CCMP2464) used by Trench and Blank (1987) in their emended description, and two strains of type *A3* (CCMP832 and rt-272) cultured from Indo-Pacific giant clams in the subfamily Tridacninae.

In chapter 3, morphological analysis of two *Symbiodinium* species belonging to clade B, S*ymbiodinium minutum* and *Symbiodinium psygmophilum* were provided for the first time. The morphological analysis of these two clade B *Symbiodinium* species were conducted by using scanning and transmission electron microscopy, and complemented all characteristics of these two dinoflagellates. Then, based on the results obtained from this study and from chapter 2, overall comparisons of morphological characteristics of currently reported *Symbiodinium* species were analysed. In addition, exploring the morphological characteristics of these species may provide more detailed information to understand these species.

In the Chapter 4, to understand genetic influence to the trophic types of dinoflagellate species, transcriptome of two closely related nematocyst-bearing dinoflagellate, *Paragymnodinium shiwhaense* and *Gyrodiniellum shiwhaense* were analyzed. The mixotrophic dinoflagellate *Paragymnodinium shiwhaense* and the heterotrophic dinoflagellate *Gyrodiniellum shiwhanese* are positioned in the same clade and both have nematocysts. In addition, these two species both have "peduncle" or so called "feeding tube" and thus, can feed on the prey species larger than its own size. Moreover, these two species were first isolated from Korea, therefore, can serve as possible predator species for the red tide species occur in Korea. Thus, exploring the expressed genes, and especially the genes related to Calvin cycle by transcriptome analysis of these two dinoflagllate, will provide better understandings of dinoflagellate trophic modes.

In chapter 5, the new species-specific primer set and new method to improve a quantitative qPCR method of detecting *Cochlodinium polykrikoides* have been developed. For the comparative evaluation of the efficiencies, 4 different DNA extraction methods were used to determine standard curves and the standard curves were determined by using the following 4 different preparations. Each methods yielded different results and to confirm their efficiencies, the abundance of *C. polykrikoides* in the samples collected from the coastal waters of South Sea, Korea, in 2014–2015, obtained were analyzed using these methods. Based on these results, most effective method to detect and quantify the *C. polykrikoides* from seawater samples were developed.

Conclusively, this study will show overall studies of dinoflagellate species including phylogenetic and genetic researches. Furthermore, I reported one new species, three modification of morphological characteristics, report of photosynthesis related genes from mixotrophic

and heterotrophic dinoflagellates recently isolated from Korea, and modification of the most effective method to detect and quantify the red tide species which can be applied to diverse dinoflagellate species. Thus, the results obtained in this study may be helpful to identify exact information of target species, and based on this information, rapid detection of target species were available.
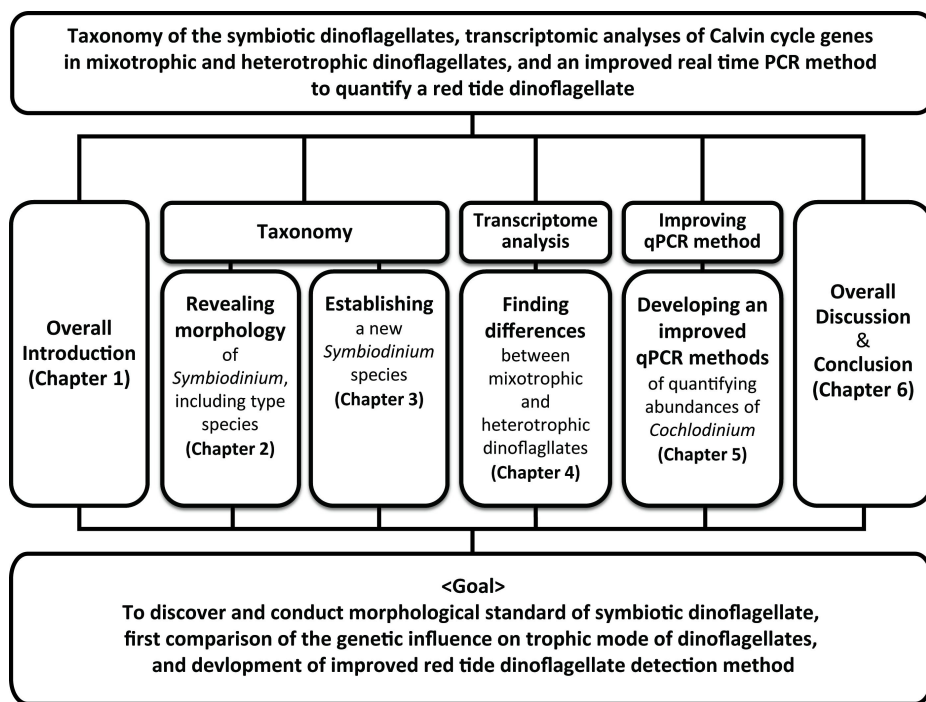
Fig. 1.1. Overall outline of this thesis

Chapter 2. Report of new symbiotic dinoflagellate *Symbiodinium tridacnidorum* sp. nov., a revised morphological description of *S. microadriaticum* Freudenthal, emended Trench et Blank.

2.1. Introduction

Dinoflagellates in the genus *Symbiodinium*, commonly known as 'zooxanthellae,' are symbiotic with various invertebrates such as corals, sponges, sea anemones, jellyfish, nudibranchs, clams, and single-cell hosts including ciliates and foraminifera (Trench, 1993; LaJeunesse, 2002; Lobban et al., 2002; Pochon et al., 2007), although some occur free-living on various substrata and in the water column (Hirose et al., 2008; Porto et al., 2008; Yamashita and Koike 2013; Jeong et al., 2012, 2014a). The symbioses that many form with a broad diversity of stony corals, order Scleractinia, are crucial for building tropical reef ecosystems. However, despite their ecological and economic importance in marine ecosystems, the taxonomy of *Symbiodinium* remains limited because few biologically discrete entities have formal binomials.

After *Symbiodinium microadriaticum* was initially described by Freudenthal (1962), the description was emended by Kevin et al. (1969). Owing to the prevailing dogma which assumed that *Symbiodinium* was a monotypic genus (McLaughlin and Zahl 1966; Kevin et al., 1969; Taylor 1974), there was little interest to investigate species diversity further

until Loeblich and Sherley (1979) attempted to rename the species *Zooxanthella microadriatica* on the basis that no previous effort had been made to differentiate it from the symbiont cells that Brandt (1881) had examined from the radiolarian, *Collozoum inerme*. Loeblich and Sherley (1979) were the first to provide Kofoidian plate tabulations, based on scanning electron microscopy (SEM), for an isolate obtained from the cnidarian *Cassiopeia xamachana*, in the Florida Keys, USA (isolate 406). They included in their study an environmental isolate from the temperate northwestern Atlantic Ocean (isolate 395) whose tabulation was distinct, yet too similar to justify describing it as a separate species.

The revelation that *Symbiodinium* was species began with Trench and Blank (1987), who introduced *S goreauii*, *S. pilosum*, and *S. kawagutii*, as well as providing another emendation to *S. microadriaticum* (Trench and Blank 1987; Trench 2000). The criteria used in the justification of these additional species relied on differences in cell size and ultrastructure including the number of chromosomes, pyrenoids, and pyrenoid stalks, as well as in the relative volumes of chromosomes, nuclei, chloroplast, and mitochondria. This work was also the first to utilize molecular evidence on photosystem proteins to substantiate these claims that the lineages were genetically distinct (Trench and Blank 1987). Molecular sequence data eventually revealed large genetic differences among members of this genus, clades of which were designated as Clades "A", "B", "C", etc. (Rowan and Powers 1991). The subsequent application of various genetic methods and markers to identify ecologically distinct lineages facilitated a surge in discovery about processes underlying the ecology and evolution of these dinoflagellates (Sampayo et al 2009; Thornhill et al., 2014; Baums et al., 2014).

Since the early 1990s, genetic analyses have dominated many aspects of *Symbiodinium* research (Coffroth and Santos 2005; Sampayo et al., 2009), and are the de facto diagnostic to examine ecological and geographical patterns of diversity (LaJeunesse et al., 2010). While there is some contention regarding how rDNA data are interpreted (Stat et al., 2011; LaJeunesse and Thornhill 2011), the convergence of evidence from a combination of several genetic markers can delimit reproductively isolated lineages (LaJeunesse and Thornhill 2011; Pochon et al., 2012; Thornhill et al., 2014); and has led to the collective use of these data in formally describing species including *Symbiodinium* spp. that are not in culture (LaJeunesse et al., 2012, 2014). However, it is important to relate, when possible, these new approaches with more traditional methods for describing dinoflagellate species.

While most *Symbiodinium* are unable to flourish in artificial growth media, there are some that proliferate in vitro. Preliminary genetic evidence suggests that many of these strains represent undescribed species for which a combination of modern and conventional taxonomic approaches can be applied (e.g. Jeong et al., 2014a). When viewed with light microscopy, *Symbiodinium* are morphologically nondescript, except for obvious differences in cell size. Scanning electron microscopy (SEM) allows the resolution of Kofoidian plate patterns on the motile cells (mastigotes) of cultured isolates (Jeong et al., 2014a). Amphiesmal plate formulae are different between *S. natans* (Clade A; Hansen and Daughberg 2009) and *S. voratum* (Clade E; Jeong et al., 2014a), yet these species are genetically divergent from each other. It is not known whether closely-related species (i.e. members of the same clade) differ in the number and arrangement of their amphiesmal plates. An assessment of morphological variation and evolution among distantly and closely related *Symbiodinium* would benefit from expanding our

comparative analyses of thecal morphology, using SEM, when new species are described.

In this report, we have characterized the amphiesmal plate morphology and pattern found on *S. microadriaticum* (*Symbiodinium* strain CCMP2464, or rt-061) isolated from the jellyfish *Cassiopeia xamachana* (ITS2 type *A1*, *sensu* LaJeunesse, 2001) because the plate tabulation of this isolate was not described by Trench and Blank (1987). The genetic identities of the isolates Loeblich and Sherley (1979) characterized morphologically and assigned to the species *Zooxanthella microadriatica* as reported above, were used to resolve their phylogenetic relationships within the genus *Symbiodinium*. We combined these results with the morphological characterization of two cultured strains (CCMP832 and rt-272) isolated from giant clams in the Pacific Ocean and for which genetic evidence indicated that they represented a novel species in Clade A (initially designated *ITS2* type *A3*, *sensu* LaJeunesse, 2001). The morphological comparison between *S. microadriaticum* and isolates from two giant clam hosts were combined with additional sequence analyses of the large subunit (LSU) rDNA, partial chloroplast large subunit (cp23S), and mitochondrial cytochrome b (cob). The genetic variation in these markers was analyzed from multiple cultures as well as field-collected specimens from several ecological and geographical sources. Finally, we examined to what extent morphological differences (i.e. plate tabulations) were concordant with phylogenetic relationships among *Symbiodinium* spp. for which these data were available.

2.2. Materials and methods

2.2.1. Cultures and growth conditions of *Symbiodinium* spp.

Symbiodinium microadriaticum (CCMP2464, formally rt-061 *sensu* Trench and Blank, 1987) and strain CCMP832 were obtained from the National Center for Marine Algae and Microbiota (NCMA) (Table 1.1). Strain CCMP2464 of *S. microadriaticum* was originally isolated from the jellyfish *Cassiopeia xamachana* in the Florida Keys, USA. The culture CCMP832 was originally obtained from the giant clam *Hippopus hippopus* living on the Great Barrier Reef, Australia; and isolate rt-272 was cultured from *Tridacna gigas* from Palau (LaJeunesse, 2001). The cultured isolates 395 and 406 analyzed by Loeblich and Sherley (1979) were obtained from the University of Texas at Austin culture collection (UTEX LB 2281 and UTEX LB 2282, respectively). Cultures were grown in L1 seawater medium without silicate (Guillard and Hargraves, 1993), at a temperature of 25 °C with continuous illumination of $20\,\mu$mol photons m^{-2} s^{-1} cool white fluorescent light under a 14:10 h light-dark cycle. They were transferred approximately every 2–3 weeks to new 250 ml PC bottles containing fresh media. When culture volumes were large enough to analyze, genetic and morphological characterizations were performed.

Table 1.1. The list of strains used for morphological analyses including, strain name, rDNA genetic identity, location (LC) and data of original collection, and Genbank accession numbers for rDNA sequences.

Species	Strain	Clade-ITS2 type	LC	Host	Collection date	Genbank (ITS)	Genbank (LSU)	Reference
Symbiodinium tridacnidorum sp. nov.	CCMP 832	A3	Great Barrier Reef	*Hippopus hippopus* (giant clam)	1966	HG939435	HG939436	This paper
Symbiodinium tridacnidorum sp. nov.	rt-272	A3	Palau	*Tridacna gigas* (giant clam)	1982		KF364600	This paper
Symbiodinium microadriaticum	CCMP 2464 (rt061)	A1	Florida, USA	*Casiopeia xamachana* (jelly)	1977	FJ823602	AF060896	Trench & Blank (1987)

2.2.2. Morphological analysis of *Symbiodinium* using Scanning electron microscopy (SEM)

Cell size and the analyses of the amphiesmal plate shape, number, and arrangement of *S. microadriaticum* culture CCMP2464 and clade *A3 Symbiodinium* sp. CCMP832, and rt-272 were performed by SEM. Cells from dense cultures were fixed for 3 min in osmium tetroxide (OsO_4) at a final concentration of 0.3% in seawater medium. Then fixed cells were collected on a PC membrane filter (pore size 3.0 μm) without additional pressure and rinsed serially with filtered and autoclaved sea water (FSW) and distilled waters to remove the salt. Then filters were dehydrated in an ethanol series of 10%, 30%, 50%, 70%, 90% for 2 min each, and dehydrated in the 100% EtOH for 2 min, two times. Then, filters were placed in the holder, placed in a critical point dryer (BAL-TEC, CPD 300, Balzers, Liechtenstein, Germany) and then maintained for 10 min in 100% EtOH to remove waters from the sample completely. When samples were ready, EtOH is replaced with liquid CO_2 and dehydrated and dried with heat. After filters were dried, the dried filters were mounted on a stub and coated with platinum. The coaded samples were viewed with a FE-SEM (S-4800, HORIBA: EX-250, Hitachi, Hitachinaka, Japan) and SEM (JSM-840A, SEM JEOL Ltd., Tokyo, Japan) and the plate patterns were photographed using a digital camera. Furthermore, cell length and cell width of live vegetative cells were measured using an image analysis system on images collected with a compound microscope (Image-Pro Plus 4.5, Media Cybernetics, Silver Spring, MD).

2.2.3. Ultrastructure analysis of *Symbiodinium* using Transmission electron microscopy (TEM)

The transmission electron microscopy (TEM) was used for counting the permanently condensed chromosome bodies typical of dinoflagellates. For sample preparation and sectioning, cells from dense cultures were fixed in 2.5% (final concentration) glutaraldehyde (final concentration). After 1.5–2 h, cells were concentrated at 1,610 x g for 10 min in a Vision Centrifuge VS-5500 (Vision Scientific Company, Bucheon, Korea). Next, the supernatant was discarded, and the pellets were transferred to 1.5 ml tubes and rinsed several times with 0.2 M pH 7.4 sodium cacodylate buffer. Then, the pellets were post fixed with 1% (final concentration) OsO_4 in deionized water for 90 min. After fixation, the pellets were embedded in agar. Dehydration was performed via a graded ethanol series (50%, 60%, 70%, 80%, 90%, and 100% ethanol, followed by 2 changes in 100% ethanol). The agar-embedded pellet was then re-embedded in Spurr's low-viscosity resin (Spurr 1969) and dried for 3 days in 70 ℃. Samples were then serially sectioned (80–100 nm) using an RMC MT-XL ultramicrotome (Boeckeler Instruments Inc., Tucson, AZ, USA), and stained with 3% (w/v) aqueous uranyl acetate followed by lead citrate. Finally, samples were observed with a JEOL-1010 transmission electron microscope (JEOL Ltd., Tokyo, Japan). The chromosome number (± SE) for the strains was determined using these serial sections.

Table 1.2. List of sample ID, type, host, geographic origin, and minimum (Min) and maximum (Max) depths from which isolates were collected.

	Sample I.D	*Symbiodinium* ITS-DGGE type	Culture origin /Host Species	Region	Location	Site	Collection Depth	Min (m)	Max (m)
Isolates in culture	CCMP 832	A3	*Hippopus hippopous*	Western Pacific	Great Barrier Reef	unknown	unknown		
	EL-1	A3	*Cassiopea sp.*	Central Pacific	O'ahu, Hawaii	Kaneohe Bay	shallow	1	3
	rt-174	A3	*Tridacna maxima*	Western Pacific	Palau	unknown	unknown		
	rt-243	A3	*Tridacna derasa*	Western Pacific	Palau	unknown	unknown		
	rt-265	A3	*T. derasa*	Western Pacific	Palau	unknown	unknown		
	rt-272	A3	*Tridacna gigas*	Western Pacific	Palau	unknown	unknown		
	TG3A	A6	*Tridacna gigas*	Western Pacific	Philippines	unknown	unknown		
	TD1E	A3a	*Tridacna derasa*	Western Pacific	Philippines	unknown	unknown		
	rt-77	A3	*Cassiopea mertensii*	Central Pacific	Hawaii	unknown	unknown		

<continued>

	Sample I.D	*Symbiodinium* ITS-DGGE type	Culture origin /Host Species	Region	Location	Site	Collection Depth	Min (m)	Max (m)
Field collections	Haw02_80	A3	*Cassiopea sp.*	Central Pacific	O'ahu Hawaii	Kaneohe Bay	intermediate	5	10
	OF 008	A3x	*Tridacna maxima*	Western Pacific	American Samoa	Ofu Island	shallow		
	OF 009	A3	*Tridacna maxima*	Western Pacific	American Samoa	Ofu Island	shallow		
	Pal09_511	A3	*Tridacna maxima*	Western Pacific	Palau	Ulang Channel	deep	12	18
	Pal14_cassio1	A3	*Cassiopea andromeda*[2]	Western Pacific	Palau	Korror	shallow	1	2
	Pal14_cassio2	A3	*Cassiopea andromeda*[2]	Western Pacific	Palau	Korror	shallow	1	2
	Pal13_cassio_Nikko	A3	*Cassiopea andromeda*[2]	Western Pacific	Palau	Nikko Bay	shallow	1	2
	TM PHU 2	A6	*Tridacna maxima*	Eastern Indian Ocean	Andaman Sea, Thialand	Phuket	shallow	2	5
	TM PHU 3	A6	*Tridacna maxima*	Eastern Indian Ocean	Andaman Sea, Thialand	Phuket	shallow	2	5
	TM PHU 4	A6	*Tridacna maxima*	Eastern Indian Ocean	Andaman Sea, Thialand	Phuket	shallow	2	5
	TM PHU 5	A6	*Tridacna maxima*	Eastern Indian Ocean	Andaman Sea, Thialand	Phuket	shallow	2	5
	Zan07_23	A3	*Agalophenia sp.*	Western Indian Ocean	Zanzibar	Changuu	shallow	1	5
	Zan07_48	A3	*Agalophenia sp.*	Western Indian Ocean	Zanzibar	Changuu	shallow	1	5

<continued>

	Sample I.D	*Symbiodinium* ITS-DGGE type	Culture origin /Host Species	Region	Location	Site	Collection Depth	Min (m)	Max (m)
Isolates in culture	rt-061	A1	*Cassiopea xamachana*	Northwest Atlantic	Floriday Keys, USA	Key Largo	shallow		
	Mac04_508	A1	*Orbicella faveolata*[1]	Western Atlantic	Floriday Keys, USA	Key Largo	shallow		
	rt-362	A1	*Stylophora pistulata*[1]	Red Sea	Gulf of Aquaba	Elat	unknown		
	rt-370	A1	*Stylophora pistulata*[1]	Red Sea	Gulf of Aquaba	Elat	unknown		
	Kb8	A1	*Cassiopea sp.*	Central Pacific	O'ahu, Hawaii	Kaneohe Bay	shallow	1	4
Field collections	Be03_34	A1	*Cassiopea xamachana*	Caribbean Sea	Belize	Carrie Bow Cay	shallow	1	2
	FL01_01	A1	*Cassiopea xamachana*	Caribbean Sea	Floriday Keys, USA	Key Largo	shallow	1	2
	PM99_01	A1	*Cassiopea xamachana*	Caribbean Sea	Mexico	Puerto Morelos	shallow	1	2

2.2.4. Nucleic acid extraction, PCR amplification, sequencing, and phylogenetic analyses

Nucleic acids were extracted from 10 to 15 ml of a dense culture of CCMP832 using the *AccuPrep*® Genomic DNA Extraction Kit (Bioneer Cooperation, Daejeon, Korea). The DNA extracts from cultures and field collected samples corresponding to *S. microadriatiucum* (= type *A1*), *S. pilosum* (= type *A2*), and that of type *A3* from the Pacific Ocean obtained and used in previously published or unpublished research were included in subsequent genetic analyses. Details such as culture number, host, depth, and geographic origin as well as journal citations where particular samples were initially analyzed are listed in the Table 1.2. A request to acquire DNA from *S. natans* to complete sequencing of the cp23S and cob genes was denied.

PCR amplifications for the ITS region of CCMP832 (ITS1, 5.8S, and ITS2) were performed using the forward primer Euk1209F (Giovannoni et al., 1988) and the reverse primer ITR2 (Litaker et al., 2003). All other ITS2 amplifications used the primer-set and reaction conditions specified in Sampayo et al. (2009). Amplifications of the LSU region D1–D3 was performed using the forward primer D1RF (Scholin et al., 1994) and the reverse primer LSUB (Litaker et al., 2003), or using the primer set and conditions developed by Zardoya et al. (1995). For PCR amplification, Solg™ f-Taq DNA Polymerase© (SolGent Co., Daejeon, Korea) was used according to the manufacturer's instructions. The partial chloroplast cp23S and mitochondrial cob genes were amplified and directly sequenced for all cultures and field collected samples according to Zhang et al. (2000) and Zhang et al. (2005), respectively (Table 1.2). Sanger sequencing of these plastid markers and the LSU was performed using Big Dye 3.1 reagents (Life Sciences) and the

products analyzed on an Applied Biosystems 3730XL instrument.

The phylogenetic analysis of the ITS (ITS1, 5.8S, ITS2) and LSU rDNA regions of the *Symbiodinium* strains was conducted using MEGA v.4 (Tamura et al., 2007) and Clustal X2 (Larkin et al., 2007), and the sequences from outgroup *Symbiodinium* from Clades D and E were obtained from recently published results (Jeong et al., 2014a; LaJeunesse et al., 2014). Maximum likelihood (ML) analyses were conducted using the RAxML 7.0.4 program with a GTR+Γ model (Stamatakis 2006). Further, 200 independent tree inferences were used to identify the best tree. ML bootstrap values were determined using 1,000 replicates. Bayesian analyses were conducted using MrBayes v.3.1 (Ronquist and Huelsenbeck 2003) in the default GTR + G + I model to determine the best available model for the data for each region. For all sequence regions, 4 independent Markov Chain Monte Carlo runs were performed as described in Kang et al. (2010).

2.3. Results

2.3.1. Taxonomic descriptions

Symbiodinium microadriaticum Freudenthal 1962, emend. by Trench and Blank 1987, emend. by Lee, Jeong, Kang & LaJeunesse (Figs 2.1A-C, 2.2, 2.3)

Emendation: This dinoflagellate has a Kofoidian plate formula of x, EAV, 4', 5a, 8'', 9-13s, 2 row cingulum, 6''', 2''''. Nucleotide sequences of the large ribosomal subunit rDNA (Accession No. KM972549), partial chloroplast large subunit, cp23S (Accession No. KF740693) and mitochondrial cytochrome b, cob, (Accession No. KF206025) genetically define this species.

Type Locality: Key Largo, Florida, USA (25°00′ 00″ N, 80°50′ 00″ W).
Habitat: Isolated from the mangrove, or upside-down, jellyfish *Cassiopeia xamachana*.

Symbiodinium tridacnidorum Lee, Jeong, Kang, & LaJeunesse sp. nov. (Figs 2.1D-I, 2.4, 2.7)

Diagnosis: Mastigote cells are 8.14–10.1 μm in length and 5.6–7.1 μm in width. The cell episome is slightly larger than the hyposome. An EAV is present on the apex. The cingulum consists of 2 rows of pentagonal plates. The cingulum is displaced by 0.06–0.2 cell lengths and 0.2–0.7 cell widths. Plates are arranged as x, EAV, 5', 6a, 8'', 9–11s, 17–19c, 7''', and 2–3''''. The 5a plate is hexagonal.

The 6'' plate is pentagonal. The 2' plate touches the 4' plate. The size of the 5' plate is similar to that of the 2' plate. A single, 2-stalked pyrenoid is present. A type E eyespot is located beneath the sulcus in motile cells. A well-developed PE emerges between the longitudinal and transverse flagella. The nucleus contains a nucleolus and 77–83 condensed chromosomes. Nucleotide sequences of the large ribosomal subunit rDNA (Accession Nos. KM816405, KM816406, KM972551), *ITS2* rDNA (Accession Nos. KM816410), partial chloroplast large subunit, cp23S (Accession Nos. KM816407– KM816409) and mitochondrial cytochrome b, cob, (Accession No. KM816411) genetically define this species.

Holotype: A holotype slide labeled USNM stub 1251931 of a culture fixed with 0.3% (w/v) osmium tetroxide has been deposited in the Protist Type Specimen Slide Collection, US Natural History Museum, Smithsonian Institution, Washington, DC, USA.

Type Locality: Tridacna Reef, Great Barrier Reef, Australia (20° 00′00″ S, 149° 00′00″E).

Habitat: Isolated from mantel tissue of the giant clam species *Hippopus hippopus*.

Etymology: The specific name "*tridacnidorum*" is based on the subfamily of bivalves (Family Cardioidea Lamark, 1809), commonly referred to as giant clams.

2.3.2. Morphology of *Symbiodinium microadriaticum*

Motile cells of *S. microadriaticum* (strain CCMP2464) were mushroom shaped, with an episome (epitheca) slightly larger than the hemispherical hyposome (hypotheca; Figs 2.1A–C). The cells (n = 30) in log phase culture were 8.0–13.8 μm in length and 6.3–11.9 μm in width, respectively (Table 1.3). In addition, the ratio of the length to width of the living cells was 1.1–1.9 μm (Table 1.3). However, when fixed and observed under SEM, the cells were slightly smaller and were 7.6–10.0 μm in length and 5.8–7.7 μm in width (Table 1.3). The ratio of the length to the width under SEM was 1.2–1.5 μm (Table 1.3).

The Kofoidian plate formula of *S. microadriaticum* cells was x, EAV, 4', 5a, 8'', 13s, the 2 cingulum rows 22–24c, 6''', and 2'''' (Table 1.3; Figs 2.2 and 2.3). At the cell's apex, the elongated amphiesmal vesicle (EAV) possessed 6–8 aligned knobs and measured 1.33–2.65 μm in length and 0.13–0.33 μm in width. This structure was bordered ventrally by the x plate and surrounded by apical plates, 2', 3', and 4' (Figs 2.2F, 2.2H, 2.3C). Apical plates consisted of a rhomboid-shaped and relatively large 1', a quadrangular 2' plate, and hexagonal 3' plate. Surrounding these were the pentagonal 4' apical plate and 1a–5a intercalary plates (Figs 2.2F, 2.2G, 2.3C). The 5 intercalary plates were hexagonal (plates 1a and sometimes 3a) pentagonal (plates 2a, 5a, and sometimes 3a), and heptagonal (plate 4a) (Fig. 2.2B-D, 2.2F, 2.2G, 2.3A-C). Of the 8 precingular plates, 1'', 4'', and 6'' plates were quadrangular, whereas 2'', 3'', 4'', 5'', 7'', and 8'' plates were pentagonal (Table 1.3; Figs 2.2A-D, 2.3A, 2.3B). Two wide cingulum rows consisting of 22–24 pentagonal amphiesmal plates were located in the center of the cell. The cingulum was displaced by ~0.1–0.2 times the cell length and ~0.4–0.7 times the cell width (Table 1.3). There were 6 postcingular plates (Table

1.3; Figs 2.2I, 2.3D). The 1''', 2''', 4''', 5''', and 6''' plates were quadrangular, but the 3''' plate was pentagonal (Figs 2.2I, 2.3D). Both antapical plates, 1'''' and 2'''', were pentagonal or hexagonal (Table 1.3; Figs 2.2I, 2.3D). A total of 13 sulcal plates, including 2S(?) plates and 1 S.p. plate were located in the sulcus. A peduncle (PE) was present in the middle of the sulcal plates (Table 1.3; Figs 2.2A, 2.2E, 2.3A).

Table 1.3. Morphological differences among Clade A *Symbiodinium* in comparison to *S. voratum* (Clade E) based on scanning electron microscopy. Mean values are shown in parentheses.

	S. tridacnidorum	*S. microadriaticum*	*S. natans*	*S. voratum*
AP length, (μm; living cells)	9.4–12.9 (10.9)	7.6–10.0 (9.2)	9.5–11.5 (10)	10.8–16.2 (13.1)
Cell width, (μm; living cells)	7.5–10.6 (8.8)	5.8–7.7 (7.1)	7.4–9.0 (8)	7.8–11.5 (9.5)
Ratio of length to width (living cells)	1.08–1.43 (1.3)	1.1–1.9 (1.2)	Unk.	1.1–1.8 (1.4)
AP length, (μm; SEM)	8.1–10.1 (9.2)	7.6–10.0 (9.2)	10.38*	8.5–12.4 (10.5)
Cell width, (μm; SEM)	5.6–7.1 (6.5)	5.8–7.7 (7.1)	8.25*	6.4–9.8 (8.2)
Ratio of length to width (SEM)	1.3–1.5 (1.4)	1.2–1.5 (1.3)	1.26*	1.2–1.4 (1.3)
EAV length, (μm)	0.76–1.84 (1.42)	1.33–2.65 (1.94)	2	1.75–3.09 (2.45)
EAV width, (μm)	0.09–0.37 (0.18)	0.13–0.33 (0.21)	0.2	0.15–0.27 (0.2)
Numbers of aligned knobs on EAV	7–9	6–8	12	9–13
Cingulum displaced by cell length	0.06–0.20 (0.12)	0.06–0.24 (0.14)	0.23*	0.13–0.21
Cingulum displaced by cell width	0.23–0.70 (0.40)	0.18–0.72 (0.41)	1.0	0.48–0.85 (0.65)
Numbers of cingular plates	17–19	22–24	20	17–20
Numbers of sulcal plates	9–11	9–13	Unk.	9
Numbers of apical plates	5	4	4	5
Numbers of intercalary plates	6	5	5	5
Numbers of precingular plates	8	8	8	8
Numbers of postcingular plates	7	6	6	6
Numbers of antapical plates	3 (rarely 2)	2	2	2
No. of chromosomes	80 ± 3 (n=4)	97 ± 2 (n=6)[#]	Unk.	74 ± 1.5 (n=5)
Plate formula	x, EAV, 5', 6a, 8'', 9–11s, 17–19c, 7''', 2–3'''', PE	x, EAV, 4', 5a, 8'', 9–13s, 22–24c, 6''', 2'''', PE	x, EAV, 4', 5a, 8″, ?s, ?c, 6‴, 2⁗, PE	x, EAV, 5′, 5a, 8″, 9s, 17–20c, 6‴, 2⁗, PE
Reference	(1)	(1)	(3)	(4)

AP, anteroposterior; EAV, elongated amphiesmal vesicle; PE, Peduncle; Unk, Unknown; [#]Obtained from Trench and Blank (1987). *Obtained from Jeong et al (2014a) (1) This study. (2) Trench and Blank (1987). (3) Hansen and Daugbjerg (2009). (4) Jeong et al. (2014a)
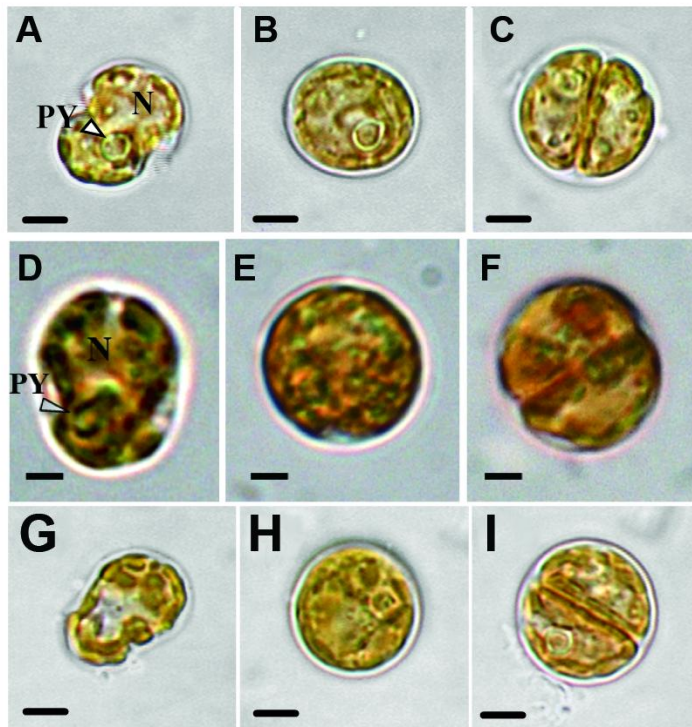
Figs 2.1. Light micrographs of the mastigote (motile), coccoid (spherical), and doublet (dividing) cells from *Symbiodinium microadriaticum* (A–C), *S. tridacnidorum* n. sp. (D–F) and *S. tridacnidorum* n. sp. strain rt272 (G–I). **A.** *S. microadriaticum* mastigote; pyrenoid (PY), nucleus (N). **B.** *S. microadriaticum* coccoid. **C.** *S. microadriaticum* doublet. A single PY is generally located in the center of the cell. **D.** *S. tridacnidorum* mastigote; pyrenoid (PY), nucleus (N). **E.** *S. tridacnidorum* coccoid. **F.** *S. tridacnidorum* doublet. **G.** *S. tridacnidorum* mastigote. **H.** *S. tridacnidorum* coccoid. **I.** *S. tridacnidorum* doublet. All cells contained a reticulated chloroplast located at the periphery of the cell. All scale bars = 2 μm.
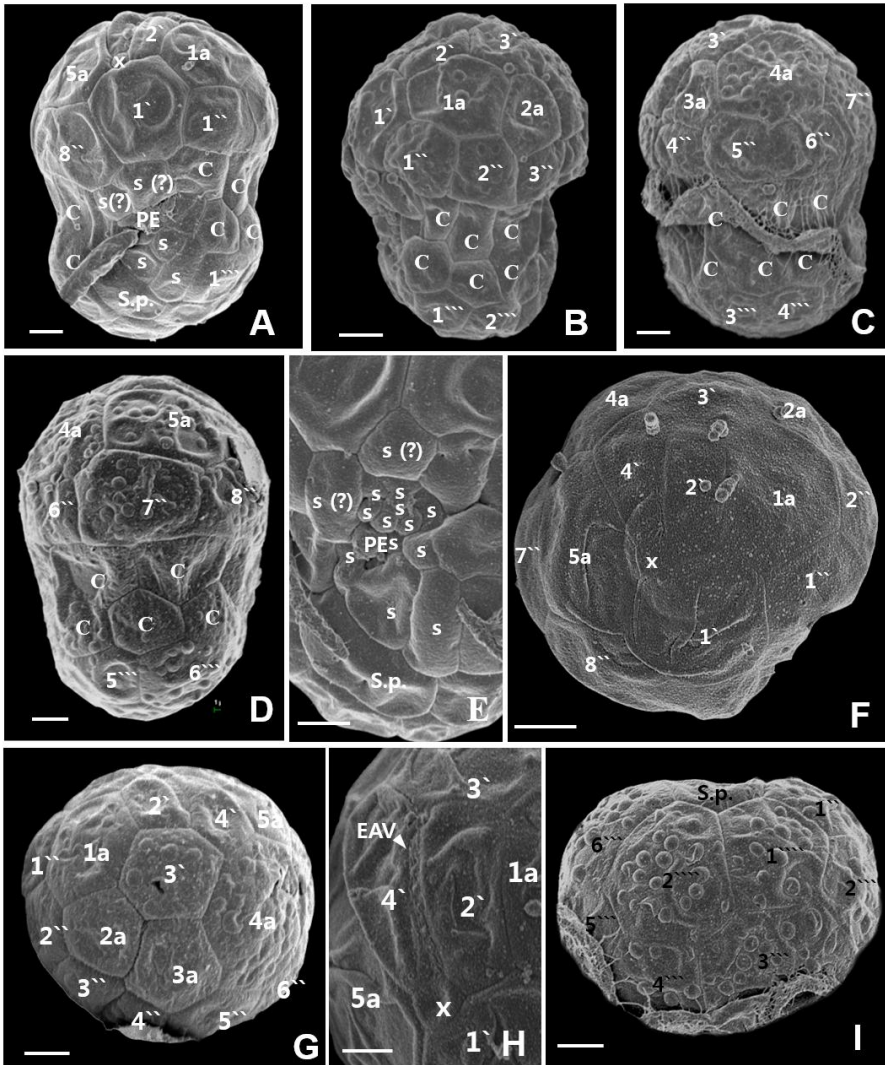
Figs 2.2. Scanning electron micrographs of *Symbiodinium microadriaticum* motile cells. **A.** Ventral view showing the episome, cingulum (C), sulcal plates (s), and hyposome. **B.** Ventral–left lateral view showing the episome, cingulum (C), and hyposome. **C.** Dorsal view showing the episome, cingulum (C), and hyposome. **D.** Ventral–right lateral view showing the episome, cingulum (C), and

hyposome. **E.** Antapical-ventral view showing the sulcal plates (s) and peduncle (PE). **F.** Apical view showing the episome and elongated amphiesmal vesicle (EAV) plate. **G.** Apical view showing the dorsal view of episome and EAV plate. **H.** Apical view showing the EAV plate with small knobs (arrowhead). **I.** Antapical view showing the hyposome. All scale bars = 1 μm.
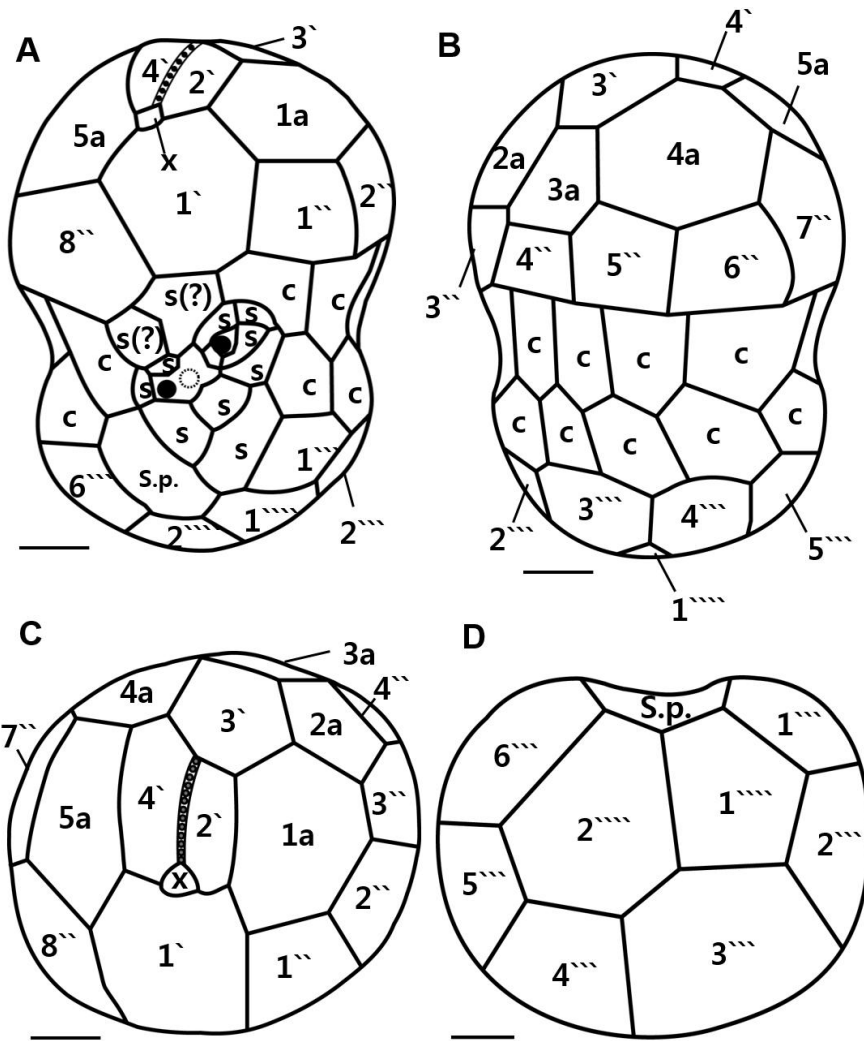
Figs 2.3. Drawings of *Symbiodinium microadriaticum* motile cells strain showing the external morphology. **A.** Ventral view. **B.** Dorsal view. **C.** Apical view. **D.** Antapical view. All scale bars = 1 μm.

2.3.3. Morphology of *Symbiodinium tridacnidorum*

The motile cells of this culture were mushroom shaped, with an episome that was slightly larger than the hemispherical hyposome (Figs 2.1D–I). The cells (n = 30) in log phase growth were found to be 9.4–12.9 μm in length and 7.5–10.6 μm in width (Table 1.3). In addition, the ratio of the length of the living cells to the width was 1.1–1.4 μm (Table 1.3). When fixed and observed under SEM, the cells were found to be 8.1–10.1 μm in length and 5.6–7.1 μm in width, and the ratio of the length to width was 1.3–1.5 μm (Table 1.3).

The Kofoidian plate formula of *S. tridacnidorum* cells is x, EAV, 5', 6a, 8'', 9-11s, 2 cingulum rows 17–19c, 7''', and 3'''' (rarely 2''''; Table 1.3; Figs 2.4, 2.5). At the cell's apex, the EAV possessed 7–9 aligned knobs and measuring 0.76–1.84 μm in length and 0.09–0.37 μm in width (Table 1.3). This structure was bordered ventrally by the x plate and surrounded by 4 apical amphiesmal plates (2', 3', 4', and 5' plates; (Figs 2.4E, 2.4F, 2.5E, 2.5F, 2.7C). Apical plates consisted of a rhomboid-shaped and relatively large 1' plate, a quadrangular 2' plate, a 3' plate that appeared pentagonal or hexagonal, and a pentagonal 4' plate (Figs 2.4E, 2.4F, 2.5E). There are 6 intercalary plates. Of these 4 are hexagonal (plates 1a, 3a, 4a, and 5a), one was pentagonal (2a), and one is either pentagonal-, hexagonal-, or heptagonal-shaped depending on the cell imaged (6a) (Figs 2.4A-E, 2.5A-E, 2.7A-C). For the 8 precingular plates, the 1'' plate is invariably quadrangular, the 2'', 5'', 6'', and 8'' plates are pentagonal, however the 3'', 4'', and 7'' plates are variable and either

quadrangular or pentagonal (Table 1.3; Figs 2.4A-E, 2.5A-E, 2.7SA, 2.7B). Two wide cingulum rows consisting of 17–19 pentagonal plates create the groove around the middle of the cell where the transverse flagellum lies. The cingulum is displaced in the region of the sulcus grove by ~0.1–0.2 times the cell length and ~0.4–0.7 times the cell width (Table 1.3). Of the 7 postcingular plates, 1''', 2''', 5''', 6''', and 7''' plates are quadrangular, while the 3''' and 4''' plates are pentagonal (Table 1.3; Figs 2.4G, 2.7D). There are usually 3, but sometimes 2, antapical plates (Table 1.3; Figs 2.5G, 2.6). The 1'''' and 2'''' plates are either pentagonal or hexagonal, while the 3'''' is hexagonal when present (Fig. 2.4G, 2.5A, 2.6). A total of between 9–11 sulcal plates including 2 S (?) plates and one posterior sulcal plate (S.p.) was observed. An accessory sulcal plate positioned between where the transverse and longitudinal flagella emerge from the cell (Table 1.3; Figs 2.4H, 2.5H, 2.7A).

Through TEM analysis, the periphery of the cell interior of *S. tridacnidorum* (CCMP832) is often occupied by chloroplast lobes. A single pyrenoid located in the central part of each cell is connected by 2 stalks to the adjacent chloroplast and surrounded by a distinct starch cap (Figs 2.8A, 2.8D). No chloroplast thylakoid lamellae penetrated the pyrenoid. A large number of lipid globules and starch were observed (Fig. 2.8A). Furthermore, an eyespot (type E), consisting of multiple layers of rectangular electron-translucent vesicles or crystalline deposits, was observed in sectioned mastigote cells (Fig. 2.8B). A mean of 80 ± 3 (SE) condensed chromosomes were estimated from serial sections of cell nuclei (n = 4 cells; Table 1.3; Fig. 2.8C).
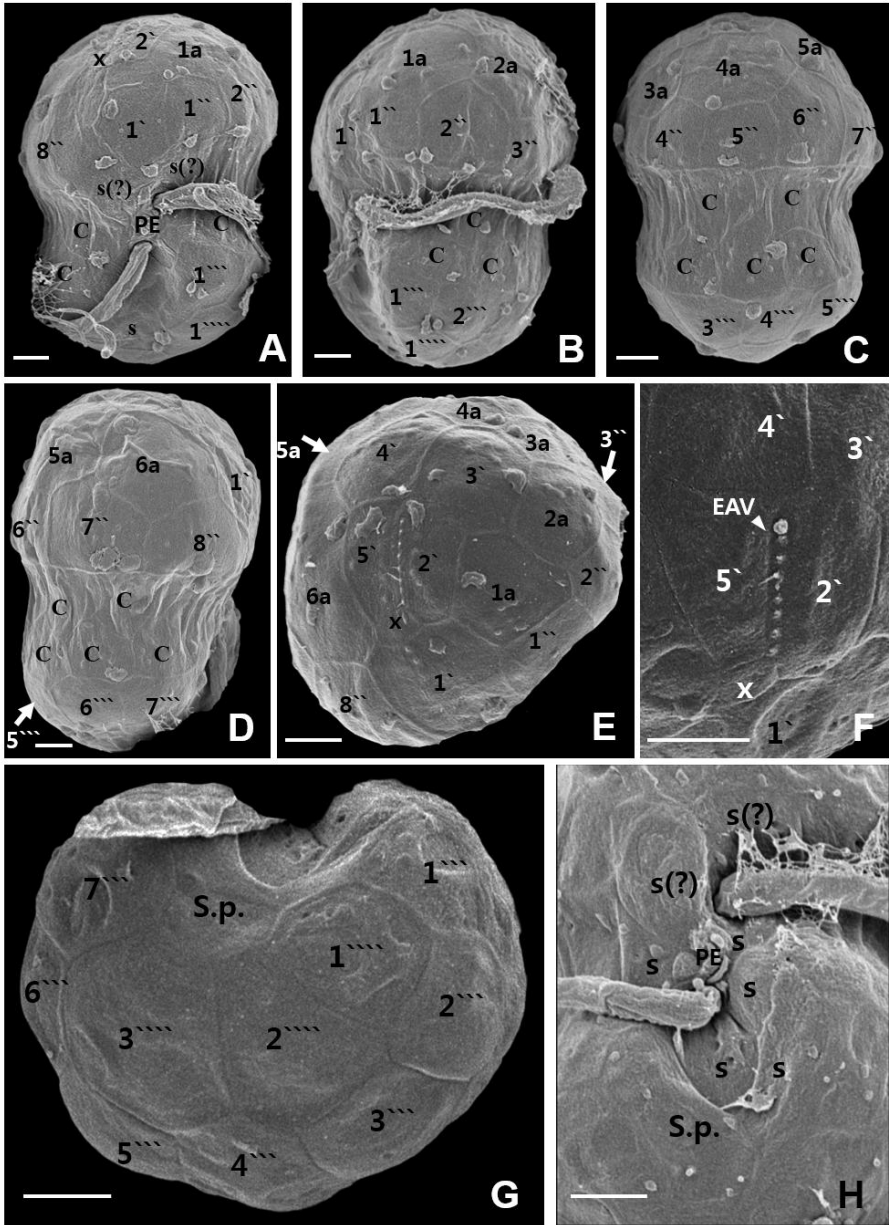
Figs 2.4. Scanning electron micrographs of *Symbiodinium tridacnidorum* motile cells. **A.** Ventral view showing the episome, cingulum (C), sulcal plates (s), peduncle (PE) and hyposome. **B.** Ventral-left lateral view showing the episome, cingulum (C), and

hyposome. **C.** Dorsal view showing the episome, cingulum (C), and hyposome. **D.** Ventral-right lateral view showing the episome, cingulum (C), sulcus (s) and hyposome. **E.** Apical view showing the episome and elongated amphiesmal vesicle (EAV) plate. **F.** Apical view showing the EAV plate with small knobs (arrowhead). **G.** Antapical view showing the hyposome. **H.** Antapical-ventral view showing the sulcal plates (s) and peduncle (PE). All scale bars = 1 μm.
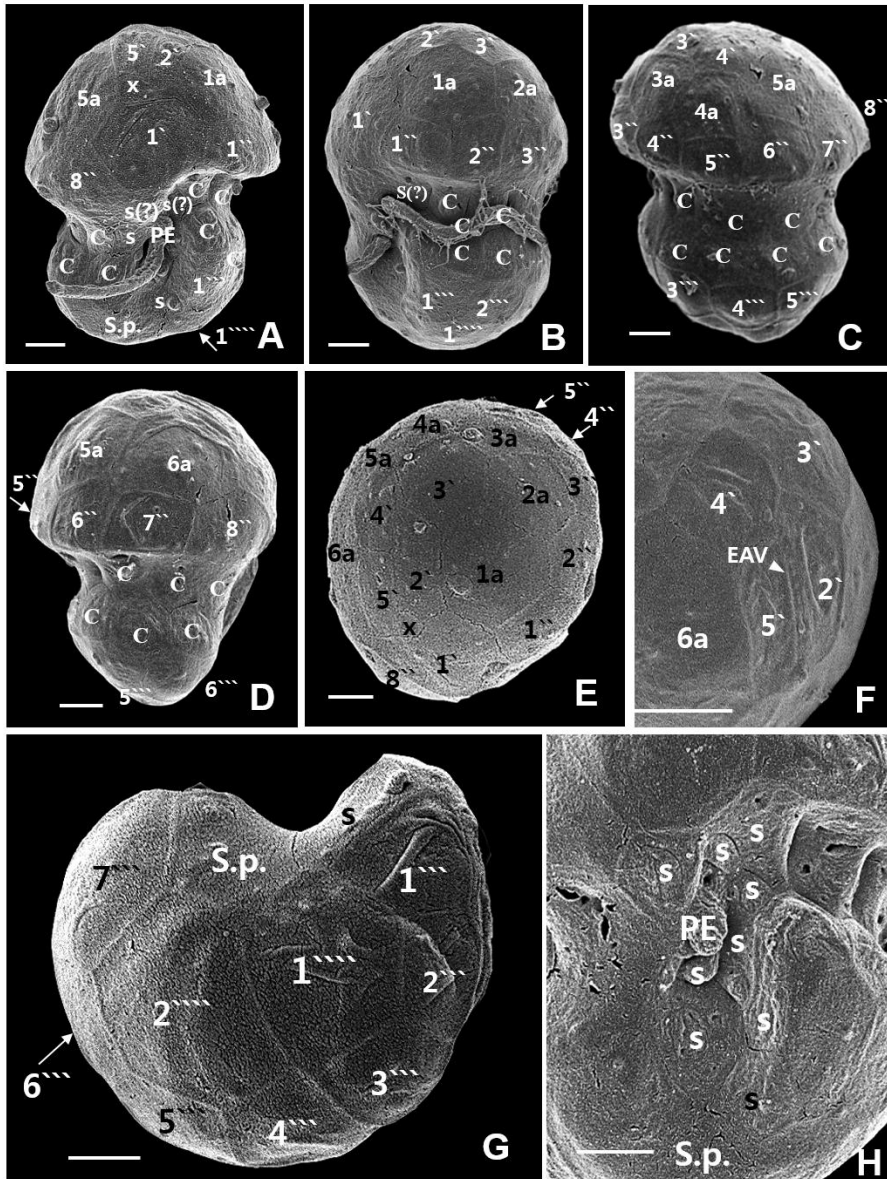
Figs 2.5 Scanning electron micrographs of motile cells of *Symbiodinium tridacnidorum* (strain rt-272). **A.** Ventral view showing the episome, cingulum (C), sulcus (s), peduncle (PE), and hyposome. **B.** Ventral-left lateral view showing the episome, cingulum (C), and hyposome. **C.** Dorsal view showing the episome, cingulum (C), and

hyposome. **D.** Ventral-right lateral view showing the episome, cingulum (C), sulcus (s) and hyposome. **E.** Apical view showing the episome and elongated amphiesmal vesicle (EAV) plate. **F.** Apical view showing the EAV plate with small knobs (arrowhead). **G.** Antapical view showing the hyposome. **H.** Antapical-ventral view showing the sulcus (s) and peduncle (PE). All scale bars = 1 μm.
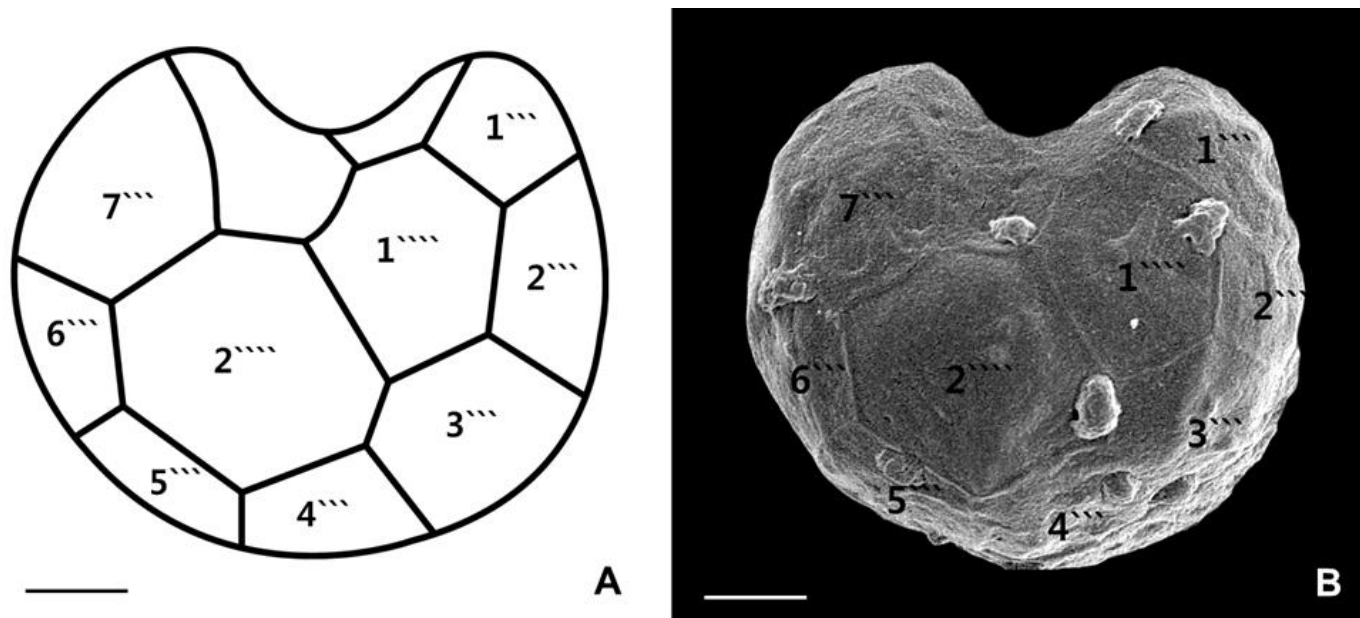
Figs 2.6. Drawings and micrographs of the antapical plate of *Symbiodinium tridacnidorum* taken using scanning electron microscopy. **A.** Drawings of the antapical view showing 2 antapical plates. **B.** Micrographs of the antapical view showing 2 antapical plates. All scale bars = 1 μm.
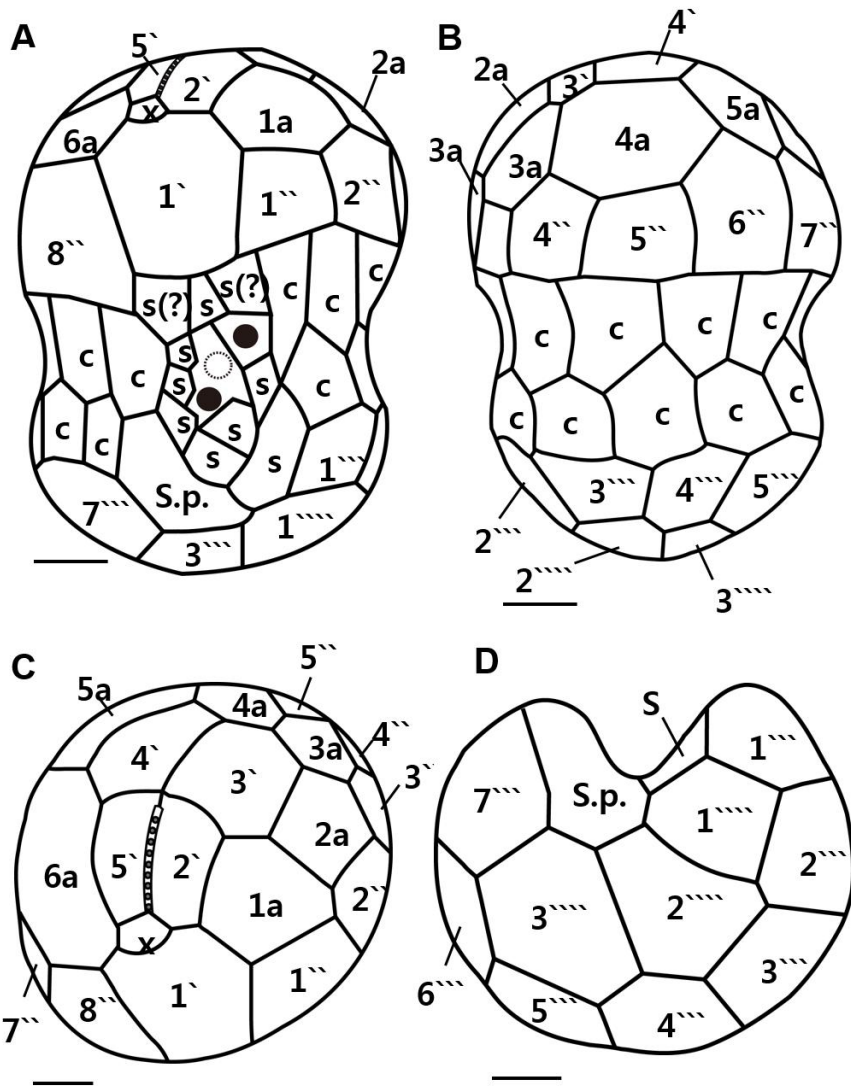
Figs 2.7. Drawings of *Symbiodinium tridacnidorum* motile cells showing the external morphology. **A.** Ventral view. **B.** Dorsal view. **C.** Apical view. **D.** Antapical view. All scale bars = 1 μm.
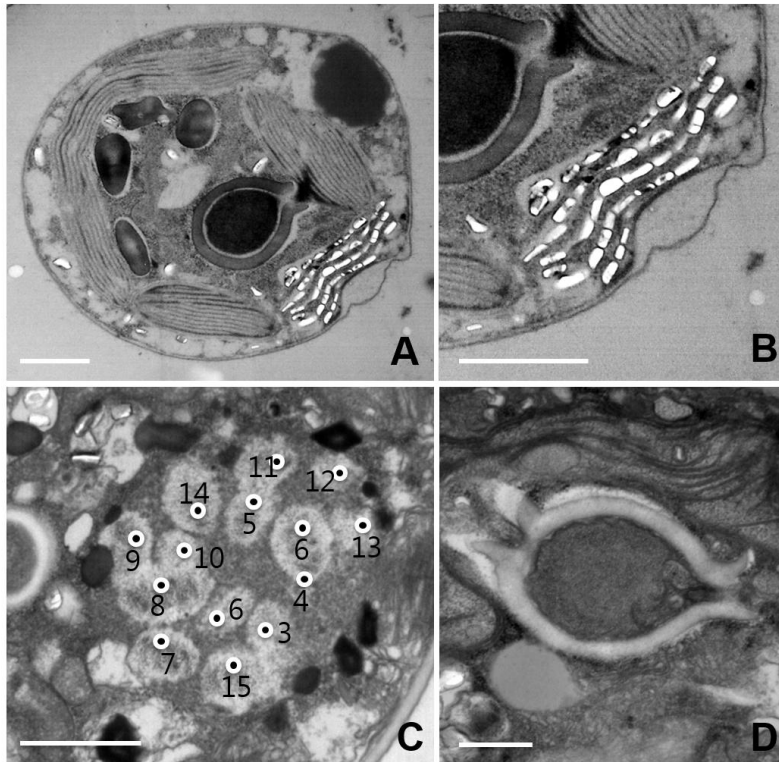
Figs 2.8. Transmission electron micrographs of *Symbiodinium tridacnidorum* cells. **A.** A transverse section of a mastigote cell from *S. tridacnidorum* showing the position of the pyrenoid in the middle of cell, the chloroplasts and type E eyespot (stigma) near the cell's surface, lipid globules, and starch. **B.** A magnified view of the type E eyespot consisting of multiple layers of rectangular electron-translucent vesicles, or crystalline deposits. **C.** Serial sectioning through the nucleus showing large number of condensed chromosomes (approximately 80 ± 3). **D.** A magnified view of a single pyrenoid with 2 stalks, located in the central part of each cell and surrounded by a distinct polysaccharide cap. Scale bar = 1 μm for **A-C** and 0.5 μm for **D.**

2.3.4. Phylogenetic delineation of Clade A *Symbiodinium*

Concordant data from ribosomal DNA (*ITS2* and *LSU*), mitochondrial cob, and chloroplast cp23S sequences show that *S. tridacnidorum* is a reproductively isolated, evolutionarily divergent, lineage and therefore distinct from other described Clade A species (Figs 2.9, 2.10). Some sequence variation in rDNA was found among cultured and field collected specimens originating from giant clams in the subfamily Tradacninae (formerly the family Tridacnidae) and the upside-down jellyfish (*Cassiopeia*; Figs 2.9A, 2.10; Table 1.2). In addition to the *ITS2* "*A3*" sequence, several additional sequence variants, *A3a*, *A6*, and *A3** ('*A3x*' *sensu* Weber, 2009) were found to be diagnostic of this *Symbiodinium* lineage (Fig. 2.9A). These sequences were recovered from direct sequencing of PCR products or from screening using denaturing gradient electrophoresis (DGGE; see Sampayo et al., 2009 for explanation of the method for identifying those ITS sequences of diagnostic value in organisms with high intragenomic rDNA variation). The culture CCMP832 is characterized by the *A3** *ITS2* sequence, which differentiated from *Symbiodinium A3* by a single base substitution (Fig. 2.9A). The *LSU* sequence of *A3** (e.g. CCMP832) also contained two base substitutions (Fig. 2.10). The rDNA variant of CCMP832 matched with a field collected sample of *Tridacna maxima* originating from 12-15 metre depth in Palau (Fig. 2.10) and from samples obtained from the Indo West Pacific, West Pacific, and Central South Pacific (Fig. 2.9; Weber, 2009).
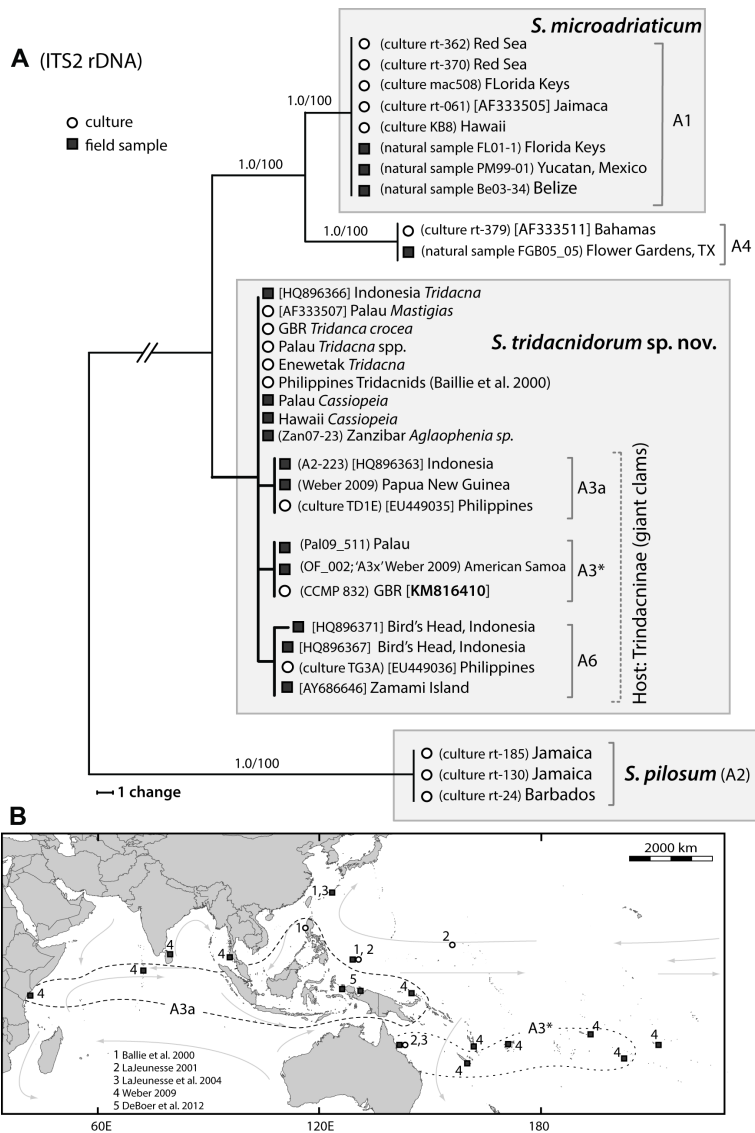
Figs 2.9. Maximum parsimony (MP) tree and a summary of the known geographical distributions. **A.** Maximum parsimony (MP) tree created from the alignment of *ITS2* data from Clade A *Symbiodinium* identified as *S. microadriaticum* (types *A1*), *S. pilosum* (*A2*), *S. tridacnidorum* sp. nov. (comprising mostly Indo-Pacific

samples from tridacnid clams and *Cassiopeia* sp.), and type *A4* found in the Western tropical Atlantic. The numbers above the branches correspond to Bayesian posterior probabilities (left) and MP boot strap values (right). **B.** A summary of the known geographical distributions for *S. tridacnidorum* associated with *Tridacna maxima* across the Indo-Pacific. The known ranges of *ITS2* variants *A3a* and *A3** (*A3x sensu* Weber, 2009) suggest the possibility that genetic structure among geographically distant populations may exist. Numbers correspond to the publications where these distributions were reported.

(culture rt-362) Red Sea
(culture rt-370) Red Sea [KF364598]
(culture mac508)
(culture CCMP 2464; rt-061) Florida Keys, USA [**KM972549**] ◁
(isolate 406; Loeblich & Sherley 1979)
(culture KB8) Hawaii
(natural sample FL01-1) Florida Keys, USA
(natural sample PM99-01) Yucatan, Mexico
(natural sample Be03-34) Belize

S. microadriaticum (A1)

1.0/98

.90/81

FGB05 05 typeA4 [KF364602]
rt-378 typeA4

A4

(CCMP 832) GBR *Hippopus hippopus* [**KM816405**] ◁ A3*
(natural sample Pal09-511) Palau *T. maxima*
(natural sample Phu002) Phuket *T. maxima*
(natural sample Phu003) Phuket *T. maxima*
(natural sample Phu004) Phuket *T. maxima* [**KM972551**]
(natural sample Phu005) Phuket *T. maxima*

A6

1.0/ 94

.97/85

.95/84

(culture rt-272) Palau *Tridacna gigas* [**KM816406**] ◁ A3
(culture rt-77) Hawaii *Cassiopeia*
(culture rt-243) Palau *T. derasa*
(culture rt-174) Enewetak *T. maxima*
(culture EL1) Hawaii *Cassiopeia* sp.
(natural sample Zan07-23) Zanzibar *Aglaophenia sp.*
(natural sample Zan07-48) Zanzibar *Aglaophenia sp.*
(natural sample Pal14-01) Palau *C. andromeda*
(natural sample Pal14-02) Palau *C. andromeda*
(natural sample Haw02-80) Hawaii *Cassiopeia* sp.

S. tridacnidorum sp. nov.

1.0/ 98

(culture rt-315) Palau *T. squamosa* [**KM972550**] ——— A5

Clade A

1.0/ 100

S. natans [EU315917]

(culture rt-185) Jamaica [KF740671]
(culture rt-130) Jamaica
(culture rt-24) Barbados

S. pilosum (A2)

1.0/ 100

Clade D

S. eurythalpos [KF740686]
S. trenchii [KF740689]
S. boreum [KF740688]

1.0/ 100

Clade E

Eastern Pacific [KF364605]
(isolate 395) Northwest Atlantic
Western Pacific [HF568830]
Mediterranean [KF364606]

S. voratum

1.0/ 100

⊢—⊣ 5 changes

Fig. 2.10. Maximum parsimony (MP) tree Clade A diversity based on 620 bp aligned positions encompassing the D1/D2 domains of the *LSU*. Species representatives from Clades D and *S. voratum* (Clade E) were used as outgroup taxa. The branch lengths are proportional to the number of character differences (branch lengths separating Clade A from the other lineages are abbreviated). The numbers associated with branches relate to Bayesian posterior probabilities (left) and MP bootstrap values (right). Posterior probabilities ≥0.8 are shown. Grey arrowheads signify those cultured isolates used for morphological analysis.

The *LSU* (and cp23S; data not shown) sequences from the two isolates examined by Loeblich and Sherley (1979) placed them in the genus *Symbiodinium*. Isolate 406 is a strain of *S. microadriaticum* (Fig. 2.10), while isolate 395 matched sequences of *S. voratum* obtained from populations in the northwestern Pacific (Fig. 2.10).

Mitochondrial cob and partial chloroplast cp23S sequences were identical for most samples of *S. tridacnidorum*. The only exceptions found were from samples of Cassiopeia andromeda collected in Palau. These were differentiated from the others by a single base substitution in domain V of the cp23S marker (Fig. 2.11).

The rDNA (*ITS2* and *LSU*) and plastid (cp23S and cob) sequences used to diagnose cultures and field-collected samples of *S. microadriaticum* were invariant despite originating from several locations in the north central and western Caribbean (Florida Keys, the Mexican Yucatan, and Belize), Red Sea (Gulf of Aqaba), and one culture (KB8) from O'ahu, Hawaii (Figs 2.9, 2.10). Similarly, the sequences of these markers were identical for each of three cultures of *S. pilosum* (type *A2*; *sensu* LaJeunesse, 2001) obtained from 3 host genera and two Caribbean locations (Figs 2.9A, 2.10, 2.11; Table 1.2). This species is only known from opportunistic contaminants during the culturing process, as there are no known field-collected samples of *S. pilosum* (LaJeunesse pers. obs.)

The phylogenetic reconstructions of Clade A *Symbiodinium* based on sequences from chloroplast and mitochondrial genes corresponded with rDNA phylogenies (cp23S and cob trees not shown). Fixed sequence differences in both the cob and cp23S resolved *S. tridacnidorum* and *S. microadriaticum* as evolutionary divergent entities. The phylogeny based on the concatenated

sequence alignments of chloroplast and mitochondrial markers, along with the D1/D2 region of LSU, is shown in Fig. 2.11.
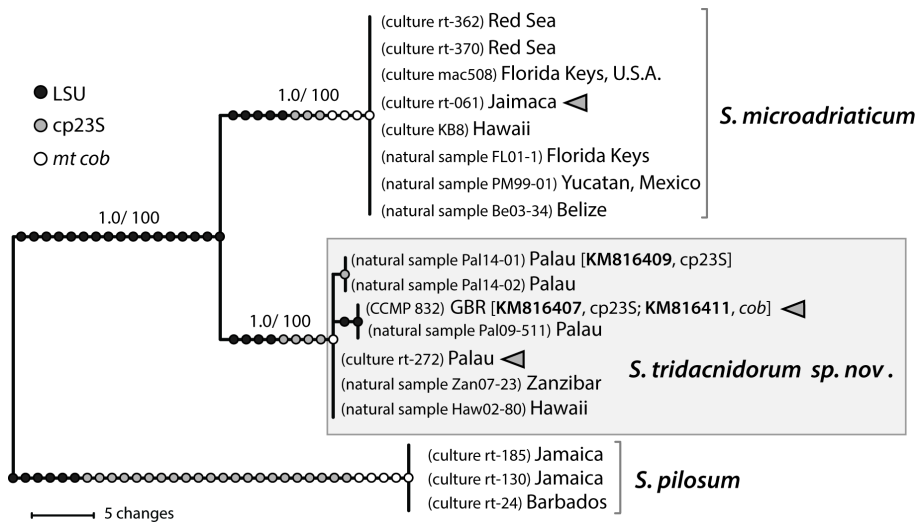
Fig. 2.11. Maximum parsimony (MP) tree created from concatenated alignments of *LSU*, cp23S, and cob sequences. The differently-shaded dot symbols along each branch indicate the relative contribution of fixed differences in each genetic marker that differentiate 3 species of Clade A. The numbers above the branches indicate the Bayesian posterior probability (left) and MP bootstrap values (right). Grey arrowheads signify the cultured isolates used for morphological analysis.

2.4. Discussion

Clade A *Symbiodinium* contains phylogenetically and ecologically distinct entities that exhibit unique geographical distributions (LaJeunesse et al., 2009). This group also comprises many species that are both ecologically common and are capable of growth in culture media, which allows for detailed morphological analysis of the motile phase and experimental manipulation (Hennige et al., 2009).

2.4.1. Morphological comparisons among Clade A *Symbiodinium*

The new description of *S. tridacnidorum* sp. nov. and emended description of *S. microadriaticum* shows that the mastigotes of genetically similar species are morphologically distinct (Fig. 2.12). Our analyses of two genetically distinct strains of *S. tridacnidorum* obtained from different regions of the Pacific Ocean (GBR and Palau) indicate that morphology is stable among individuals (i.e. strains) of this species (Figs 2.5, 2.9A, 2.10).

The size, shape, number, and arrangement of amphiesmal plates can also be used to discern Clade A species that were initially recognized by genetic and ecological differences (Table 1.3). Each species possesses different numbers of sulcal and cingular plates (Table 1.3). The number of knobs arranged on the EAV are similar for *S. microadriaticum* and *S. tridacnidorum* (6-8 and 7-9, respectively), but differ significantly from *S. natans*, which has at least 12 knobs. However, similarities and differences in plate

formulae do not necessarily correspond to phylogenetic relationships. *S. microadriaticum* (CCMP2464) and *S. natans* contain the same number of apical, intercalary, postcingular, and antapical plates whereas *S. tridacnidorum* had different totals for these plate types (Fig. 2.12; Table 1.3); making the overall plate arrangement for *S. tridacnidorum* more distinctive than the plate tabulation established for *S. voratum* (Clade E), a distantly related species (Fig. 2.12). Furthermore, the shapes of specific plates when compared between species corresponded only partially with phylogenetic data. For example the 5a and 6'' plates were distinct for *S. tridacnidorum* being hexagonal and pentagonal, respectively; whereas the shapes of these plates for *S. microadriaticum* and *S. natans* matched with *S. voratum*, pentagonal and quadrangular, respectively. Therefore, while the comprehensive analyses of morphological evidence can define these 'morphologically cryptic' species, the overlap in trait values creates some ambiguity when reconciled against gene-based phylogenies.

This work provides morphological analysis of the *S. microadriaticum* strain (CCMP2464, or rt-061) used by Trench and Blank (1987) to further emend the description of *S. microadriaticum*, the type species in the genus *Symbiodinium* (Freudenthal). LaJeunesse (2001) genetically analyzed CCMP2464 and designated it as type *A1*. From the incomplete description provided by Freudenthal (1962), for which the original type material is not available, it is not possible to know whether the particular culture he based his diagnosis was morphologically and genetically the same as the specimens analyzed by Loeblich and Sherley (1979) and by Trench and Blank (1987). However, the entity isolated as CCMP2464 by Trench and Blank (1987),

accurately represents the identity of *Symbiodinium* found in field collected samples of *C. xamachana* from the Greater Caribbean (LaJeunesse, 2002; Fig. 2.10), and not an opportunistic species isolated during the culture process (Santos et al., 2001).

The two isolates described as *Zooxanthella microadriatica* by Loeblich and Sherley (1979) are morphologically similar to *S. microadriaticum* (CCMP2464). These included strain 406 isolated from *Cassiopeia xamachana* from the Florida Keys, which had a thecal plate formula of 5', 5–6a, 9–10', 8–9s, 20c, 7–8''', and 3''''; and strain 395 isolated from a decaying red alga, *Chondrus crispus*, collected off the coast of Massachusetts, USA, which had a plate formula of 5', 4–6a, 10–11'', 8–9s, 20c, 7–8''', and 3''''. Our genetic characterization of these isolates unambiguously resolved their identity. Isolate 406 (given to Loeblich by Trench's student, Schoenberg) is likely to be the same isolate later used by Trench and Blank (1987) in their emendation of *S. microadriaticum* (rt–061 synonymous with CCMP2464; Fig. 2.10). Our plate reconstruction of the isolate from *Cassiopeia xamachana* collected from the Florida Keys, USA, differs from their formulation in the number of precingular and antapical plates. The genus *Zooxanthella* was created by Brandt (1881) during his studies on the algae living in the radiolarian, *Collozoum inerme*. However, recent analysis of radiolarian dinoflagellate symbionts shows that they are evolutionarily divergent from *Symbiodinium* and the genus *Zooxanthella* has been replaced with the new genus *Brantodinium* (Probert et al., 2014).

The free-living strain Loeblich & Sherley (1979), obtained from cold temperate waters of the Northwest Atlantic, isolate 395, corresponds to *S. voratum* (Fig. 2.10). Their morphological

characterization was similar to that of Jeong et al. (2014a), but there appears to be a difference in how antapical vs. postcingular plates were designated by each set of researchers. Also, the number of precingular plates estimated by Loeblich and Sherley (1979) was higher than that reported by Jeong et al. (2014a). However, these morphological differences also correspond to exceptional morphological characterizations referred to in the supplementary figure reported by Jeong et al. (2014a). Further, despite these apparent morphological differences, which may stem from differences in technique, the large cell size, high latitudinal origin, and free-living habit of isolate 395 are consistent with genetic analysis identifying this isolate as *S. voratum*, and not *Zooxanthella microadriatica*.
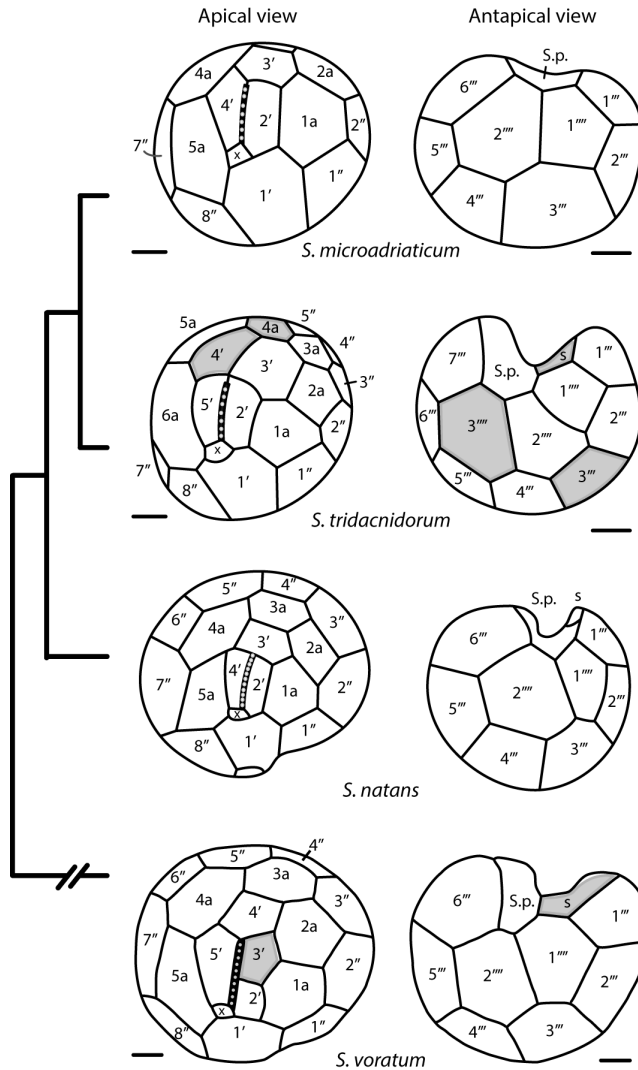
Fig. 2.12. A comparison of apical and antapical plate morphologies from *S. microadriaticum*, *S. tridacnidorum* and *S. natans* (Clade A), and *S. voratum* (Clade E). The occurrence of additional plates and plate connections that differ from *S. microadriaticum* are highlighted in grey. Genetic relationships based on LSU rDNA are drawn to the left.

2.4.2. The genetic, ecological, and geographical attributes of described species in *Symbiodinium* Clade A

Symbiodinium tridacnidorum is probably the most prevalent Clade A species from the Indo-Pacific that is mutualistic with very different kinds of animal. Independent researchers, working in the West Indo-Pacific, have commonly identified (genetically) and cultured *S. tridacnidorum* from giant clams in the molluscan subfamily Tradacninae (Rowan et al., 1996; Carlos et al., 1999; Baillie et al., 2000; LaJeunesse, 2001; LaJeunesse et al., 2004a, 2004b; Weber, 2009; DeBoer et al., 2012). This symbiont has also been identified and cultured from species of the mangrove upside-down jellyfish in the genus, *Cassiopeia*, a rhizostomate group in the Class Scyphozoa (Fig. 2.9; LaJeunesse et al., 2004a, 2004b). *Cassiopeia andromeda* from Palau, a likely native of the Pacific Ocean region (host genetic data not shown), contained *S. tridacnidorum* populations, diagnosed by a slightly distinct cp23S sequence variant (Fig. 2.9). In the Indian Ocean, it occurs in the large stinging hydroid (Aglaophenia; Figs 2.9A, 2.10). Experiments with *S. tridacnidorum* have shown that isolates from *Tridacna* spp. (rt-272) can infect and induce strobilation in the scyphistome of *Cassiopeia xamachana* (Fitt, 1985). The seemingly disparate specificities of this symbiont cannot be explained by host phylogenetic relationships, nor the nature of their associations (e.g. extracellular vs. intracellular), yet suggests that unknown biotic or abiotic factors have initiated host shifts during its evolutionary history (Secord and Kareiva, 1996).

Three *ITS2* sequence variants, *A3a*, *A3** (listed as ʻ*A3x*ʼ in Weber 2009), and *A6* diagnose *Symbiodinium* populations found only in the tridacnids (Fig. 2.9). Types *A3* and *A6* are relatively widespread, but type *A3a* occurs predominantly in tridacnids from the Indo-west Pacific and Central Indian Ocean, whereas *A3** is common in clams from the Southwest and Southcentral tropical Pacific (Fig. 2.9B; Weber, 2009). These different geographic distributions indicate regional differentiation exists between some populations of *S. tridacnidorum* (Weber, 2009). The analysis of microsatellite allelic data can be used in the future to test the possibility of regional endemism/isolation across this widely distributed species (Pinzón et al., 2011; Baums et al., 2014). The broad geographic range and genetic variation among populations of *S. tridacnidorum* associated with the tridacnids indicate that this particular relationship has probably lasted millions of years (Thornhill et al., 2014).

Symbiodinium species designated type *A3* (*sensu lato*) are associated with a wide range of cnidarians that occur in the Greater Caribbean region, including species of the elk- and stag-horn coral (*Acropora*), shallow colonies of the blushing star coral (*Stephanocoenia*), finger corals from sea grass beds (*Porites porites*), the top sides of shallow colonies of boulder star corals (*Orbicella* sp.), and colonies of mat zoanthids (*Zoanthus* sp.; LaJeunesse 2002; Finney et al., 2010; Baums et al., 2014). Preliminary population genetic and phylogenetic comparison between Pacific and Atlantic *Symbiodinium A3* indicate that they are different species (Pinzón et al., 2011; LaJeunesse unpubl. data). The *A3* associated with Caribbean*Acropora* spp. was given the provisional name *Symbiodinium* ʻ*fitti*ʼ (Pinzón et al., 2011; Baums

et al., 2014), pending formal description (in progress). These genetic data also indicate that type *A3* from the Greater Caribbean probably comprises several species (Pinzón, 2011); and the product of a minor adaptive radiation of this lineage in the Atlantic Ocean following its separation from the Pacific 3-4 MYA (Thornhill et al., 2014).

All the genetic variants attributed to *S. tridacnidorum* (i.e. *A3*, *A3a*, *A3** and *A6*) have been isolated and maintained in stable culture at one time or another (Fig. 2.9A). However, the lineages diagnosed as *A3* from the Greater Caribbean have yet to be successfully cultured despite numerous attempts (M. A. Coffroth, SUNY Buffalo, pers. comm.). This hints at the fundamental differences in physiology between Pacific and Atlantic members of the '*A3*' lineage. *S. triadacnidorum* lives at high densities in the tubular system of digestive diverticula that ramify the mantle tissues of giant clams (Norton et al., 1992). Perhaps this capacity for extracellular existence explains why it is readily cultured in artificial seawater media (Baillie et al., 2000; Carlos et al., 1999; LaJeunesse, 2001).

On several occasions, strains of *S. microadriaticum* have proliferated opportunistically during failed attempts to culture the normal symbiont found in a particular host coral (e.g. *Orbicella faveolata* from the Florida Keys and *Stylophora* sp. from the Gulf of Aqaba in the Red Sea; Fig. 2.9). Therefore *S. microadriaticum* must exist at low background concentrations in the environment, and yet are only known to occur in high densities from field-collected samples of *Cassiopeia xamachana* in the Greater Caribbean (Figs 2.9, 2.10; LaJeunesse, 2002). This particular species of upside-down jelly appears to have been introduced to shallow

tropical marine environments around the world, but there are no data to indicate from where it originated (Holland et al., 2004). The taxonomy *Cassiopeia* requires major revision and it is clear that some species lineages have been introduced by humans to regions around the world (Holland et al., 2004). Future genetic analyses of *C. xamachana* specimens collected outside the Atlantic may show that *S. microadriaticum* is found in *C. xamachana* everywhere this host occurs.

Finally, the chromosome numbers counted for *S. tridacnidorum* (n = 80 ± 3) and *S. microadriaticum* (97 ± 2; Table 1.2; Trench and Blank, 1987) differ to an extent that would make them reproductively incompatible as eukaryotes. The chromosome values for *S. pilosum* (78 ± 2) are similar to *S. tridacnidorum*, but significant sequence divergence at several DNA loci indicates that they are distantly related (Figs 2.9-2.11). Additional analysis of the chromosome number from other yet undescribed species in Clade A may offer insights into genome evolution among the closely and distantly related species that comprise this group.

Chapter 3. Morphological characterization of the two new Symbiotic dinoflagellate *Symbiodinium minutum* and *S. psygmophilum* belonging to clade B

3.1. Introduction

Dinoflagellates are often abundant and ubiquitous protists in marine environments (Gomez, 2012, Jeong et al. 2013, Kang et al. 2013, Yoo et al. 2013; Moestrup et al, 2014). They play diverse roles in marine ecosystems as primary producers but also as predators, prey, competitors, parasites, and symbiotic partners (Hansen, 1991; Jeong, 1999; Stoecker, 1999; Kim et al. 2013a; Park et al. 2013a, Seong and Jeong 2013; Lim et al. 2014; Lee et al. 2015b). The ecological niche of a dinoflagellate species is usually different from that of the other dinoflagellate species (Jeong et al. 2010; Lee et al. 2014c). Thus, to understand the roles of a dinoflagellate species in marine ecosystems, exact identification of the species are necessary.

Among these dinoflagellate species, the genus *Symbiodinium*, commonly known as zooxanthellae, comprises symbiotic dinoflagellates, most of which are symbiotic with various species such as corals, sponges, sea anemones, jellyfish, nudibranchs, clams, ciliates, and foraminifera (LaJeunesse, 2002; Rodriguez-Lanetty et al. 2003; Lewis and Coffroth 2004; Fay et al. 2009; Pochon and Gates 2010; Hill et al. 2011; Pochon et al. 2012; LaJeunesse et al. 2015), while some exist as free-living forms (Gou

et al. 2003; Hansen and Daugbjerg 2009; Jeong et al. 2012, 2014a, 2014b). These species are critical to the ecosystem because *Symbiodinium* species are crucial components of coral reef ecosystems (Iglesias-Prieto et al. 1992; Stanley, 2006; Stat et al. 2006); however, despite their ecological importance in marine ecosystems, not much information on their taxonomy is available. In particular, the morphological characters of *Symbiodinium* have been studied much less than their genetic characters (Kevin et al. 1969; Loeblich and Sherley 1979; Santos et al. 2003; Coffroth and Santos 2005; Hansen and Daugbjerg 2009; Jeong et al. 2014a) because of their difficulty in culturing and scanning electron microscopy (SEM) observations. Thus, some newly established *Symbiodinium* species provided only genetic information mostly using internal transcribed spacer region (ITS) or large subunit (LSU) region of nucleotide ribosomal DNA (rDNA) without morphological information. However, description of new species without morphological characters may cause difficulties in distinguishing species and strains in a genus. Thus, for establishment of new species, both molecular and morphological characteristics are necessary. Further, the Kofoidian plate formula was used for describing a few new species from clade A including *Symbiodinium natans* reported by Hansen and Daubjerg (2009), and clade E *Symbiodinium voratum* reported by Jeong et al. (2014a), and these species can be the morphological standard to establish new species in the genus *Symbiodinium*. Based on molecular identification, genus *Symbiodinium* comprises nine clades including clade A-I (Rowan and Powers 1991; sensu Pochon and Gates 2010), which are phylogenetically very divergent and shows global distributions as well as their abundances (Jeong et al. 2014a). Among genus

Symbiodinium, species belonging to clade B have been found inside sea anemones and corals (Rowan and Knowlton 1995; Diekmann et al. 2003; LaJeunesse et al. 2012). Until now, two species have been reported in the clade B, *Symbiodinium minutum* and *Symbiodinium psygmophilum* (LaJeunesse et al. 2012). The *S. minutum* which belongs to type B1 classified by ITS2 molecular characteristics (sensu LaJeunesse, 2001) is known to form symbiotic relationships with widespread tropical anemones, including the genus *Aiptasia*. The *S. psygmophilum*, which belongs to type B2 classified by ITS2 molecular characteristics (sensu LaJeunesse, 2001) is found mostly in subtropical and temperate stony corals such as *Astrangia*, *Cladocora*, and *Oculina* (LaJeunesse et al. 2012). However, like many other *Symbiodinium* speices, these species were only identified by genetic markers such as nuclear ribosomal ITS1 and ITS2, single copy microsatellite flanker Sym15, mitochondrial cytochrome b (cob), and the chloroplast 23S (cp23S) rRNA gene while and their detailed morphological characterizations such as plate tabulations and related diagnoses have not been provided (LaJeunesse et al., 2012). For this reason, it is worthwhile to explore morphological characters of these two species, including plate patterns of these two species. Thus, in this study, we analyzed the morphology of *S. minutum* and *S. psygmophilum* by SEM and transmission electron microscopy (TEM) to explore morphological characteristics of these two species. On the basis of plate patterns, here we provide complete plate formulae of these two species.

3.2. Materials and methods

3.2.1. Collection and culture of *Symbiodinium* spp.

Two clade B1 *Symbiodinum minutum* strains including CCMP830 from NCMA and rt-13 provided by LaJeunesse, and two clade B2 *Symbiodinium psygmophilum* strains including CCMP2459 (or also called rt-141) and PurPflex provided by LaJeunesse were used in this study (Table 2.1). Both species were cultivated at a temperature of 25℃ with continuous illumination of $20 \mu E/m^2/s$ under cool white fluorescent light and a 14:10 h light-dark cycle. When cultures became dense, they were transferred to new 250-ml PC bottles containing fresh L1 seawater medium approximately every 2-3 weeks. These cultures were used for genetic and morphological analyses.

3.2.2. Morphological analysis of *Symbiodinium* spp.

The length and width of ~30 live cells from each culture in exponential growth were measured using the program ImageJ (Abramoff et al., 2004) and images obtained with a compound microscope (Ziess-Axiovert 200M; Carl Zeiss Ltd, Göttingen, Germany) at a magnification of 1000X. Morphological analyses such as the description of the formula and shape of thecal plate of *S. minutum* and *S. psygmophilum* were performed by scanning electron microscopy (SEM). A 10-ml aliquot of each dense cultures of these two *Symbiodinium* species were fixed for 3-10 min in osmium tetroxide (OsO_4) in a final concentration of 0.3 % in

filtered and autoclaved seawater (FSW). The fixed cells were then collected on a PC membrane filter (pore size 3.0 μm) without additional pressure and serially rinsed three-five times with diluted FSW and distilled water to remove the salt. After cells were collected, they were dehydrated in an ethanol series of 10%, 30%, 50%, 70%, 90% and then two times of 100% ethanol. The dehydrated cells were transferred to critical point dryer (BAL-TEC, CPD 300, Balzers, Liechtenstein, Germany), and maintained in the 100% EtOH and filters were washed with liquid carbon dioxide (CO_2) for complete dehydration. Then filters were dried completely and then mounted on a stub and coated with platinum. The filters with cells were observed with a FE-SEM (S-4800, HORIBA: EX-250, Hitachi, Hitachinaka, Japan) and SEM (JSM-840A, SEM JEOL Ltd., Tokyo, Japan) and photographed using a digital camera. Based on obtained results and live cells, cell length and width of fixed cells and live vegetative flagellated cells were measured using an image analysis system on images collected with a compound microscope (Image-Pro Plus 4.5, Media Cybernetics, Silver Spring, MD).

For the observation of intercellular observations including chromosome counting, transmission electron microscopy (TEM) were used. For TEM analysis, cells of each strain with a seawater medium (F/2) were transferred to a 10 ml tube and fixed in glutaraldehyde with final concentration of 2.5% for 1.5-2h. After fixation, tubes containing fixed cells were centrifuged at 1,610 $\times$g for 10 min and the supernatant were discarded. The pellets were transferred to 1.5 ml tubes, rinsed several times with 0.2 M pH 7.4 sodium cacodylate buffer, and postfixed with 1% osmium tetroxide in deionized water for 90 min. After fixation, the pellets were embedded in agar. Dehydration was performed via a graded

ethanol series (50%, 60%, 70%, 80%, 90%, and 100% ethanol, followed by two changes in 100% ethanol). The agar-embedded pellet was then re-embedded in Spurr's low-viscosity resin (Spurr, 1969) and dried for 3 days at 70°C. Hardened samples were then serially sectioned (80-100 nm) using an RMC MT-XL ultramicrotome (Boeckeler Instruments Inc., Tucson, AZ, USA), and stained with 3% aqueous uranyl acetate followed by lead citrate. Finally, sectioned samples were observed with a JEOL-1010 transmission electron microscope (JEOL Ltd., Tokyo, Japan). The number of chromosomes (± SE) in each strain was determined using these serial sections.

Table 2.1. Strain, location of collection (LC), host and collection information of 2 *Symbiodinium* clade B species obtained from the National Center for Marine Algae and Microbiota (formerly the Provasoli-Guillard National Center for Culture of Marine Phytoplankton). NA: Not available.

Species	Strain name	Clade	LC	Host	Reference
Symbiodinium minutum	CCMP830	B1	Bermuda	*Aiptasia pulchella* (Sea anemone)	LaJeunesse et al. (2012)
Symbiodinium minutum	rt-13	B1	NA	NA	Provided by LaJeunesse
Symbiodinium psygmophilum	CCMP2459 (= rt-141)	B2	NA	*Occulina diffusa* (Coral)	LaJeunesse et al. (2012)
Symbiodinium psygmophilum	PurPflex	B2	NA	NA	Provided by LaJeunesse

3.3. Results

3.3.1. Morphology of *Symbiodinium minutum*

For size, approximately 30 live vegetative cells were observed and for plate tabulation analyses, approximately 150 fixed cells were observed. The size of photosynthetically grown cells observed under a compound microscope showed 8.5–11.7 μm in length and 6.9–9.8 μm in width, while the length to width ratio was 1.1–1.3 (Table 2.2). Scanning electron microscopy (SEM) result showed that the morphology of *S. minutum* CCMP830 and rt-13 were almost identical. The elongated amphiesmal vesicle (EAV) located on the apical plate was bordered by three apical plates (i.e., 2'–4' plates) with knobs lined up at the apex and small plate x associated in the ventral part (Figs 3.1E, 3.1F, 3.2C). The size of EAV measured under SEM showed 1.0–2.4 μm in length and 0.1–0.3 μm in width, and the number of knobs was 5–8 (Table 2.2; Figs 3.1F, 3.2C).

The plate formula based on Kofoidian series of *S. minutum* was x, EAV, 4', 5a, 8'', 7s, two cingulum rows, 18–20c, 5–6''', and 2'''' (Table 2.2; Figs 3.1, 3.2). The apical plates consisted of a rhomboic and relatively large plate 1' and pentagonal or hexagonal 2' touching plates 1', 3', 4', and 1a and 2a. The pentagonal or hexagonal plate 3' touched plates 2', 4', and intercalary plates 2a–4a, whereas the pentagonal 4' touched 2', 3', 4a, and 5a (Figs 3.1A-F, 3.2A-C). There were five intercalary plates: pentagonal 1a, hexagonal 2a, pentagonal or hexagonal 3a, heptagonal 4a, and pentagonal or hexagonal 5a (Figs 3.1B-E, 3.2A-C). The pentagonal plate 1a touched plates 1', 2', 2a, 1'', and 2'', while hexagonal 2a touched 2', 3', 1a, 3a, 2'', and 3'' (Figs 3.1A, 3.1B, 3.1E, 3.2C). Furthermore, the hexagonal intercalary plate 3a touched

plates 3', 2a, 4a, 3'', 4'', and 5'' (Fig. 3.1B). The hexagonal or heptagonal 4a always touched 3', 3a, 5a, 5'', 6'', and 7'' and sometimes 2', but the pentagonal 5a touched 1', 4', 4a, 7'', and 8'' (Figs 3.1D, 3.1E, 3.2C).

The *S. minutum* cells had eight precingular plates that were either quadrangular (1'', 4'', and 6'') or pentagonal (2'', 3'', 5'', 7'', and 8'') in shape (Figs 3.1A–E, 3.2A–C). The cingulum was consisted of two rows of 18 pentagonal amphiesmal (Figs 3.1A–D, 3.2A–B). The cingulum was displaced about 0.1–0.3 times the cell length and 0.2–0.4 times the cell width (Table 2.2; Figs 3.1A, 3.2A).

There were six postcingular plates; 1''', 2''', 4''', and 5''' were quadrangular, but 3''' and 6''' were pentagonal (Figs 3.1G, 3.2D). There were two antapical plates in hyposome; 1'''' was hexagonal, while 2'''' was pentagonal (Figs 3.1G, 3.2D). The 1'''' contacted 1''', 2''', 3''', 2'''', and the posterior sulcal (S.p.) plate (Figs 3.1G, 3.2D).

There were seven sulcal plates in *S. minutum*; four s plates, two S(?), and one S.p. (Table 2.2; Figs 3.1A, 3.1H, 3.2A). Furthermore, a peduncle was present in the center of the sulcal plates (Figs 3.1A, 3.1H, 3.2A).

The serially sectioned TEM analysis showed that a large portion of the peripheral cytoplasm of *S. minutum* contained chloroplast lobes, which were connected with pyrenoid (PY) (Fig. 3.3A). A single PY located in the central part of each cell was connected by two stalks to the adjacent chloroplast and surrounded by a distinct polysaccharide cap (Fig. 3.3A, 3.3D). No chloroplast thylakoid lamellae penetrated the PY. Further, a large number of large lipid globules was present (Fig. 3.3C). In the sectioned cells of *S. minutum*, a type E eyespot consisting of multiple layers of rectangular electron-translucent vesicles or crystalline deposits was observed (Fig. 3.3B).

Table 2.2. Comparison of morphologically reported *Symbiodinium* species based on figures obtained under scanning electron microscopy. Mean values are shown in the parentheses.

	S. minutum	*S. psygmophilum*	*S. tridacnidorum*	*S. microadriaticum*	*S. natans*	*S. voratum*
AP length, μm (living cells)	6.75−9.38 (8.15)	7.87−12.27 (9.64)	8.1−10.1 (9.2)	7.6−10.0 (9.2)	10.38 [a]	8.5−12.4 (10.5)
Cell width, μm (living cells)	5.47−7.81 (6.67)	6.40−9.72 (7.82)	5.6−7.1 (6.5)	5.8−7.7 (7.1)	8.25 [a]	6.4−9.8 (8.2)
Ratio of length to width (living cells)	1.10−1.31 (1.22)	1.1−1.48 (1.23)	1.3−1.5 (1.4)	1.2−1.5 (1.3)	1.26 [a]	1.2−1.4 (1.3)
EAV length, μm	1.01−2.40 (1.56)	0.95−1.76 (1.43)	0.76−1.84 (1.42)	1.33−2.65 (1.94)	2	1.75−3.09 (2.45)
EAV width, μm	0.10−0.26 (0.19)	0.08−0.15 (0.11)	0.09−0.37 (0.18)	0.13−0.33 (0.21)	0.2	0.15−0.27 (0.2)
No. of small knobs in EAV	5−8	6−9	7−9	6−8	12	9−13
Cingulum displaced by length	0.10−0.27 (0.16)	0.12−0.23 (0.17)	0.06−0.20 (0.12)	0.06−0.24 (0.14)	0.23 [a]	0.13−0.21
Cingulum displaced by width	0.15−0.34 (0.21)	0.15−0.28 (0.21)	0.23−0.70 (0.40)	0.18−0.72 (0.41)	1.0	0.48−0.85 (0.65)
No. of cingular plates	18−20	20−22	17−19	22−24	20	17−20
No. of apical plates	4	4	5	4	4	5
No. of intercalary plates	5	5	6	5	5	5
No. of precingular plates	8	8	8	8	8	8
No. of postcingular plates	6	6 (rarely 5)	7	6	6	6
No. of antapical plates	2	1 (rarely 2)	3 (rarely 2)	2	2	2
Plate tabulation	X, EAV, 4', 5a, 8", 7S, 18−20c, 5−6''', 2''''	X, EAV, 4', 5a, 8", 7−10S, 20−22c, 5−6''', 1−2''''	x, EAV, 5', 6a, 8", 9−11s, 17−19c, 7''', 2−3''''	x, EAV, 4', 5a, 8", 9−13s, 22−24c, 6''', 2''''	x, EAV, 4', 5a, 8", ?s, ?c, 6''', 2''''	x, EAV, 5', 5a, 8", 9s, 17−20c, 6''', 2''''
Reference	(1)	(1)	(2)	(2)	(3)	(4)

AP, anteroposterior; EAV, elongated amphiesmal vesicle; [a] Obtained from Jeong et al. (2014a) **(1)** This study; **(2)** Lee et al. (2014b) ; **(3)** Hansen and Daugbjerg (2009) ; **(4)** Jeong et al. (2012).
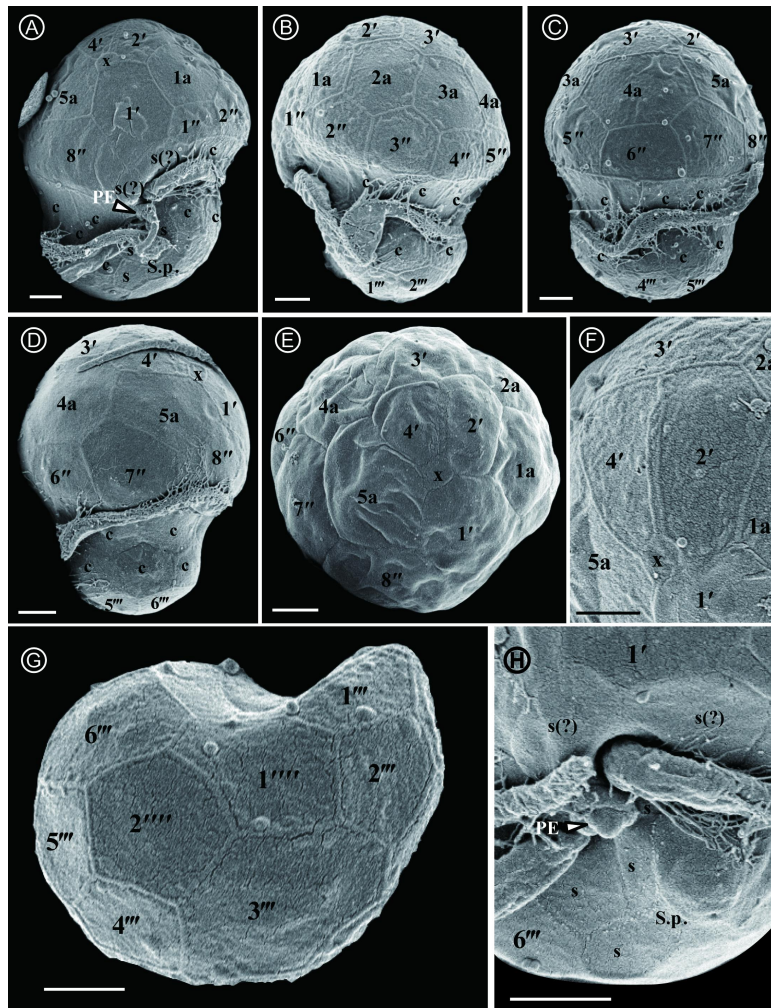
Fig. 3.1. Scanning electron micrographs of *Symbiodinium minutum* motile cells. **A.** Ventral view showing the episome, cingulum (C), sulcus (s), peduncle (PE), and hyposome. **B.** Ventral-left lateral view showing the episome, cingulum (C), and hyposome. **C.** Dorsal view showing the episome, cingulum (C), and hyposome. **D.** Ventral-right lateral view showing the episome, cingulum (C), sulcus (s), and hyposome **E.** Apical view showing the episome and elongated amphiesmal vesicle (EAV) plate. **F.** Apical view showing the EAV plate with small knobs (arrowhead). **G.** Antapical view showing the hyposome. **H.** Antapical-ventral view showing the sulcus (s) and peduncle (PE). All scale bars = 1 μm.

Fig. 3.2. Drawings of *Symbiodinium minutum* motile cells showing the external morphology. **A.** Ventral view. **B.** Dorsal view. **C.** Apical view. **D.** Antapical view. All scale bars = 1 μm.
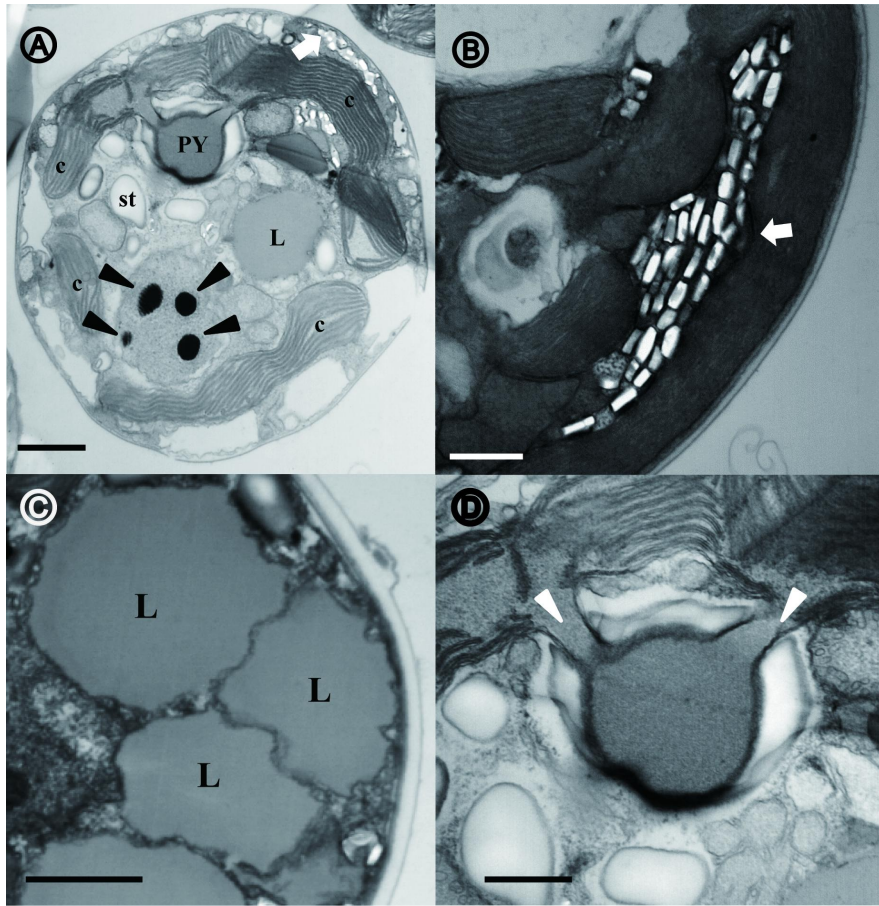
Fig. 3.3. Transmission electron micrographs of *Symbiodinium minutum* cells. **A.** Transverse section of a mastigote cell showing the position of the nucleus possessing chromosomes (black arrowheads) in the middle of cell, chloroplasts (c), two stalked pyrenoid (PY), type E eyespot (stigma, white arrow) near the cell's surface, lipid globules (L), and starch (s). **B.** Type E eyespot (white arrow) consisting of multiple layers of rectangular electrontranslucent vesicles, or crystalline deposits. **C.** Serial sectioning showing the large number of lipid globules. **D.** Pyrenoid with two stalks (white arrowheads) connected to chloroplasts around the cell's surface and surrounded by a distinct polysaccharide cap. Scale bar = 1 μm for panels A and C and 0.5 μm for panels B and D.

3.3.2. Morphology of *Symbiodinium psygmophilum*

For size, approximately 30 cells were observed and for plate tabulation analyses, approximately 300 cells were observed. The size of photosynthetically grown cells observed under a compound microscope showed 7.87-12.27 μm in length and 6.40-9.72 μm in width, while the length to width ratio was 1.1-1.5 (Table 2.2). The SEM showed that the morphologies of *S. psygmophilum* CCMP2459 and PurPflex were almost identical. The EAV with knobs lined up at the apex was located on the apical plate and was bordered by three apical plates (2'-4') and a small plate x associated with the ventral part (Figs 3.4E, 3.4F, 3.5C). The EAV was 1.0-1.8 μm in length and 0.1-0.2 μm in width and the number of knobs was 6-9 (Table 2.2; Figs 3.4F, 3.5C).

The plate formula based on Kofoidian series of *S. psygmophilum* was x, EAV, 4', 5a, 8'', 7-10S, two cingulum rows, 20-22c, 5-6''', and 1'''' (Table 2.2; Figs 3.4, 2.5). The apical plates consisted of a rhomboic and relatively large hexa- or heptagonal plate 1' and pentagonal plate 2' touching plates 1', 3', 1a, and 2a. The pentagonal 3' always touched apical plates 2', 4' and intercalary plates 2a-4a and sometimes touched 5a. The quadrangular or pentagonal 4' usually touched 1'-3' and 4a, but sometimes touched 5a (Figs 3.4A-F, 3.5A-C). There were five intercalary plates including pentagonal 1a and hexagonal 2a-5a (Figs 3.4A-D, 3.5A-C). The pentagonal 1a touched apical plates 1' and 2', intercalary 2a, and precingular 1'' and 2'' (Figs 3.4A, 2.4B, 3.4E, 3.5A, 3.4C). Furthermore, the hexagonal 3a touched 3', 2a, 4a, 3'', 4'', and 5'' (Figs 3.4B, 3.4C, 3.5B). The hexagonal 4a usually touched 3', 3a, 5a, 5'', 6'', and 7'', while hexagonal 5a touched 1', 3', 4', 4a, 7'', and 8'' (Figs 3.4C, 3.4D, 3.5B, 3.5C).

The precingular plates of *S. psygmophilum* consisted of eight plates:

quadrangular 1'' and 6''; pentagonal 2'', 3'', 5'', 7'', and 8''; and quadrangular or pentagonal 4'' (Figs 3.4A-D, 3.5A, 3.5B). The cingulum was consisted of two rows of 22 pentagonal amphiesmal plates (Figs 3.4A-D, 3.5A, 3.5B). The cingulum was displaced about 0.1–0.2 times the cell length and 0.2–0.3 times the cell width (Table 2.2; Figs 3.4A, 3.5A).

There were five quadrangular postcingular plates, while there was one hexagonal antapical plate (Figs 3.4G, 3.5D). The antapical plate touched all five postcingular plates and the S.p. plate (Figs 3.4G, 3.5D).

The *S. psygmophilum* cells possessed seven to 10 sulcal plates (Table 2.2; Figs 3.4A, 3.4H, 3.5A); four to seven s plates, two S(?), and one S.p.. A peduncle was present in the center of the sulcal plates (Figs 3.4A, 3.4H, 3.5A).

The serially sectioned TEM analysis showed that a large portion of the peripheral cytoplasm of *S. psygmophilum* cells contained chloroplast lobes connected to pyrenoid (PY) (Fig. 3.6A). A single PY located in the central part of each cell was connected by two stalks to the adjacent chloroplast and surrounded by a distinct polysaccharide cap (Fig. 3.6A, 3.6D). No chloroplast thylakoid lamellae penetrated the PY. A large number of lipid globules and starch were observed (Fig. 3.6A). Furthermore, a type E eyespot, consisting of multiple layers of rectangular electron-translucent vesicles or crystalline deposits, was observed in sectioned mastigote cells (Fig. 3.6B).
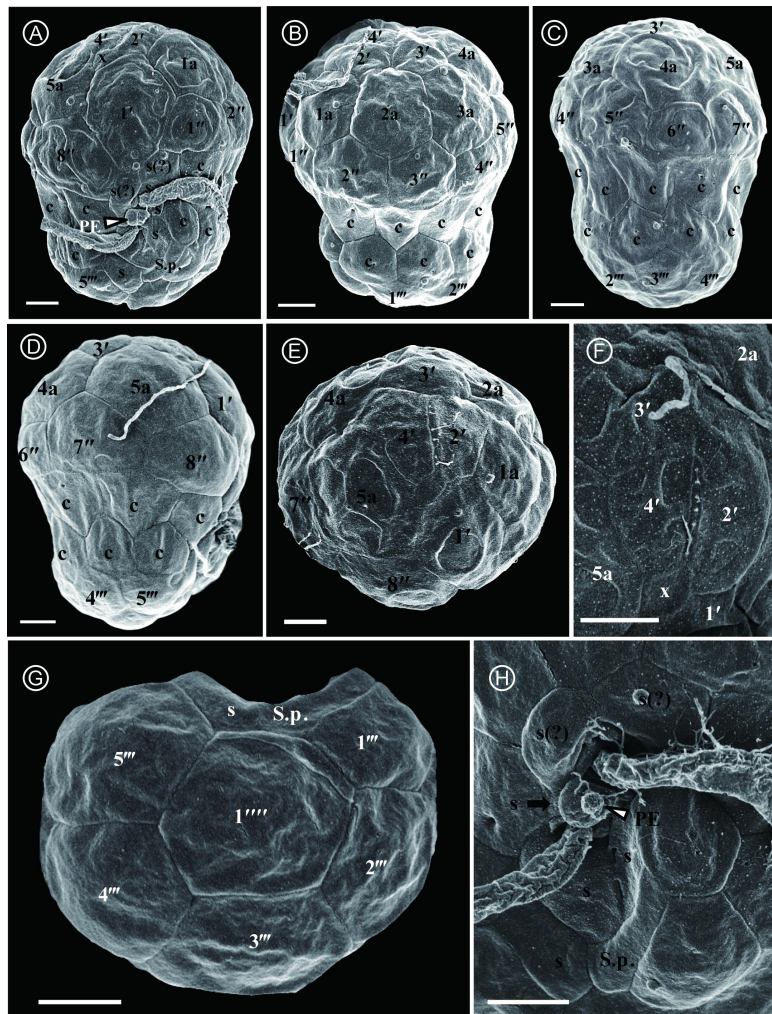
Fig. 3.4. Scanning electron micrographs of *Symbiodinium psygmophilum* motile cells. **A.** Ventral view showing the episome, cingulum (C), sulcus (s), peduncle (PE), and hyposome. **B.** Ventral-left lateral view showing the episome, cingulum (C), and hyposome. **C.** Dorsal view showing the episome, cingulum (C), and hyposome. **D.** Ventral-right lateral view showing the episome, cingulum (C), sulcus (s), and hyposome **E.** Apical view showing the episome and elongated amphiesmal vesicle (EAV) plate. **F.** Apical view showing the EAV plate with small knobs (arrowhead). **G.** Antapical view showing the hyposome. **H.** Antapical-ventral view showing the sulcus (s) and peduncle (PE). All scale bars = 1 μm.

Fig. 3.5. Drawings of *Symbiodinium psygmophilum* motile cells showing the external morphology. **A.** Ventral view. **B.** Dorsal view. **C.** Apical view. **D.** Antapical view. All scale bars = 1 μm.
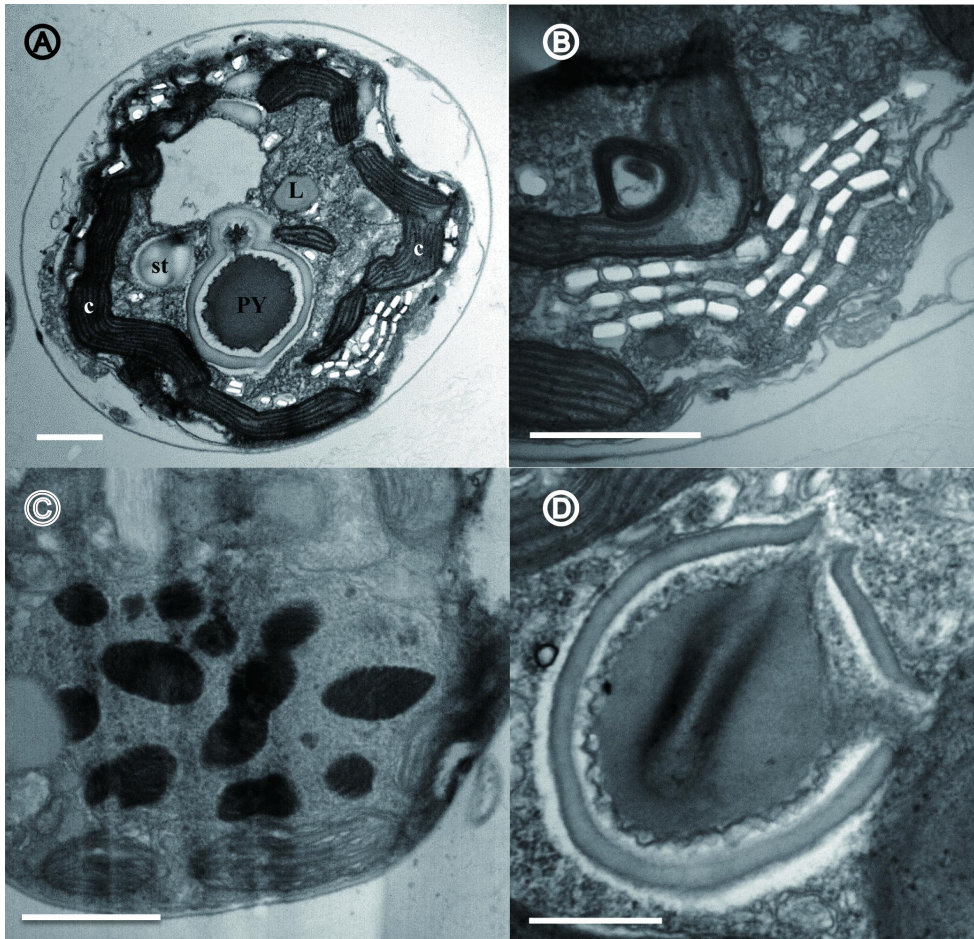
Fig. 3.6. Transmission electron micrographs of *Symbiodinium psygmophilum* cells. **A.** Transverse section of a mastigote cell showing the pyrenoid, nucleus, chloroplast, type E eyespot (stigma), lipid globules, and starch. **B.** Type E eyespot consisting of multiple layers of rectangular electron-translucent vesicles, or crystalline deposits (stigma, white arrow). **C.** Cell with many chromosomes in the nucleus. **D.** Single pyrenoid with two stalks, located in the central part of each cell and surrounded by a distinct polysaccharide cap. Scale bar = 1 μm for panels A and C and 0.5 μm for panels B and D.

3.4. Discussion

This study is the first report of the plate formulae and some other detailed morphological characters of the *Symbiodinium* species belonging to clade B, showing clear differences from species belonging to other clades and even the within-clade difference, that *S. minutum* (type B1) has a plate formula clearly different from *S. psygmophilum* (type B2) (Table 2.2).

The plate formula of *S. psygmophilum* is clearly different from *S. natans* (x, EAV, 4', 5a, 8'', 6S, two cingulum rows, 6''', 2'''') in clade A, *S. voratum* (x, EAV, 5', 5a, 8'', 9S, two cingulum rows, 6 to 7''', 2'''') in clade E, the only two *Symbiodinium* species with known complete plate formula (Hansen and Daugbjerg 2009; Jeong et al. 2014a). However, *S. minutum* has a plate formula similar to *S. natans* (Table 2.2). Thus, this study suggests that there may be similarities despite its molecular differences such as clades, or ecological differences such as hosts or locations in the species belonging to genus *Symbiodinium*. Therefore, further exploration on morphological speciation and identification may be needed in the study of genus or species in *Symbiodionium*.

Contrary to the similarity in plate formulae, *S. minutum* has plate shapes different from *S. natans*; 1a and 2a intercalary plates of *S. minutum* are pentagonal and hexagonal, respectively, whereas those of *S. natans* are hexagonal and pentagonal, respectively; the 2'''' antapical plate of *S. minutum* is pentagonal, while that of S. natans is hexagonal. Based on the plate formulae and plate shapes, this study confirms that *S. minutum* and *S. psygmophilum* are morphologically distinct from other known species.

The postcingular 3''' of *S. psygmophilum* is rectangular shape in the

antapical view, while *S. minutum* and *S. voratum* showed pentagonal. The *S. psygmophilum* had a quadrangular 4' apical plate, and hexagonal 4a and 5a intercalary plates, while *S. minutum* had a pentagonal 4' apical plate and hexa- or heptagonal 4a and pentagonal 5a intercalary plates. Thus, in addition to the differences in plate formula, *S. psygmophilum* has plates whose shapes are different from *S. minutum*. Hence, the species in the same clade may have somewhat different plate shapes. Therefore, both molecular genetic and morphological characterizations should be combined to fully describe a species in *Symbiodinium*.

In the analysis of the ultrastructures, both *S. minutum* and *S. psygmophilum* had type E eyespot and a two-stalk PY like the other *Symbiodinium* species (e.g., Jeong et al. 2014a). However, *S. minutum* had many variously sized lipid globules, unlike the other *Symbiodinium* species which have only a few lipid globules (Hansen and Daugbjerg 2009; Jeong et al. 2014a). Therefore, further studies of other strains are needed to test whether this feature can be used for differentiating *S. minutum* from other *Symbiodinium* species.

To conclude, this study suggests that not all the species in a clade may have the same plate formula. Even different types within a clade, which are categorized by genetic divergences, may differ in morphology. The clade B1 *S. minutum* was originally isolated from a sea anemone, while the clade B2 *S. psygmophilum* from a stony coral. Therefore, different hosts may be related to a different morphology and genetics of the species belonging to the same clade.

Chapter 4. Comparative *de novo* transcriptome analysis of the heterotrophic dinoflagellate *Gyrodinium shiwhaense* and the mixotrophic dinoflagellate *Paragymnodinium shiwhaense*.

4.1. Introduction

Marine dinoflagellates are ubiquitous and play diverse roles in marine food webs as prey, predators, parasites, and endosymbiotic organisms (Jeong, 1999; Jeong et al., 2010; Bayer et al., 2012; Lee et al., 2014a, 2014b, 2015a, 2015b; Murray et al. 2016). Some dinoflagellates have caused red tides or harmful algal blooms (Heisler et al., 2008; Kudela and Gobler, 2012; Jeong et al., 2015). These ubiquity, diverse roles, and predominating plankton assemblages may be related to their diverse trophic modes (Stoecker, 1999; Sherr and Sherr, 2007); they have all 3 major trophic modes, i.e., exclusive autotrophy, heterotrophy, and mixotrophy (i.e., combination of photosynthesis and heterotrophy). These diverse trophic modes may be related to evolution of dinoflagellates responding to diverse environmental changes in geological scales (Porter, 1988). Recently, many dinoflagellate species that had been thought to be exclusively autotrophic and some newly described species have been revealed to be mixotrophic (Jeong et al., 2012; Lee et al., 2014a, 2014b, 2015a, 2015b). Differences in metabolisms, enzymes, gene expression, and eventually genomes among exclusive autotrophy, heterotrophy, and mixotrophy of dinoflagellates are not well understood yet. Theoretically, mixotrophic dinoflagellates can conduct both photosysnthesis and feeding and thus they may have more genes than

exclusive autotrophic dinoflagellates or heterotrophic dinoflagellates. However, this hypothesis has not been proved yet.

The genome sizes of dinoflagellates are very large and thus it is very difficult to analyze whole genomes of a dinoflagellate at this time; there have been only two dinoflagellates whose genomes have been reported (Shoguchi et al., 2013; Lin et al., 2015). Thus, transcriptomes (i.e., gene expression) of dinoflagellates have been analyzed as proxy of their genomes (Yang, et al., 2011; Richardson et al., 2014; Ryan et al., 2014; Zhang et al., 2014; Pozdnyakov and Skarlato, 2015). So far, transcriptomes of only 50 dinoflagellates species have been reported (Erdner et al., 2006; Lowe et al., 2011; Morey et al., 2011; Salcedo et al., 2012; Kim et al., 2013a; Shoguchi et al., 2013; Barshis et al., 2014; Richardson et al., 2014; Ryan et al., 2014; Keeling et al., 2014; Wang et al., 2014; Zhang et al., 2014; Gavelis et al., 2015; Lin et al., 2015; Pozdnyakov and Skarlato, 2015; Guo et al., 2016). Thus, *de novo* assembly of transcriptomes of more dinoflagellates species and also comparing the transcriptomes among dinoflagellates are needed to find new genes and understand relationships and possible evolutions in dinoflagellates.

The mixotrophic dinoflagellate *Paragymnodinium shiwhaense* and the heterotrophic dinoflagellate *Gyrodinium shiwhaense* were isolated from Shiwha Bay, Korea and described as new species in the new genera (Kang et al., 2010, 2011; Yoo et al., 2010; Jeong et al., 2011). They have high similarity in their morphology and ribosomal DNA and edible prey species, although their trophic modes are largely different (Kang et al., 2010, 2011); they have woloszynskioid surface structures and nematocysts and also form a clade in the phylogenetic trees based on SSU and LSU ribosomal DNA. The kind of the prey species that *G. shiwhaense* is able to feed on is very similar to that of *P. shiwhaense*

(Yoo et al., 2010; Jeong et al., 2011). Interestingly, like *G. shiwhaense*, *P. shiwhaense* cannot grow without feeding on prey, whereas it can divide ca. twice a day with feeding on the optimal prey *Amphidinim carterae* (maximum mixotrophic growth rate = 1.1 d^{-1}). This rate is similar to the maximum growth rate of *G. shiwhaense* feeding on the same prey. Thus, *P. shiwhaense* has been treated as one of the mixotrophic dinoflagellates that are very close to heterotrophic dinoflagellates. Thus, several critical questions arise here; (1) Does *P. shiwhaense* have more expressed genes than *G. shiwhaense*? or vice versa. (2) Does *G. shiwhaense* have any gene related to photosynthesis? The photosynthetic carbon reduction process, known as Calvin cycle, is the primary pathway of carbon fixation and is an essence in photosynthesis (Wilson and Calvin, 1955; Raines, 2003). This cycle consists of the processes of carbon fixation, reduction reactions, and ribulose 1,5-bisphosphate (RuBP) regeneration (Salvucci et al., 1986; Streusand and Portis, 1987). There are 7 different pathways in this cycle in the RuBP regeneration process. (3) Therefore, if *G. shiwhaense* has genes related to photosynthesis, the next question is whether these genes can run any pathway in the regeneration in Calvin cycle or not. If so, acquisition of chloroplasts from ingested prey may help in conducting kleptoplastidy (Kim et al., 2013a). To answer these questions, in this study, transcriptomes of these two dinoflagellates grown the same conditions (i.e., feeding on the raphidophyte *Heterosigma akashiwo*, non-dinoflagellate prey) were de novo assembled and then compared.

The results of this study provide data on de novo assembled transcriptomes and molecular characterizations of two newly described dinoflagellates and a basis on understanding differences in gene expressions between closely related hetereotrophic and mixotrophic dinoflagellates and eventually evolution in dinoflagellates.

4.2. Materials and methods

4.2.1. Sample preparations and cell harvest

The clonal cultures of *Gyrodiniellum shiwhaense* (GSGJ1408) and *Paragymnodinium shiwhaense* (PSSH0605-1) used in this study were originally isolated from the coastal water of Shiwha Bay, Korea, in 2009 and from Shiwha bay, Korea in 2006, respectively (Table 3.1). Both cultures were maintained with providing *Heterosigma akashiwo* as prey at 20 ℃ under the illumination of 20 mE m^{-2} s^{-1} under a 14:10 h light-dark cycle. Both cultures maintained in 2-L polycarbonate (PC) bottles were transferred to new 2-L PC bottles containing freshly filtered seawater and prey cells every week. On every transfer day, the cultures were thoroughly checked under a fluorescence microscope to make sure that there was no visible bacterial contamination. Further, the possible bacterial mRNA contaminations were easily removed from EST dataset by existence of poly-A tail as Kim et al. (2013a) described. Approximately 8 L of the dense cultures with cell densities of ca. 10,000 $cell^{-1}$ mL^{-1} were used for pyrosequencing analysis. To eliminate any cell in the ambient waters or ingested cells inside the protoplasms of *G. shiwhaense* and *P. shiwhaense* cells, the cultures maintained without added prey for 6 days. To harvest cells, the cultures were centrifuged at 800 × g for 15 min. Total of 300 mg of each culture was obtained as pellet forms. The pellets were washed with PBS (Bioneer, Daejeon, Korea) several times and collected in a 1.5-ml tube, frozen immediately using liquid nitrogen, and then stored in a deep freezer maintained at −75 ℃ ca. 3 days before the RNA being extracted.

Table 3.1. Species information of *Gyrodiniellum shiwhaense* and *Paragymnodinium shiwhaense* used in this study.

Species	*Gyrodiniellum shiwhaense*	*Paragymnodinium shiwhaense*
Collection date	September, 2009	May, 2006
collection area	Shiwha Bay, Korea	Shiwha Bay, Korea
T (℃)	26.5	18.8
Salinity	33.4	30.4
Prey species		
Diatoms		
Skeletonema costatum	N	N
Prymnesiophyceae		
Isochrysis galbana	Y	Y
Cryptophytes		
Teleaulex sp.	Y	Y
Rhodomonas salina	Y	Y
Rhaphidophytes		
Heterosigma akashiwo	Y	Y
Mixotrophic dinoflagellates		
Heterocapsa rotundata	Y	Y
Amphidinium carterae	Y	Y
Prorocentrum minimum	**Y**	**N**
Heterocapsa triquetra	N	N
Scrippsiella trochoidea	N	N
Cochlodinium polykrikoides	N	N
Prorocentrum micans	N	N
Akashiwo sanguinea	N	N
Gonyaulax polygramma	N	N
Alexandrium tamarense	N	N
Lingulodinium polyedrum	N	N

4.2.2. RNA isolation and sequencing

The total RNA from *P. shiwhaense* and *G. shiwhaense* were isolated using Trizol (MRC INC.) method according to manufacturer's protocol (Rio et al., 2010). The mRNA were purified according to manufacturer's protocol using Invitrogen Dynabead mRNA Purification Kit (Invitrogen, Carslbad, CA) and 200ng of mRNA were fragmented by using magnetic particle concentrator (Dynal MPC®-50, Dynal Biotech, France). The double strand cDNA of these fragmented RNA were synthetizaed using Transcriptor First Strand cDNA Synthesis Kit (Roche Diagnostic Systems, Branchburg, NJ) according to the manufacturer's protocol. Then the pyrosequencing assembly and annotation of sequencing data were conducted using GS FLX titanium platform of 454 pyrosequencing (Rogers and Venter, 2005). To analyze the sequence data, a web-based pipeline program for EST data analysis (PESTAS) developed by Kongju University was used (http://genebank.kongju.ac.kr).

4.2.3. Identification of plastid-derived genes and bioinformatics.

The obtained unigenes were used for the homology searches against various protein database including NCBInr, InterProScan, Gene Ontology (GO), and KEGG (BLASTx, E-value < 1.00 E^{-5}) (Figs 4.2-4.5). Basically, a BLASTx homology search against the NCBI nr protein database and InterProScan was performed using the Blast2GO program (Conesa et al., 2005). The the evolutionary genealogy of genes:Non-supervised Orthologous Groups (eggNOG) database (Huerta-Cepas et al., 2015) was used to predict and classify the protein functional groups. While the nucleotide and amino acid sequence homology searches and comparison

were carried out using BLAST on the NCBI GenBank database (http://blast.ncbi.nlm.nih.gov). With obtained data, the putative plastid-derived genes were manually searched by keywords related to chloroplast, photosynthesis, chlorophyll, and light harvesting from spreadsheets. Additional homology searches were carried out by comparing our translated EST database directly with comprehensive chloroplast protein database of *Arabidopsis thaliana* (Kleffmann et al., 2004) (Plastid protein database: http://www.plprot.ethz.ch. and AT_Chloro database: http://www.grenoble.prabi.fr/at_chloro).

4.2.4. Phylogenetic analysis of photosynthesis related gene and ribosomal DNA.

The 18S ribosomal small subunit sequences were performed by using sequences of *G. shiwhaense*, *P. shiwhaense*, and diverse dinoflagellate species obtained from NCBI GenBank sequence database. A representative dataset of the SSU ribosomal DNA (rDNA) regions were aligned using MEGA v.4 (Tamura et al. 2007). The rDNA dataset of the SSU region was analyzed using the GTR+Γ model. The phylogeny of each gene was inferred by maximum-likelihood (ML) using the RAxML 7.0.3 program (Stamatakis, 2006) For ML, bootstrapping with 100 replications was conducted.

4.2.5. Gene-specific primer-probe set design, DNA extraction and RT-PCR amplification.

The presence or absence of target genes related to the Calvin cycle in the *P. shiwhaense* and *G. shiwhaense* genomes was confirmed using the SYBR Green qPCR method with gene-specific primers and qPCRBIO

SyGreen Mix Hi-ROX (PCR Biosystems Ltd., London, UK) on Rotor-Gene Q (Qiagen, Hilden, Germany) (Table 3.2). The specific primer for the Ribulose 5-phosphate isomerase (Rpi) gene were directly designed by ourselves based on the universally conserved regions of diverse dinoflagellate species obtained from NCBI, and the universally conserved regions were used for the forward and reverse primers (Table 3.2). In addition, the gene-specific primers of the Sedoheptulose bisphosphatase (SBPase) gene and the Phosphoribulokinase (PRK) gene were obtained from Teich et al. (2007) and Jiang et al. (2012), respectively (Table 3.2). For the real-time PCR (RT-PCR) amplification, DNA was extracted from dense cultures of *P. shiwhaense* and *G. shiwhaense* using the *AccuPrep*® Genomic DNA Extraction Kit (Bioneer Cooperation, Daejeon, Korea), and amplified by using Rotor-Gene Q (Qiagen, Hilden, Germany) under the following thermal cycling conditions; 2 min at 95 ℃, followed by 45 cycles of 10 s at 95 ℃, 45 s at 60 ℃, and 20 s at 72 ℃ in series.

Table 3.2. Information on the primers and probes used in this study.

Target gene	Primer Type	Name	Sequence (5'–3')	Reference
Rpi	Forward	Rpi_DinoF	ATCGATGGCGCTGACGAGGTGG	This study
Rpi	Reverse	Rpi_DinoR	CAAAAGGGCACAATCTCCAC	This study
PRK	Forward	PRK_DinoF	ACAGGTTGCTTAGATGGC	Jiang et al (2012)
PRK	Reverse	PRK_DinoR	TTGTTTGATGAAGGCTCG	Jiang et al (2012)
SBPase	Forward	SBP_DinoF	GTSGTSTTCGACCCSCTNGAYGG	Teich et al (2007)
SBPase	Reverse	SBP_DinoR	ACSGGSACCATSCCSCCSGTRTA	Teich et al (2007)

Rpi : Ribulose 5–phosphate isomerase; **PRK** : Phosphoribulokinase; **SBPase** : Sedoheptulose bisphosphatas

4.3. Results

4.3.1. Sequence analysis and assembly

In the phylogenetic tree based on small subunit (SSU) rDNA sequences sequences of dinoflagellates, *P. shiwheaense* and *G. shiwhaense* were confirmed to form a clade, which showed that these two species had a genetically close relationship (Fig. 1).

A total of 216 Mbp of ESTs were sequenced from *P. shiwheaense* and assembled to total 21,932 contigs with an average length of 878 bp (Table 3). In addition, a total of 192 Mbp of ESTs were sequenced from *G. shiwhaense* and assembled to 10,805 contigs with an average length of 780 bp (Table 3.3).

Among the 21,932 unigenes expressed in *P. shiwheaense*, 3615 unigenes (16.5%) were expressed in *G. shiwhaense* as well (Fig. 4.7). Furthermore, Among the 10,805 unigenes expressed in *G. shiwhaense*, 3449 unigenes (31.9%) were expressed in *P. shiwheaense* as well (Fig. 4.7).
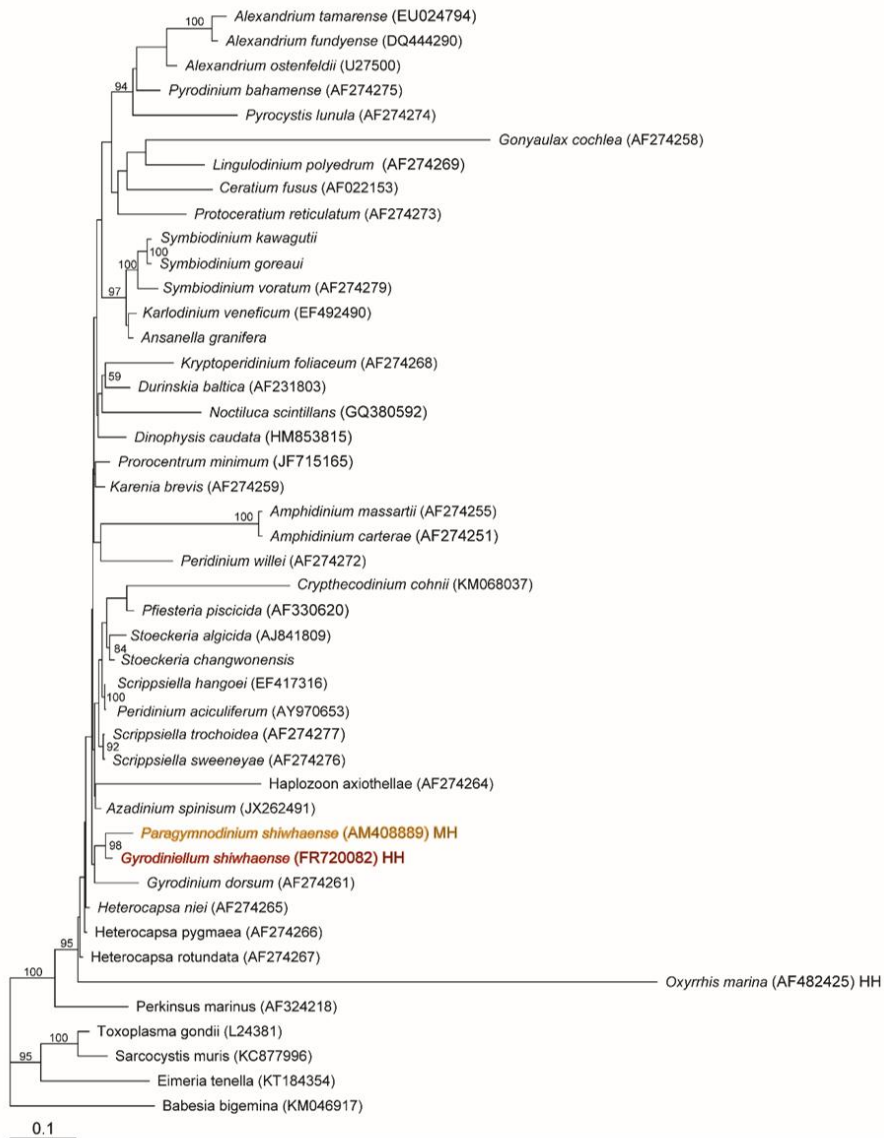
Fig. 4.1. The SSU rDNA phylogenetic tree of dinoflagellate species. The trophic type of each species are marked after the accession number. **HH**: Exclusively heterotrophic (dark red), **MH**: mixo-heterotrophic (Orange),

Table 3.3. Summary of *Paragymnodinium shiwhaense* and *Gyrodiniellum shiwhaense* transcriptome.

	P. shiwhaense	*G. shiwhaense*
RNA sequencing		
number of reads	488,523	469,923
Total length	216,376,233	192,291,907
Assembly		
Length of assembled sequence (bp)	19,257,096	8,431,599
Total number of contig	21,932	10,805
N50 (bp) contig size	1053	992
Q39 minus bases (%)	984,778 (5.1%)	408,490 (4.8%)
Q40 plus bases (%)	18,572,318 (96.4%)	8,023,109 (95.2%)
Average contig size	878	780
Largest contig size	8506	8913

4.3.2. Functional classification by "eggNOG" and "Gene Ontology"

For annotation of the assembled transcripts, BLAST sequence similarity searches were performed using various gene function databases such as GO, KEGG, InterProScan, and NCBI nr. When protein functional groups of *P. shiwheaense* and *G. shiwhaense* were predicted and classified using eggNOG database, total 10,581 unigenes of *P. shiwhaense* were functionally clustered into 25 categories (Fig. 4.2, Table 3.4). However, total of 5,377 unigenes were clustered into 25 categories of the eggNOG category from *G. shiwhaense* (Fig. 4.2, Table 3.4). Among the eggNOG categories analysed, 1,756 unigenes (32.7%) were function unknown genes. In addition, the sequence of the number of the clustered unigenes of *P. shiwhaense* was "Posttranslational modification, protein turnover, chaperones" category (1,002 unigenes, 9.5%) > "Translation, ribosomal structure and biogenesis" category (999 unigenes, 9.4%) > "energy production and conversion" (830 unigenes, 7.8%) (Figs 4.2, Table 3.4). However, 3,467 unigenes (32.8%) were function unknown genes. Furthermore, the sequence of the number of the clustered unigenes of *G. shiwhaense* was "Translation, ribosomal structure and biogenesis" category (641 unigenes, 11.9%) > "Posttranslational modification, protein turnover, chaperones" category (594 unigenes, 11.0%) > "energy production and conversion" (415 unigenes, 7.7%) (Figs 4.2, Table 3.4).

In the gene ontology (GO) analysis, 29 known functional terms of unigenes for both *P. shiwheaense* and *G. shiwhaense* were matched (Fig. 3, Table 5). The sequence of the number of the clustered unigenes of *P. shiwhaense* (total of 18,785 unigenes) was genes related to metabolic process (2,897, 15.4%) > catalytic activity (2,889, 15.4%) > cell (2,486, 13.2%) > binding (2,361, 12.6%) > cellular process (1,978, 10.5%)

(Fig. 4.3, Table 3.5). In addition, the sequence of the number of the clustered unigenes of *G. shiwhaense* (total of 11,780 unigenes) was genes related to metabolic process (1,638, 13.9%) > binding (1,525, 12.9%)> catalytic activity (1,508, 12.8%) > cell (1,461, 12.4%) > cellular process (1,244, 10.6%) (Fig. 4.3, Table 3.5).

4.3.3. Photosynthesis and carbon fixation related genes classified by KEGG in *G. shiwhaense* and *P. shiwhaense*.

Based on the KEGG pathway assignments, numerous genes coding for proteins involved in the photosynthesis pathway were identified. The pathway was sub-classified by the categories of Photosystem 1, Photosystem 2, Cytochrome b6/f complex, Photosynthetic electron transport, and F-type ATPase (Fig. 4.4). More than 3 genes were identified from all above 6 sub-categories. When genes related to photosynthesis were analyzed based on KEGG pathway analysis, *P. shiwhaense* had 9 unigenes (i.e., *psbL*, *psbP*, *psbQ*, *psbT*, *psb27*, *psaC*, *psaE*, *petG*, and *b* in F-type ATPase) which *G. shiwhaense* did not have (Fig. 4.4). However, in this analysis, there was no unigene which *G. shiwhaense* had, but *P. shiwhaense* did not have.

Table 3.4. The eggNOG comparison data of *Gyrodiniellum shiwhaense* and *Paragymnodinium shiwhaense*.

Name of gene	G. shiwhaense		P. shiwhaense	
	No. of unigenes	%	No. of unigenes	%
RNA processing and modification	22	0.4	65	0.6
Chromatin structure and conversion	14	0.3	23	0.2
Energy production and conversion	415	7.7	830	7.8
Cell cycle control, cell division, chromosome partitioning	85	1.6	136	1.3
Amino acid transport and metabolism	203	3.8	479	4.5
Nucleotide transport and metabolism	101	1.9	165	1.6
Carbogydrate transport and metabolism	240	4.5	672	6.4
Coenzyme transport and metabolism	83	1.5	201	1.9
Lipid transport and metabolism	107	2.0	269	2.5
Translation, ribosomal structure and biogenesis	641	11.9	999	9.4
Transcription	58	1.1	122	1.2
Replication, recombination and repair	115	2.1	233	2.2
Cell wall/membrane/envelop biogenesis	52	1.0	94	0.9
Cell motility	4	0.1	0	0.0
Posttranslational modification, protein turnover, chaperones	594	11.0	1002	9.5
Inorganic ion transport and metabolism	132	2.5	403	3.8
Secondary metabilites biosynthesis, transport and catabolism	22	0.4	81	0.8
General functional prediction only	0	0.0	0	0.0
Function unknown	1756	32.7	3467	32.8
Signal transduction mechanisms	246	4.6	577	5.5
Intracellular trafficking, secretion, and vesicular transport	172	3.2	321	3.0
Defense mechanisms	20	0.4	62	0.6
Extracellular structures	0	0.0	1	0.0
Nuclear structures	0	0.0	2	0.0
Cytoskelecton	295	5.5	377	3.6
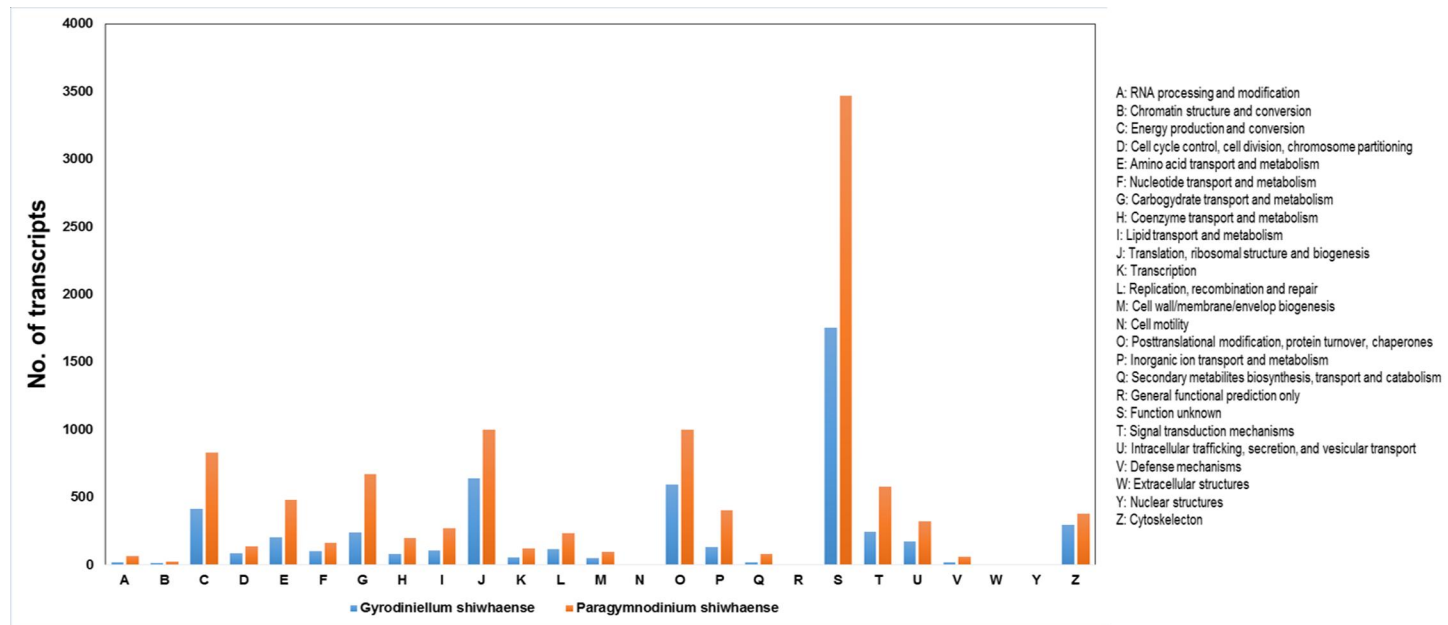
Fig. 4.2. The eggNOG classification of the *Paragymnodinium shiwhaense* and *Gyrodiniellum shiwhaense*. **A.** *Paragymnodinium shiwhaense* **B.** *Gyrodiniellum shiwhaense*.

Table 3.5. Gene ontology data analysis and comparison of *Gyrodiniellum shiwhaense* and *Paragymnodinium shiwhaense*.

Name of gene	G. shiwhaense		P. shiwhaense	
	No. of unigenes	%	No. of unigenes	%
metabolic process	1638	13.9	2897	15.4
cellular process	1244	10.6	1978	10.5
single-organism process	391	3.3	554	2.9
biological regulation	267	2.3	416	2.2
localization	316	2.7	404	2.2
response to stimulus	250	2.1	310	1.7
cellular component organization or biogenesis	184	1.6	233	1.2
developmental process	81	0.7	126	0.7
multicellular organismal process	76	0.6	119	0.6
signaling	65	0.6	108	0.6
reproduction	27	0.2	43	0.2
growth	13	0.1	21	0.1
multi-organism process	6	0.1	8	0.0
cell	1461	12.4	2486	13.2
organelle	992	8.4	1698	9.0
macromolecular complex	891	7.6	1169	6.2
membrane	109	0.9	144	0.8
membrane-enclosed lumen	54	0.5	60	0.3
extracellular region	19	0.2	30	0.2
extracellular matrix	1	0.0	0	0
catalytic activity	1508	12.8	2889	15.4
binding	1525	12.9	2361	12.6
structural molecule activity	378	3.2	438	2.3
transporter activity	217	1.8	193	1.0
electron carrier activity	36	0.3	75	0.4
enzyme regulator activity	13	0.1	11	0.1
antioxidant activity	7	0.1	7	0.0
molecular transducer activity	5	0.0	5	0.0
nucleic acid binding transcription factor activity	6	0.1	2	0.0
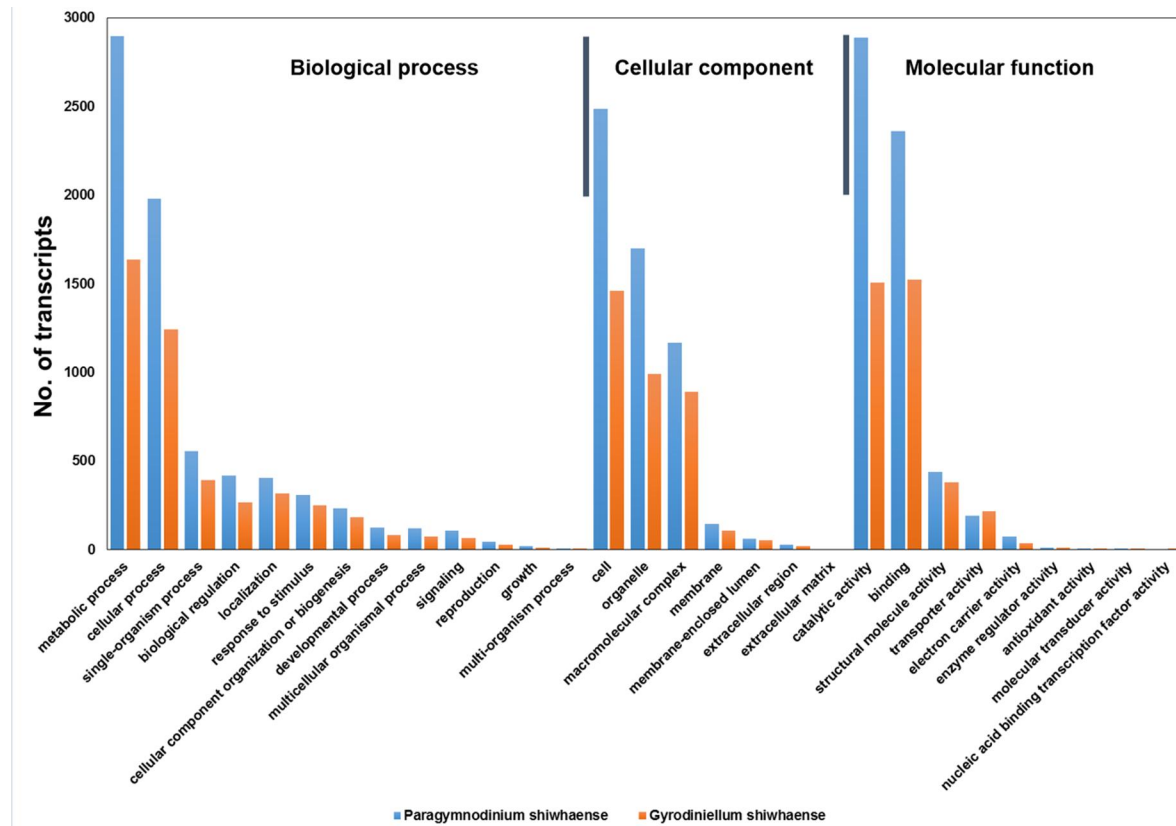
Fig. 4.3. Comparison of gene ontology (GO) terms between the *Gyrodiniellum shiwhaense* and *Paragymnodinm shiwhaense.*
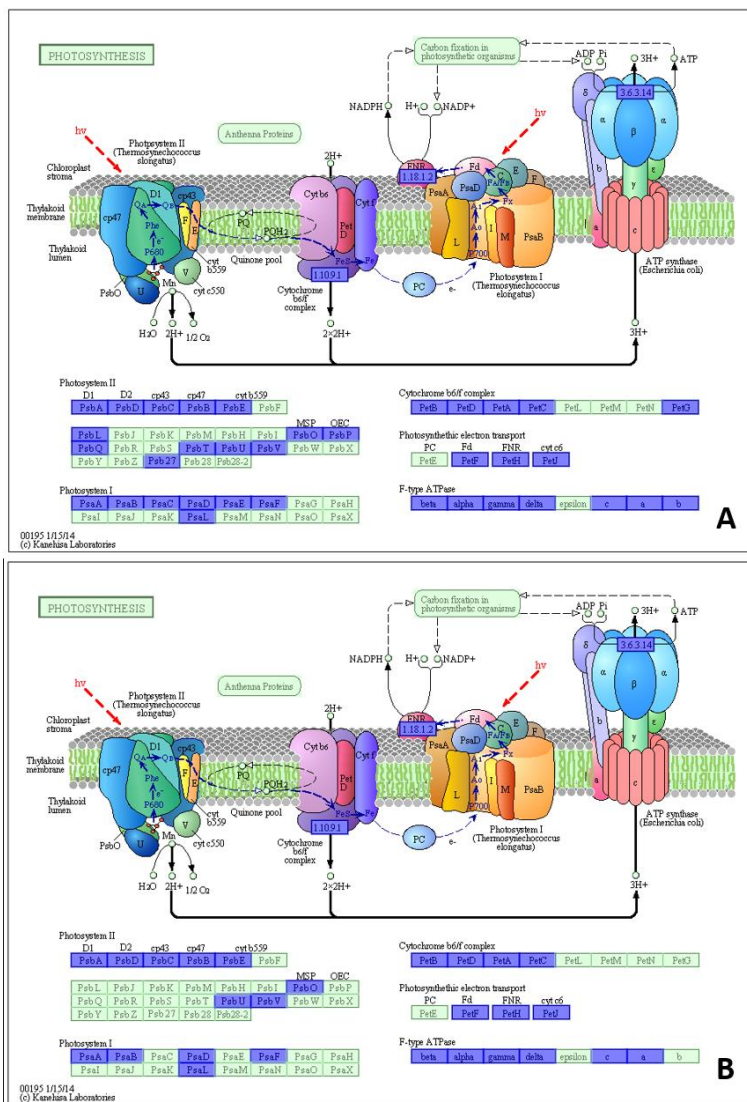
Fig. 4.4. The photosynthesis related analysis of KEGG pathway. **A.** KEGG pathway analysis of *P. shiwhaense*. Genes appearing in *P. shiwhaense* transcriptome database are represented in purple color and absent genes in green color. **B.** KEGG pathway analysis of *G. shiwhaense*. Genes appearing in *G. shiwhaense* transcriptome database are represented in purple color and absent genes in green color.

4.3.4. Calvin cycle related gene expression in *G. shiwhaense* and *P. shiwhaense*

Based on the transcriptome data of *P. shiwhaense* and *G. shiwhaense*, the expression of genes related to Calvin cycle were explored. *P. shiwhaense* had all 12 expressed genes [1165 contigs; Glyceraldehyde 3-phosphate dehydrogenase (GAPDH), Phosphoglycerate kinase (PGK), Fructose-bisphosphate aldolase, Fructose 1,6 bisphosphatase (FBPase), Transketolase, Triosephosphate isomerase (TPI), Ribulose-1,5-bisphosphate carboxylase/ oxygenase (RuBisCO), Phosphoribulokinase (PRK), Ribose 5-phosphate isomerase (Rpi), Ribulose 5-phosphate epimerase (PPE), Sedoheptulose bisphosphatase (SBPase), Aldolase, and Phosphoketolase] which can be found in the Calvin cycle (Fig. 4.5B; Table 4.6, Table 3.8). These genes can run all 7 complete pathways which can be run in the cycle (Fig. 4.5; Table 3.6). However, *G. shiwhaense* had 10 express genes (377 contigs; none of Rpi and PRK genes) (Fig. 4.5C; Table 3.7). These genes cannot run any complete pathways in the Calvin cycle.

Based on the BlastX hits, the Calvin cycle genes discovered in *P. shiwhaense* had several isoforms with diverse dinoflagellate species (Table 3.8). For example, the RuBisCO gene of *P. shiwhaense* had highest similarity hits to the mixotrophic dinoflagellates *Prorocentrum donghaiense, P. minimum*, and symbiotic dinoflagellate *Symbiodinium* sp. Furthermore, *P. shiwhaense* had highest similarity hit to the dinoflagellates *Karenia brevis* and *Lingulodinium polyedrum* in FBPase gene, *Alexandrium fundyense, Amphidinium carterae, Karenia mikimotoi, Lepidodinium chlorophorum, Pyrocystis lunula*, and *Pyrocystis noctiluca* in GAPDH gene, *Heterocapsa triquetra* and *Pfiesteria piscicda* in FBA gene, *Pyrocystis lunula* in PRK gene, *H. triquetra* in Rpi gene, and *L. polyedrum* in SBPase gene. However, *P. shiwhaense* had highest sim-

ilarity hit to the cyanobacterium *Synechococcus* sp. in Transketolase gene, the haptophyte *Emiliania huxleyi* in TPI, the chlorophyte *Dunaliella salina* in PPE, the cyrptophyte *Guillardia theta* and the haptophyte *Pavlova lutheri* in PGK, and the proteobacterium *Roseomonas* sp. in Aldolase gene.

Based on the BlastX hits, the Calvin cycle genes discovered in *G. shiwhaense* had several isoforms with diverse dinoflagellate species (Table 3.9). For example, the GAPDH gene of *G. shiwhaense* had highest similarity hit to the mixotrophic dinoflagellate *Amphidinium operculatum, L. chlorophorum* or *Karlodinium veneficum* and heterotrophic dinoflagellate *P. piscicida*. Furthermore, *G. shiwhaense* had highest similarity hit to dinoflagellates *P. piscicida, H. triquetra* and *A. carterae* in FBA gene, *H. triquetra* in PGK gene, *P. donghaiense, P. minimum*, and *L. polyedrum* in RuBisCO gene, *L. polyedrum* in SBPase gene, *Karlodinium veneficum* in Transketolase gene. However, *G. shiwhaense* had highest similarity hit to the euglenozoan *Euglena gracilis* in FBPase gene, the land plant *Arabidopsis thaliana* in PPE gene, and the apicomplexan *Eimeria maxima* in TPI gene.

The presence or absence of the genes which were expressed or not expressed in this transcriptome analyses was confirmed by the SYBR green method using gene-specific primer sets (Fig. 4.6); the RPI gene was not expressed in *G. shiwhaense* and the absence of this gene in this dinoflagellate was confirmed (Fig. 4.6A). To the contrary, the SBPase gene was expressed in *G. shiwhaense* and the presence of this gene was confirmed (Fig. 4.6B). However, the PRK gene of *G. shiwhaense* was not expressed, but this gene was found in the SYBR green method (Fig. 4.6C). Four pathways in the Calvin cycle could be compeleted because the PRK gene was found. However, if the PRK gene was absent, there might be no complete pathway in Calvin cycle. In addition, the RPI, SBPase, and PRK genes of *P. shiwhaense* were ex-

pressed and the presence of these genes were confirmed by the SYBR green method (Fig. 4.6)
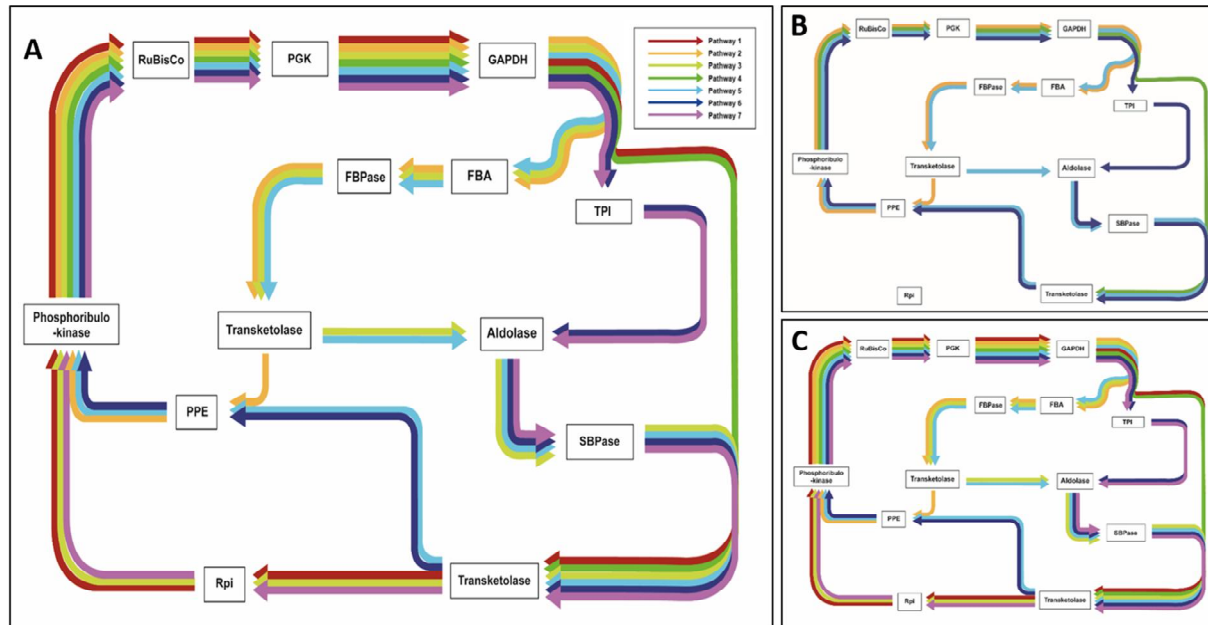
Fig. 4.5. The 7 pathway with combinations of 12 genes that are considered to run Calvin cycle. **A.** The 7 pathways of Calvin-Benson cycle. **B.** Pathways that were complemented in the mixotrophic dinoflagellate *Paragymnodinium shiwhaense*. **C.** Pathways that were complemented in the heterotrophic dinoflagellate *Gyrodiniellum shiwhaense*. **RuBisCO**: Ribulose-1,5-bisphosphate carboxylase/oxygenase, **PGK**: Phosphoglycerate kinase, **GAPDH**: Glyceraldehyde 3-phosphate dehydrogenase, **Rpi**: Ribose 5-phosphate isomerase, **FBPase**: Fructose 1,6 bisphosphatase, **TPI**: Triosephosphate isomerase, **PPE**: Ribulose 5-phosphate epimerase, **SBPase**: Sedoheptulose bisphosphatase,
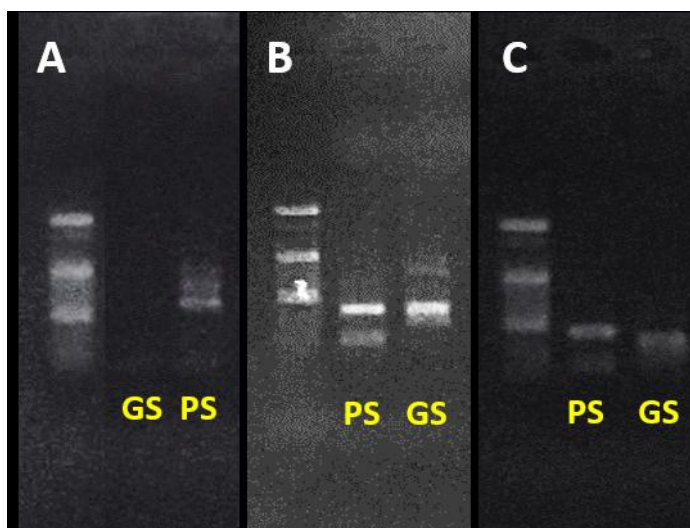
Fig. 4.6. The gel elusion figures of presence and absence of genes obtained using SYBR green RT-PCR with gene-specific primer set of *Paragymnodinium shiwhaense* and *Gyrodiniellum shiwhaense*. **A.** Ribose 5-phosphate isomerase (Rpi) gene, **B.** Sedoheptulose bisphosphatase (SBPase) gene, **C.** Phosphoribulokinase (PRK) gene. **GS:** *Gyrodiniellum shiwhaense*, **PS:** *Paragymnodinium shiwhaense*

Table 3.6. The 7 pathways of Calvin cycle and related genes.

Order of direction	Pathway 1	Pathway 2	Pathway 3	Pathway 4	Pathway 5	Pathway 6	Pathway 7
	RuBisCO	RuBisCO	RuBisCO	RuBisCO	RuBisCO	RuBisCO	RuBisCO
	PGK	PGK	PGK	PGK	PGK	PGK	PGK
	GAPDH	GAPDH	GAPDH	GAPDH	GAPDH	GAPDH	GAPDH
						TPI	TPI
		FBA	FBA		FBA		
		FBPase	FBPase		FBPase		
		Transketolase	Transketolase		Transketolase		
			Aldolase		Aldolase	Aldolase	Aldolase
			SBPase		SBPase	SBPase	SBPase
	Transketolase		Transketolase	Transketolase	Transketolase	Transketolase	Transketolase
		PPE		PPE	PPE	PPE	
	Rpi		Rpi				Rpi
	PRK	PRK	PRK	PRK	PRK	PRK	PRK

Species	Total No. of Pathways	Availability	Availability	Availability	Availability	Availability	Availability	Availability
PS	7	Y	Y	Y	Y	Y	Y	Y
GS	4	N	Y	N	Y	Y	Y	N

PGK: Phosphoglycerate kinase, **GAPDH**: Glyceraldehyde 3-phosphate dehydrogenase, **FBA**: Fructose-bisphosphate aldolase, **FBPase**: Fructose 1,6 bisphosphatase, **TKT**: Transketolase, **RuBisCO**: Ribulose-1,5-bisphosphate carboxylase/oxygenase, **TPI**: Triosephosphate isomerase, **PRK**: Phosphoribulokinase, **Rpi**: Ribose 5-phosphate isomerase, **PPE**: Ribulose 5-phosphate epimerase, **SBPase**: Sedoheptulose bisphosphatase, **PKT**: Phosphoketolase, **PS**: *Paragymnodinium shiwhaense*, **GS**: *Gyrodiniellum shiwhaense*.

4.4. Discussion

The results of this study show that mixotrophic *P. shiwhaense* and heterotrophic dinoflagellate *G. shiwhaense* have similarity and dissimilarity in their transcriptomes (Table 4.7); in the cases of similarity, in the the eggNOG analysis, the functional groups containing the 3 largest numbers of the clustered unigenes in *P. shiwhaense* and *G. shiwhaense* are identical; "Translation, ribosomal structure and biogenesis", "Posttranslational modification, protein turnover, chaperones", and "energy production and conversion" (Table 4.7). In addition, in the GO analysis, the functional groups containing the 5 largest numbers of the clustered unigenes in both species are also identical; "metabolic process", "binding", "catalytic activity", "cell", and "cellular process" (Table 4.7). Based on these results, it is suggested that *P. shiwhaense* and *G. shiwhaense* may allocate similar functional unigenes.

In the cases of dissimilarity, in the the eggNOG analysis, total unigenes expressed in *P. shiwhaense* was 49 % (1,711 unigenes) greater than that in *G. shiwhaense* (Table 4.7). Furthermore, in the GO analysis, total unigenes expressed in *P. shiwhaense* were relatively 37 % (7,005 unigenes) greater than in *G. shiwhaense* (Table 4.7). Thus, these results show that this mixotrophic dinoflagellate has more functional unigenes than the heterotropic dinoflagellate. Theoretically, mixotrophic dinoflagellates are likely to have more diverse functional charcteristics in genetic level than heterotropic dinoflagellates because the former must conduct both photosynthesis and phagotrophy, while the latter only phagotrophy. However, this hypothesis had not been proved yet, but the results of the present study support it. In the KEGG analysis, the number of the photosynthesis related genes expressed in *P. shiwhaense* is 53% greater than that in *G. shiwhaense*. In particular, the number of the expressed genes in photosystem II of *P. shiwhaense* is 63% greater

than that in *G. shiwhaense*. As expected, the mixotrophic dinoflagellate has more photosynthesis related genes than the heterotrophic dinoflagellate. Many photosynthesis related genes, in particular 10 of 12 genes in the Calvin cycle, were expressed in *G. shiwhaense*. The RPI and PRK genes in the Calvin cycle were not expressed in *G. shiwhaense*, while *P. shiwhaense* has all 12 genes. Due to deficit of RPI and PRK genes, *G. shiwhaense* cannot run any complete pathway in the regeneration process in the Calvin cyle, while *P. shiwhaense* can run all 7 complete pathways. However, *G. shiwhaense* has the PRK gene even though it was not expressed, whereas it does not have the RPI gene. Thus, if the PRK gene is expressed, *G. shiwhaense* may run 4 complete pathways in the Calvin cycle. *G. shiwhaense* dose not have some essential genes realted to photosystem I and II. In addition to the absence of chloroplasts, lacking these photosynthetic genes may make *G. shiwhaense* to survive only when it feeds on prey. Based on this results, it is suggested that *G. shiwhaense* may be evolved from *P. shiwhaense* or sister species with losing many functional genes including photosynthesis. However, in the KEGG analysis, the photosynthetic electron transport system related genes expressed by both species are identical. Thus, *G. shiwhaense* may not lose the photosynthetic electron transport system related genes in this evolution. The presence of photosynthesis related genes of some heterotrophic dinoflagellate such as *Oxyrrhis marina*, *Crypthecodinium cohnii*, and *Pfiesteria piscicida* has been reported (Sanchez-Puerta et al., 2007; Slamovits and Keeling, 2008, 2010; Hartz et al., 2011; Kim et al., 2013a, Keeling et al., 2014; Lee et al., 2014c). However, thes studies did not explore any complete pathway in Calvin cycle using discovered genes. When the Calvin cycle related genes of these species were reanalyzed using the transcriptome data obtained from MMETSP and from Kim et al. (2013a) in this study, all 12 genes were expressed in *O. marina* and *C. cohnii*, but 10 genes

in *P. piscicda*. *P. piscicda* does not have PRK and SBPase. Thus, theoretically, *O. marina* and *C. cohnii* have all genes which can run all 7 complete pathways in the Calvin cylcle, but *P. piscicda* has genes which can run only 3 complete pathways. Many genes related to the Calvin cycle were expressed in *G. shiwhaense*, *O. marina*, *C. cohnii*, and *P. piscicida* without photosynthesis because they do not have chloroplasts. This may cause energy loss without gaining glucose.

The sequence of rDNA of *P. shiwhaense* is known to be ca. 4% different from that of *G. shiwhaense* and these two species have nematocysts (Kang et al., 2010, 2011). In addition to these two species, only a few genera such as *Polykrikos*, *Pheopolykrikos*, and *Nematodinium* are known to have nematocysts (Jeong et al., 2011). Thus, the present of the nematocysts is a distinct feature in dinoflagellates. However, they have considerably different transcriptomes even though they were cultivated under the same conditions (i.e., same prey item, light, temperature etc.); approximately 17% of the unigenes expressed in *P. shiwheaense* were expressed in *G. shiwhaense* and 32% of the unigenes expressed in *G. shiwhaense* were expressed in *P. shiwheaense*. Therefore, different trophic modes may cause large difference in their transcriptomes. It is worthwile to analyze transcriptomes, in particular expression of genes related to photosysnthesis, of more dinoflagellates to explore evolution among exlusively autotrophic, mixotrophic and heterotrophic dinoflagellates.

Table 3.7. Similarities and dissimilarities of *Paragymnodinium shiwhaense* and *Gyrodiniellum shiwhaense* compared from transcriptome data. Difference were marked with bold. **PGK**: Phosphoglycerate kinase, **GAPDH**: Glyceraldehyde 3-phosphate dehydrogenase, **FBA**: Fructose-bisphosphate aldolase, **FBPase**: Fructose 1,6 bisphosphatase, **TKT**: Transketolase, **RuBisCO**: Ribulose-1,5-bisphosphate carboxylase/oxygenase, **TPI**: Triosephosphate isomerase, **PRK**: Phosphoribulokinase, **Rpi**: Ribose 5-phosphate isomerase, **PPE**: Ribulose 5-phosphate epimerase, **SBPase**: Sedoheptulose bisphosphatase, **PKT**: Phosphoketolase.

A. Similarities

Terms	*P. shiwhaense*	*G. shiwhaense*
Top 3 unigenes matched in eggNOG database	1. Post-translational modification, protein turnover, chaperones 2. Translation, ribosomal structure & biogenesis 3. Energy production & conversion	1. Translation, ribosomal structure & biogenesis 2. Post-translational modification, protein turn over, chaperones 3. Energy production & conversion
Top 5 unigenes matched in GO database	1. Metabolic process 2. Catalytic activity 3. Cell 4. Binding 5. Cellular process	1. Metabolic process 2. Binding 3. Catalytic activity 4. Cell 5. Cellular process
Photosynthethic electron transport related genes in KEGG analysis	petF, petH, petJ	petF, petH, petJ

B. Dissimilarities

Terms	*P. shiwhaense*	*G. shiwhaense*
Photosystem II related genes in KEGG analysis	psbA, psbD, psbC, psbB, psbE, **psbL**, psbO, **psbP, psbQ, psbT**, psbU, psbV, psb27	psbA, psbD, psbC, psbB, psbE, psbO, psbU, psbV
Photosystem I related genes in KEGG analysis	psaA, psaB, **psaC**, psaD, **psaE**, psaF, psaL	psaA, psaB, psaD, psaF, psaL
Cytochrome b6/f complex related genes in KEGG analysis	petB, petD, petA, petC, **petG**	petB, petD, petA, petC
F-type ATPase related genes in KEGG analysis	beta, alpha, gamma, delta, c, a, **b**	beta, alpha, gamma, delta, c, a
Presence number of main 12 genes related to Calvin cycle	All present	Rpi gene absent
No. of Calvin cycle related main genes confirmed in transcriptome	12	10
No. of Calvin cycle related main genes confirmed with gene specific primers	All present	Presence of PRK gene was additionally confirmed
Number of avilable Calvin cycle pathway	7	4
Dinophyte originated genes in Calvin cycle	GAPDH, FBA, RuBisCO, SBPase, **FBPase**, PRK, Rpi	GAPDH, FBA, RuBisCO, SBPase, PGK, Transketolase
Origin diversities of Calvin cycle related genes	20 phylum	8 phylum

Table 3.8. List of photosynthesis genes involved in Calvin cycle in *Gyrodiniellum shiwhaense*.

Gene Name	Contig No.	No. Of Reads	Length (bp)	Genbank Accession No.	E-Value (Blastx)	Origin	Phylum
phosphoglycerate kinase	EPT001TT0700C000146	4	1284	AAW79323	5.81E-170	Heterocapsa triquetra	Dinophyta
	EPT001TT0700C000422	3	1827	AAU11483	1.63E-65	Euglena gracilis	Euglenozoa
	EPT001TT0700C000504	4	1745	AAU11483	8.24E-160	Euglena gracilis	Euglenozoa
	EPT001TT0700C001499	4	1284	AAW79323	9.54E-173	Heterocapsa triquetra	Dinophyta
	EPT001TT0700C002783	3	1018	AAU11483	4.44E-76	Euglena gracilis	Euglenozoa
	EPT001TT0700C007232	4	553	AAW79324	3.42E-65	Heterocapsa triquetra	Dinophyta
	EPT001TT0700C009806	4	150	AAW79327	1.45E-08	Pavlova lutheri	Haptophyta
	EPT001TT0700C009811	4	151	AAW79327	9.14E-14	Pavlova lutheri	Haptophyta
GAPDH	EPT001TT0700C001185	5	1385	BAC87932	7.14E-161	Amphidinium operculatum	Dinophyta
	EPT001TT0700C001831	5	1198	ACF28670	2.51E-156	Amphidinium carterae	Dinophyta
	EPT001TT0700C002446	5	1078	ABI14256	1.87E-168	Pfiesteria piscicida	Dinophyta
	EPT001TT0700C003261	5	947	ABI14256	2.77E-138	Pfiesteria piscicida	Dinophyta
	EPT001TT0700C004682	5	791	CDJ57266	3.22E-96	Eimeria maxima	Apicomplexa
	EPT001TT0700C004798	5	779	BAC87932	7.86E-131	Amphidinium operculatum	Dinophyta
	EPT001TT0700C005817	5	689	ABI14256	3.56E-108	Pfiesteria piscicida	Dinophyta
	EPT001TT0700C005826	5	685	BAC87933	4.31E-94	Amphidinium operculatum	Dinophyta
	EPT001TT0700C005920	4	678	AAF44719	7.19E-58	Achlya bisexualis	Heterokontophyta
	EPT001TT0700C005933	5	677	BAC87933	7.34E-103	Amphidinium operculatum	Dinophyta
	EPT001TT0700C006359	5	641	BAG11483	1.39E-89	Lepidodinium chlorophorum	Dinophyta
	EPT001TT0700C006558	5	624	ABI14256	2.01E-66	Pfiesteria piscicida	Dinophyta
	EPT001TT0700C006734	5	607	ABI14256	2.97E-88	Pfiesteria piscicida	Dinophyta
	EPT001TT0700C006755	4	605	BAC87937	1.27E-91	Scrippsiella trochoidea	Dinophyta
	EPT001TT0700C006868	5	594	ABI14256	6.10E-88	Pfiesteria piscicida	Dinophyta
	EPT001TT0700C007049	5	573	BAG11483	3.69E-92	Lepidodinium chlorophorum	Dinophyta
	EPT001TT0700C007618	5	498	BAD72939	5.22E-78	Karlodinium veneficum	Dinophyta
	EPT001TT0700C007759	5	476	ADV03068	7.56E-69	Amphidinium carterae	Dinophyta
	EPT001TT0700C008005	5	434	ABI14392	5.42E-51	Karlodinium veneficum	Dinophyta

<Continued>

Gene Name	Contig No.	No. Of Reads	Length (bp)	Genbank Accession No.	E-Value (Blastx)	Origin	Phylum
GAPDH	EPT001TT0700C008117	5	415	BAD72933	3.19E-46	Karenia mikimotoi	Dinophyta
	EPT001TT0700C008255	5	386	ABO47862	2.13E-47	Alexandrium fundyense	Dinophyta
	EPT001TT0700C008313	5	373	ABI14256	1.51E-29	Pfiesteria piscicida	Dinophyta
	EPT001TT0700C008441	5	349	ABI14392	1.15E-40	Karlodinium veneficum	Dinophyta
	EPT001TT0700C008534	5	330	BAD72933	6.96E-43	Karenia mikimotoi	Dinophyta
	EPT001TT0700C008546	5	328	ABI14256	1.54E-29	Pfiesteria piscicida	Dinophyta
	EPT001TT0700C009446	5	195	BAG11483	1.55E-29	Lepidodinium chlorophorum	Dinophyta
	EPT001TT0700C010194	5	109	BAC87933	3.26E-11	Amphidinium operculatum	Dinophyta
	EPT001TT0700C010227	5	108	ABO47862	4.71E-10	Alexandrium fundyense	Dinophyta
Fructose-bisphosphate aldolase	EPT001TT0700C000067	2	2729	ACU44982	2.24E-72	Pfiesteria piscicida	Dinophyta
	EPT001TT0700C000805	4	1540	AAV71135	1.66E-169	Heterocapsa triquetra	Dinophyta
	EPT001TT0700C001308	4	1340	XP_004497605	7.60E-120	Cicer arietinum	Tracheophyta
	EPT001TT0700C001933	3	1177	WP_005510124	7.53E-97	Corynebacterium amycolatum	Actinobacteria
	EPT001TT0700C002260	4	1111	ACF28635	1.60E-162	Amphidinium carterae	Dinophyta
	EPT001TT0700C003703	5	893	ACU44982	1.57E-124	Pfiesteria piscicida	Dinophyta
	EPT001TT0700C004037	5	858	ACU44982	1.67E-120	Pfiesteria piscicida	Dinophyta
	EPT001TT0700C005496	4	710	XP_005769338	3.92E-97	Emiliania huxleyi	Haptophyta
	EPT001TT0700C006138	4	659	ACF28635	1.87E-84	Amphidinium carterae	Dinophyta
	EPT001TT0700C006201	5	651	AAV71134	2.46E-87	Heterocapsa triquetra	Dinophyta
	EPT001TT0700C007289	4	543	XP_005769338	1.69E-74	Emiliania huxleyi	Haptophyta

<Continued>

Gene Name	Contig No.	No. Of Reads	Length (bp)	Genbank Accession No.	E-Value (Blastx)	Origin	Phylum
Fructose-bisphosphate aldolase	EPT001TT0700C008158	5	406	ACU44985	5.63E-48	Pfiesteria piscicida	Dinophyta
	EPT001TT0700C008251	5	387	ACU44982	4.89E-60	Pfiesteria piscicida	Dinophyta
	EPT001TT0700C008455	4	346	XP_005769338	1.41E-43	Emiliania huxleyi	Haptophyta
	EPT001TT0700C008860	4	279	ACU44985	1.68E-28	Pfiesteria piscicida	Dinophyta
	EPT001TT0700C008921	5	267	ACU44985	2.15E-31	Pfiesteria piscicida	Dinophyta
Fructose 1,6 bisphosphatase	EPT001TT0700C003910	1	869	ABF68600	2.75E-86	Euglena gracilis	Euglenozoa
transketolase	EPT001TT0700C001844	3	1197	ABQ23347	5.94E-174	Karlodinium veneficum	Dinophyta
	EPT001TT0700C001942	4	1172	ABQ23347	5.25E-159	Karlodinium veneficum	Dinophyta
	EPT001TT0700C002045	4	1151	ABQ23347	1.45E-129	Karlodinium veneficum	Dinophyta
	EPT001TT0700C003002	4	984	ABQ23347	3.40E-118	Karlodinium veneficum	Dinophyta
	EPT001TT0700C003578	2	908	ABQ23347	2.05E-117	Karlodinium veneficum	Dinophyta
	EPT001TT0700C003640	2	901	CBJ48487	3.48E-103	Ectocarpus siliculosus	Heterokontophyta
	EPT001TT0700C004832	4	775	ABQ23347	2.08E-76	Karlodinium veneficum	Dinophyta
	EPT001TT0700C005855	2	684	CBJ48487	1.21E-84	Ectocarpus siliculosus	Heterokontophyta
	EPT001TT0700C006380	3	640	ABQ23346	2.72E-77	Karlodinium veneficum	Dinophyta
	EPT001TT0700C008397	2	356	ABQ23347	8.70E-41	Karlodinium veneficum	Dinophyta
	EPT001TT0700C008474	2	342	ABQ23347	1.90E-40	Karlodinium veneficum	Dinophyta
	EPT001TT0700C009587	3	180	ABQ23345	9.52E-08	Isochrysis galbana	Haptophyta
	EPT001TT0700C010028	1	127	CBJ48487	6.23E-15	Ectocarpus siliculosus	Heterokontophyta

<Continued>

Gene Name	Contig No.	No. Of Reads	Length (bp)	Genbank Accession No.	E-Value (Blastx)	Origin	Phylum
RuBisCO	EPT001TT0700C001973	4	1167	AAQ04822	0	Prorocentrum minimum	Dinophyta
	EPT001TT0700C003289	3	946	AAO13086	8.44242E-87	Prorocentrum minimum	Dinophyta
	EPT001TT0700C003714	4	891	AAO13026	3.2296E-154	Prorocentrum minimum	Dinophyta
	EPT001TT0700C004371	3	822	AAQ04822	5.0816E-140	Prorocentrum minimum	Dinophyta
	EPT001TT0700C004419	4	818	AGW32485	1.5148E-144	Prorocentrum donghaiense	Dinophyta
	EPT001TT0700C004450	3	815	AAQ04822	2.246E-140	Prorocentrum minimum	Dinophyta
	EPT001TT0700C004879	4	772	AGW32485	7.9729E-137	Prorocentrum donghaiense	Dinophyta
	EPT001TT0700C004974	4	763	AAQ04822	3.90768E-88	Prorocentrum minimum	Dinophyta
	EPT001TT0700C005663	4	701	AAC37234	4.28114E-32	Lingulodinium polyedrum	Dinophyta
	EPT001TT0700C005761	3	691	AGW32491	1.7793E-123	Prorocentrum donghaiense	Dinophyta
	EPT001TT0700C006209	4	654	AGW32485	2.9149E-114	Prorocentrum donghaiense	Dinophyta
	EPT001TT0700C006404	3	637	AGW32491	5.1692E-113	Prorocentrum donghaiense	Dinophyta
	EPT001TT0700C006528	4	627	AAQ04822	1.4959E-101	Prorocentrum minimum	Dinophyta
	EPT001TT0700C007565	4	504	AAQ04822	9.38762E-80	Prorocentrum minimum	Dinophyta
	EPT001TT0700C008513	5	336	ACI63584	5.21041E-54	uncultured eukaryote	
	EPT001TT0700C008616	5	316	AAC37234	1.07176E-51	Lingulodinium polyedrum	Dinophyta
	EPT001TT0700C008681	4	304	AAC37234	2.14652E-07	Lingulodinium polyedrum	Dinophyta
	EPT001TT0700C008737	5	296	AAK06652	6.68136E-41	Amphidinium carterae	Dinophyta
	EPT001TT0700C008766	4	292	AGW32498	2.37917E-46	Prorocentrum donghaiense	Dinophyta

<Continued>

Gene Name	Contig No.	No. Of Reads	Length (bp)	Genbank Accession No.	E-Value (Blastx)	Origin	Phylum
RuBisCO	EPT001TT0700C008933	4	266	AAQ04822	6.46044E-36	Prorocentrum minimum	Dinophyta
	EPT001TT0700C009136	2	238	AGW32491	1.58008E-34	Prorocentrum donghaiense	Dinophyta
	EPT001TT0700C009318	4	213	AGW32498	5.21317E-30	Prorocentrum donghaiense	Dinophyta
	EPT001TT0700C009909	3	141	AAQ04822	3.15986E-11	Prorocentrum minimum	Dinophyta
	EPT001TT0700C010273	3	102	AGW32491	1.79654E-09	Prorocentrum donghaiense	Dinophyta
triosephosphate isomerase	EPT001TT0700C003880	5	873	CDJ60494	1.76224E-56	Eimeria maxima	Apicomplexa
Ribulose 5-phosphate epimerase	EPT001TT0700C003050	2	977	NP_200949	2.35238E-87	Arabidopsis thaliana	Tracheophyta
SBPase	EPT001TT0700C001592	2	1262	ABF68590	2.0301E-127	Lingulodinium polyedrum	Dinophyta
Aldolase	EPT001TT0700C001308	1	1340	XP_005649618	7.1123E-118	Coccomyxa subellipsoidea	Chlorophyta
Phosphoketolase	EPT001TT0700C005373	4	724	YP_477385	5.62919E-59	Synechococcus sp.	Cyanobacteria

Table 3.9. List of photosynthesis genes involved in Calvin cycle in *Paragymnodinium shiwhaense.*

Gene Name	Contig No.	No. Of Reads	Length (bp)	Genbank Accession No.	E-Value (Blastx)	Origin	Phylum
phosphoglycerate kinase	EPT001TT0701C000772	4	1916	AAW79327	3.22E-128	Pavlova lutheri	Haptophyta
	EPT001TT0701C000888	4	1862	AAW79325	3.09E-136	Isochrysis galbana	Haptophyta
	EPT001TT0701C000931	4	1845	XP_005821497	3.49E-132	Guillardia theta	Cryptophyta
	EPT001TT0701C001382	5	1684	XP_005821497	8.77E-127	Guillardia theta	Cryptophyta
	EPT001TT0701C001623	4	1625	ACO14839	4.73E-130	Caligus clemensi	Arthropoda
	EPT001TT0701C001721	4	1600	XP_005821497	1.00E-132	Guillardia theta	Cryptophyta
	EPT001TT0701C002271	4	1499	AAW79327	1.36E-152	Pavlova lutheri	Haptophyta
	EPT001TT0701C002371	4	1482	AAW79327	1.17E-156	Pavlova lutheri	Haptophyta
	EPT001TT0701C003985	4	1273	XP_005821497	8.09E-116	Guillardia theta	Cryptophyta
	EPT001TT0701C004198	4	1249	AAW79327	5.40E-157	Pavlova lutheri	Haptophyta
	EPT001TT0701C004798	3	1195	AAF45020	2.38E-90	Phaeodactylum tricornutum	Heterokontophyta
	EPT001TT0701C004963	4	1182	CAB61334	6.85E-106	Laminaria digitata	Heterokontophyta
	EPT001TT0701C005566	4	1130	AAF45020	3.38E-91	Phaeodactylum tricornutum	Heterokontophyta
	EPT001TT0701C006232	4	1078	AAW79327	4.23E-120	Pavlova lutheri	Haptophyta
	EPT001TT0701C006263	4	1076	AAW79327	1.59E-135	Pavlova lutheri	Haptophyta
	EPT001TT0701C011561	4	787	XP_005821497	5.71E-53	Guillardia theta	Cryptophyta
	EPT001TT0701C012264	3	760	XP_005791258	2.06E-41	Emiliania huxleyi	Haptophyta
	EPT001TT0701C012954	4	731	AAW79327	4.08E-92	Pavlova lutheri	Haptophyta
	EPT001TT0701C012955	4	731	AAW79327	2.03E-91	Pavlova lutheri	Haptophyta
	EPT001TT0701C014365	4	673	XP_005821497	1.10E-58	Guillardia theta	Cryptophyta
	EPT001TT0701C015122	4	644	XP_005821497	5.78E-51	Guillardia theta	Cryptophyta
	EPT001TT0701C016070	3	601	AAW79327	6.62E-37	Pavlova lutheri	Haptophyta
	EPT001TT0701C017427	4	520	XP_005791258	2.35E-62	Emiliania huxleyi	Haptophyta
	EPT001TT0701C017430	4	521	BAG09537	2.36E-30	Pyropia yezoensis	Rhodophyta
	EPT001TT0701C017608	2	504	AAF45020	8.71E-09	Phaeodactylum tricornutum	Heterokontophyta
	EPT001TT0701C017630	4	502	ABF69999	5.96E-50	Musa acuminata	Tracheophyta
	EPT001TT0701C017767	4	486	NP_683058	1.33E-25	Thermosynechococcus elongatus	Cyanobacteria

<Continued>

Gene Name	Contig No.	No. Of Reads	Length (bp)	Genbank Accession No.	E-Value (Blastx)	Origin	Phylum
phosphoglycerate kinase	EPT001TT0701C018179	4	439	WP_006854064	1.81E-22	Synechococcus sp.	Cyanobacteria
	EPT001TT0701C018377	5	412	XP_005791258	3.62E-47	Emiliania huxleyi	Haptophyta
	EPT001TT0701C019664	4	259	AGV54662	6.97E-30	Phaseolus vulgaris	Tracheophyta
	EPT001TT0701C019787	5	246	ESS30067	4.91E-12	Toxoplasma gondii	Apicomplexa
	EPT001TT0701C019788	5	246	ESS30067	4.91E-12	Toxoplasma gondii	Apicomplexa
	EPT001TT0701C019834	5	240	Q42962	6.44E-12	Paragymnodinium shiwhaense	Dinophyta
	EPT001TT0701C020601	4	167	AAW79324	2.54E-08	Heterocapsa triquetra	Dinophyta
	EPT001TT0701C021102	4	120	EKD15806	3.33E-08	Marssonina brunnea f. sp.	Ascomycota
GAPDH	EPT001TT0701C000085	5	2775	ABO47862	1.492E-164	Alexandrium fundyense	Dinophyta
	EPT001TT0701C000199	5	2394	ACF28654	1.1035E-144	Amphidinium carterae	Dinophyta
	EPT001TT0701C001468	5	1662	AAM68968	8.5219E-159	Pyrocystis lunula	Dinophyta
	EPT001TT0701C001722	5	1600	AAM68968	8.1595E-159	Pyrocystis lunula	Dinophyta
	EPT001TT0701C001829	4	1579	AAM68968	2.1024E-159	Pyrocystis lunula	Dinophyta
	EPT001TT0701C001897	5	1568	AAM68968	2.3059E-158	Pyrocystis lunula	Dinophyta
	EPT001TT0701C002475	5	1466	AAM68968	2.4749E-159	Pyrocystis lunula	Dinophyta
	EPT001TT0701C002491	5	1465	ADV03068	2.4927E-117	Amphidinium carterae	Dinophyta
	EPT001TT0701C002762	5	1425	AAM68968	7.9611E-155	Pyrocystis lunula	Dinophyta
	EPT001TT0701C002888	5	1406	AAM68968	6.8297E-159	Pyrocystis lunula	Dinophyta
	EPT001TT0701C003269	4	1353	BAD72933	0	Karenia mikimotoi	Dinophyta
	EPT001TT0701C003283	5	1353	AAM68968	1.4404E-158	Pyrocystis lunula	Dinophyta
	EPT001TT0701C003325	5	1349	AAM68968	9.9091E-160	Pyrocystis lunula	Dinophyta
	EPT001TT0701C003618	5	1315	BAC87932	6.6106E-161	Amphidinium operculatum	Dinophyta
	EPT001TT0701C003777	5	1295	BAD72931	2.79725E-79	Karenia mikimotoi	Dinophyta
	EPT001TT0701C003975	5	1274	BAG11483	6.1166E-172	Lepidodinium chlorophorum	Dinophyta
	EPT001TT0701C004133	4	1257	AAM68968	1.3988E-120	Pyrocystis lunula	Dinophyta
	EPT001TT0701C004204	5	1249	ACF28670	2.9682E-147	Amphidinium carterae	Dinophyta
	EPT001TT0701C004302	5	1239	BAG11483	1.7087E-171	Lepidodinium chlorophorum	Dinophyta
	EPT001TT0701C004362	5	1234	BAG11483	5.468E-162	Lepidodinium chlorophorum	Dinophyta

<Continued>

Gene Name	Contig No.	No. Of Reads	Length (bp)	Genbank Accession No.	E-Value (Blastx)	Origin	Phylum
GAPDH	EPT001TT0701C004374	5	1233	BAG11483	8.133E-174	Lepidodinium chlorophorum	Dinophyta
	EPT001TT0701C005457	5	1140	BAG11483	1.1537E-163	Lepidodinium chlorophorum	Dinophyta
	EPT001TT0701C006964	5	1028	AAM68968	1.4841E-111	Pyrocystis lunula	Dinophyta
	EPT001TT0701C007618	4	983	BAD72933	4.1213E-148	Karenia mikimotoi	Dinophyta
	EPT001TT0701C007887	5	967	AAM68968	1.8099E-108	Pyrocystis lunula	Dinophyta
	EPT001TT0701C007901	5	967	BAG11483	1.246E-149	Lepidodinium chlorophorum	Dinophyta
	EPT001TT0701C007905	4	960	BAD72933	1.7728E-140	Karenia mikimotoi	Dinophyta
	EPT001TT0701C008448	5	937	BAG11483	2.2942E-145	Lepidodinium chlorophorum	Dinophyta
	EPT001TT0701C008505	5	932	AAM68968	5.52186E-67	Pyrocystis lunula	Dinophyta
	EPT001TT0701C009422	4	883	AAM68969	1.50821E-87	Pyrocystis noctiluca	Dinophyta
	EPT001TT0701C009682	5	872	AAM68968	1.33392E-72	Pyrocystis lunula	Dinophyta
	EPT001TT0701C009733	4	869	AAM68968	4.4903E-121	Pyrocystis lunula	Dinophyta
	EPT001TT0701C010354	4	839	BAD72933	1.4511E-129	Karenia mikimotoi	Dinophyta
	EPT001TT0701C010999	4	811	AAM68969	4.87575E-87	Pyrocystis noctiluca	Dinophyta
	EPT001TT0701C011112	4	807	AAM68969	4.79896E-87	Pyrocystis noctiluca	Dinophyta
	EPT001TT0701C011173	4	803	AAM68969	1.22189E-58	Pyrocystis noctiluca	Dinophyta
	EPT001TT0701C011518	5	790	AAM68968	5.20876E-54	Pyrocystis lunula	Dinophyta
	EPT001TT0701C011755	5	780	BAD72931	9.3024E-125	Karenia mikimotoi	Dinophyta
	EPT001TT0701C012379	5	755	AAM68969	4.20472E-87	Pyrocystis noctiluca	Dinophyta
	EPT001TT0701C012418	4	753	AAM68969	8.20601E-83	Pyrocystis noctiluca	Dinophyta
	EPT001TT0701C012769	4	739	AAM68969	2.07023E-83	Pyrocystis noctiluca	Dinophyta
	EPT001TT0701C012771	5	737	AAM68968	2.4229E-116	Pyrocystis lunula	Dinophyta
	EPT001TT0701C013314	5	716	AAM68968	1.45204E-30	Pyrocystis lunula	Dinophyta
	EPT001TT0701C013494	4	709	AAM68969	3.68211E-87	Pyrocystis noctiluca	Dinophyta
	EPT001TT0701C013528	4	708	AAM68969	2.02513E-77	Pyrocystis noctiluca	Dinophyta
	EPT001TT0701C014519	5	667	BAG11483	9.9037E-97	Lepidodinium chlorophorum	Dinophyta
	EPT001TT0701C014646	5	661	BAG11483	1.8222E-95	Lepidodinium chlorophorum	Dinophyta
	EPT001TT0701C014943	5	651	AAM68968	2.5716E-102	Pyrocystis lunula	Dinophyta

〈Continued〉

Gene Name	Contig No.	No. Of Reads	Length (bp)	Genbank Accession No.	E-Value (Blastx)	Origin	Phylum
GAPDH	EPT001TT0701C015348	5	633	AAM68968	4.29576E-80	Pyrocystis lunula	Dinophyta
	EPT001TT0701C015729	5	616	ABO47862	4.52392E-63	Alexandrium fundyense	Dinophyta
	EPT001TT0701C016025	5	603	BAG11483	3.34715E-84	Lepidodinium chlorophorum	Dinophyta
	EPT001TT0701C017300	2	531	AAM68968	1.11936E-11	Pyrocystis lunula	Dinophyta
	EPT001TT0701C017338	4	528	AAM68969	6.07298E-79	Pyrocystis noctiluca	Dinophyta
	EPT001TT0701C017414	1	521	BAD72933	1.28391E-60	Karenia mikimotoi	Dinophyta
	EPT001TT0701C017522	4	513	AAM68969	2.399E-35	Pyrocystis noctiluca	Dinophyta
	EPT001TT0701C017560	4	506	AAM68969	2.42071E-35	Pyrocystis noctiluca	Dinophyta
	EPT001TT0701C017654	5	500	BAC87937	4.11811E-75	Scrippsiella trochoidea	Dinophyta
	EPT001TT0701C017792	4	484	AAM68969	2.42211E-35	Pyrocystis noctiluca	Dinophyta
	EPT001TT0701C017920	5	467	ACF28670	8.5117E-57	Amphidinium carterae	Dinophyta
	EPT001TT0701C017944	5	466	ADV03068	2.40428E-43	Amphidinium carterae	Dinophyta
	EPT001TT0701C018003	5	460	ABO47862	7.08507E-43	Alexandrium fundyense	Dinophyta
	EPT001TT0701C018312	5	423	ADV03068	2.18141E-28	Amphidinium carterae	Dinophyta
	EPT001TT0701C018315	5	423	ABO47862	1.27295E-44	Alexandrium fundyense	Dinophyta
	EPT001TT0701C018514	5	393	AAM68969	5.75717E-29	Pyrocystis noctiluca	Dinophyta
	EPT001TT0701C018801	5	355	AAM68968	5.26734E-46	Pyrocystis lunula	Dinophyta
	EPT001TT0701C018859	5	348	ADV03068	4.83889E-28	Amphidinium carterae	Dinophyta
	EPT001TT0701C018915	4	343	AAM68969	4.37253E-45	Pyrocystis noctiluca	Dinophyta
	EPT001TT0701C019025	1	328	BAD72933	1.25962E-39	Karenia mikimotoi	Dinophyta
	EPT001TT0701C019073	5	323	BAD72935	1.10236E-51	Karenia brevis	Dinophyta
	EPT001TT0701C019096	5	321	AAM68968	1.76843E-38	Pyrocystis lunula	Dinophyta
	EPT001TT0701C019447	5	282	AAM68968	4.24985E-40	Pyrocystis lunula	Dinophyta
	EPT001TT0701C019489	5	277	AAM68969	5.04927E-33	Pyrocystis noctiluca	Dinophyta
	EPT001TT0701C019547	5	270	AAM68968	5.6273E-40	Pyrocystis lunula	Dinophyta
	EPT001TT0701C019686	5	257	AAD01872	5.3389E-38	Lingulodinium polyedrum	Dinophyta
	EPT001TT0701C019824	5	241	AAM68969	5.0661E-33	Pyrocystis noctiluca	Dinophyta
	EPT001TT0701C020151	5	210	AAM68969	1.62056E-31	Pyrocystis noctiluca	Dinophyta
	EPT001TT0701C020178	5	208	BAD72935	1.05381E-30	Karenia brevis	Dinophyta
	EPT001TT0701C020223	4	205	AAM68969	9.91801E-21	Pyrocystis noctiluca	Dinophyta

<Continued>

Gene Name	Contig No.	No. Of Reads	Length (bp)	Genbank Accession No.	E-Value (Blastx)	Origin	Phylum
GAPDH	EPT001TT0701C020362	5	190	BAG11483	6.51656E-28	Lepidodinium chlorophorum	Dinophyta
	EPT001TT0701C020401	5	186	ABI14392	1.66271E-20	Karlodinium veneficum	Dinophyta
	EPT001TT0701C020933	5	135	AAM68968	1.8009E-14	Pyrocystis lunula	Dinophyta
	EPT001TT0701C021208	5	113	BAC87925	5.53601E-11	Polarella glacialis	Dinophyta
	EPT001TT0701C021281	5	106	CDJ63967	7.27266E-11	Eimeria necatrix	Apicomplexa
fructose-bisphosphate aldolase	EPT001TT0701C001330	1	1697	XP_002288320	2.6425E-155	Thalassiosira pseudonana	Heterokontophyta
	EPT001TT0701C001482	1	1659	XP_002288320	5.3502E-153	Thalassiosira pseudonana	Heterokontophyta
	EPT001TT0701C001649	1	1616	XP_002288320	1.6011E-154	Thalassiosira pseudonana	Heterokontophyta
	EPT001TT0701C002009	3	1545	AAV71135	6.7649E-179	Heterocapsa triquetra	Dinophyta
	EPT001TT0701C002113	3	1525	AAV71135	4.0235E-168	Heterocapsa triquetra	Dinophyta
	EPT001TT0701C002168	3	1518	AAV71135	2.1324E-161	Heterocapsa triquetra	Dinophyta
	EPT001TT0701C002180	3	1514	AAV71135	1.2041E-156	Heterocapsa triquetra	Dinophyta
	EPT001TT0701C002850	4	1411	ACU44982	1.5794E-155	Pfiesteria piscicida	Dinophyta
	EPT001TT0701C002918	1	1400	XP_004956796	1.381E-10	Setaria talica	Tracheophyta
	EPT001TT0701C003315	4	1348	ACU44982	9.3177E-142	Pfiesteria piscicida	Dinophyta
	EPT001TT0701C003514	5	1326	ACU44982	3.7927E-156	Pfiesteria piscicida	Dinophyta
	EPT001TT0701C004136	2	1257	XP_005840722	3.0183E-115	Guillardia theta	Cryptophyta
	EPT001TT0701C004868	2	1190	AAV71135	5.0976E-117	Heterocapsa triquetra	Dinophyta
	EPT001TT0701C004915	5	1186	ACU44982	4.5391E-158	Pfiesteria piscicida	Dinophyta
	EPT001TT0701C005223	5	1159	ACU44982	2.842E-149	Pfiesteria piscicida	Dinophyta
	EPT001TT0701C006080	4	1091	EQC41663	5.7619E-125	Saprolegnia diclina	Heterokontophyta
	EPT001TT0701C007087	2	1019	AAV71135	4.3898E-116	Heterocapsa triquetra	Dinophyta
	EPT001TT0701C007711	2	978	AAV71135	6.8824E-87	Heterocapsa triquetra	Dinophyta
	EPT001TT0701C009639	1	872	XP_004956796	2.92539E-11	Setaria talica	Tracheophyta
	EPT001TT0701C009726	5	870	ACU44982	5.2091E-93	Pfiesteria piscicida	Dinophyta
	EPT001TT0701C009869	2	862	XP_002288320	2.63864E-65	Thalassiosira pseudonana	Heterokontophyta
	EPT001TT0701C010388	2	832	XP_002288320	2.72784E-88	Thalassiosira pseudonana	Heterokontophyta
	EPT001TT0701C010482	4	831	ACU44982	3.4091E-99	Pfiesteria piscicida	Dinophyta

Gene Name	Contig No.	No. Of Reads	Length (bp)	Genbank Accession No.	E-Value (Blastx)	Origin	Phylum
fructose-bisphosphate aldolase	EPT001TT0701C010695	5	824	ACU44982	9.7021E-123	Pfiesteria piscicida	Dinophyta
	EPT001TT0701C011878	2	768	AAV71137	7.69541E-60	Isochrysis galbana	Haptophyta
	EPT001TT0701C011973	2	771	AAV71135	1.16264E-71	Heterocapsa triquetra	Dinophyta
	EPT001TT0701C014124	2	683	AAV71135	6.46406E-46	Heterocapsa triquetra	Dinophyta
	EPT001TT0701C014550	1	664	AAV71135	1.21545E-38	Heterocapsa triquetra	Dinophyta
	EPT001TT0701C016987	3	551	AAV71135	8.52769E-24	Heterocapsa triquetra	Dinophyta
	EPT001TT0701C017138	2	541	AAV71135	4.68029E-24	Heterocapsa triquetra	Dinophyta
	EPT001TT0701C017545	2	510	AAV71135	7.98618E-31	Heterocapsa triquetra	Dinophyta
	EPT001TT0701C017564	2	508	AAV71138	5.04822E-17	Guillardia theta	Cryptophyta
	EPT001TT0701C018083	2	450	AAV71138	6.55207E-17	Guillardia theta	Cryptophyta
	EPT001TT0701C018389	5	410	ACU44985	8.12116E-39	Pfiesteria piscicida	Dinophyta
	EPT001TT0701C018699	3	369	AAV71135	7.78913E-26	Heterocapsa triquetra	Dinophyta
	EPT001TT0701C018700	3	369	AAV71135	4.8788E-28	Heterocapsa triquetra	Dinophyta
	EPT001TT0701C018738	3	363	EJD08425	2.99624E-09	Fomitiporia mediterranea	Basidiomycota
	EPT001TT0701C018891	2	345	AAV71135	6.98086E-43	Heterocapsa triquetra	Dinophyta
	EPT001TT0701C018977	3	334	AAV71135	2.07283E-10	Heterocapsa triquetra	Dinophyta
	EPT001TT0701C019361	3	290	AAV71135	2.25544E-12	Heterocapsa triquetra	Dinophyta
	EPT001TT0701C020098	4	214	YP_001359106	1.73789E-09	Sulfurovum sp.	Proteobacteria
	EPT001TT0701C020135	2	211	YP_004656125	2.60164E-21	Runella slithyformis	Bacteroidetes
	EPT001TT0701C020295	2	197	AAV71135	3.11275E-22	Heterocapsa triquetra	Dinophyta
	EPT001TT0701C020367	3	190	AAV71135	1.23468E-10	Heterocapsa triquetra	Dinophyta
	EPT001TT0701C020377	2	189	AAV71137	1.90643E-19	Isochrysis galbana	Haptophyta
	EPT001TT0701C020607	3	166	AAV71135	1.81417E-14	Heterocapsa triquetra	Dinophyta
Fructose-1,6-bisphosphatase	EPT001TT0701C001054	3	1796	ABF68596	1.8445E-138	Lingulodinium polyedrum	Dinophyta
	EPT001TT0701C001068	2	1790	ABF68596	8.5917E-136	Lingulodinium polyedrum	Dinophyta
	EPT001TT0701C001205	2	1726	ABF68596	8.1863E-136	Lingulodinium polyedrum	Dinophyta
	EPT001TT0701C001330	3	1697	AFE02909	2.2318E-162	Emiliania huxleyi	Haptophyta
	EPT001TT0701C001482	3	1659	AFE02909	3.9586E-156	Emiliania huxleyi	Haptophyta

〈Continued〉

Gene Name	Contig No.	No. Of Reads	Length (bp)	Genbank Accession No.	E-Value (Blastx)	Origin	Phylum
Fructose-1,6-bisphosphatase	EPT001TT0701C001649	3	1616	AFE02909	3.8109E-156	Emiliania huxleyi	Haptophyta
	EPT001TT0701C001983	4	1550	XP_005769338	1.0931E-144	Emiliania huxleyi	Haptophyta
	EPT001TT0701C002009	1	1545	ABF73010	9.8139E-162	Karenia brevis	Dinophyta
	EPT001TT0701C002113	2	1525	ABF73010	7.6232E-151	Karenia brevis	Dinophyta
	EPT001TT0701C002168	2	1518	ABF73010	5.0991E-147	Karenia brevis	Dinophyta
	EPT001TT0701C002180	2	1514	AAM66752	1.7992E-152	Odontella sinensis	Heterokontophyta
	EPT001TT0701C002502	4	1463	XP_005769338	5.3368E-146	Emiliania huxleyi	Haptophyta
	EPT001TT0701C003716	2	1303	ABF68600	6.9146E-102	Euglena gracilis	Euglenozoa
	EPT001TT0701C004136	1	1257	CBJ48329	6.0816E-116	Ectocarpus siliculosus	Heterokontophyta
	EPT001TT0701C004339	4	1236	XP_005769338	3.9643E-120	Emiliania huxleyi	Haptophyta
	EPT001TT0701C004868	2	1190	ABF73010	1.2993E-112	Karenia brevis	Dinophyta
	EPT001TT0701C006916	4	1030	XP_005769338	4.9426E-123	Emiliania huxleyi	Haptophyta
	EPT001TT0701C007087	2	1019	ABF73010	3.2556E-111	Karenia brevis	Dinophyta
	EPT001TT0701C007711	2	978	AAM66752	2.70642E-83	Odontella sinensis	Heterokontophyta
	EPT001TT0701C009869	2	862	AFE02909	1.10603E-71	Emiliania huxleyi	Haptophyta
	EPT001TT0701C010388	2	832	AFE02909	4.64222E-96	Emiliania huxleyi	Haptophyta
	EPT001TT0701C011307	3	798	ABF68596	8.87431E-70	Lingulodinium polyedrum	Dinophyta
	EPT001TT0701C011878	2	768	ABF73010	1.01091E-62	Karenia brevis	Dinophyta
	EPT001TT0701C011973	2	771	ABF73010	8.62234E-67	Karenia brevis	Dinophyta
	EPT001TT0701C013720	2	699	ABF68596	3.81231E-49	Lingulodinium polyedrum	Dinophyta
	EPT001TT0701C014124	3	683	ABF73010	2.45634E-45	Karenia brevis	Dinophyta
	EPT001TT0701C014125	2	682	ABF68596	3.51432E-36	Lingulodinium polyedrum	Dinophyta
	EPT001TT0701C014550	2	664	ABF73010	1.13763E-36	Karenia brevis	Dinophyta
	EPT001TT0701C016987	1	551	AAM66752	1.11375E-23	Odontella sinensis	Heterokontophyta
	EPT001TT0701C017138	1	541	AAM66752	5.72126E-22	Odontella sinensis	Heterokontophyta
	EPT001TT0701C017545	2	510	AAM66752	1.79914E-30	Odontella sinensis	Heterokontophyta
	EPT001TT0701C017564	2	508	AAM66752	1.46881E-16	Odontella sinensis	Heterokontophyta
	EPT001TT0701C018083	2	450	AAO43196	6.55207E-17	Phaeodactylum tricornutum	Heterokontophyta

<Continued>

Gene Name	Contig No.	No. Of Reads	Length (bp)	Genbank Accession No.	E-Value (Blastx)	Origin	Phylum
Fructose-1,6-bisphosphatase	EPT001TT0701C018699	2	369	ABF73010	3.06298E-22	Karenia brevis	Dinophyta
	EPT001TT0701C018700	2	369	ABF73010	9.52156E-24	Karenia brevis	Dinophyta
	EPT001TT0701C018891	2	345	ACF28657	1.66156E-44	Amphidinium carterae	Dinophyta
	EPT001TT0701C018977	2	334	ABF73010	1.58711E-10	Karenia brevis	Dinophyta
	EPT001TT0701C019361	2	290	ABF73010	2.25544E-12	Karenia brevis	Dinophyta
	EPT001TT0701C020135	2	211	ACF28657	2.77962E-23	Amphidinium carterae	Dinophyta
	EPT001TT0701C020295	2	197	ABF73010	1.82487E-22	Karenia brevis	Dinophyta
	EPT001TT0701C020367	1	190	AAM66752	2.10605E-10	Odontella sinensis	Heterokontophyta
	EPT001TT0701C020377	2	189	ABF73010	1.61389E-18	Karenia brevis	Dinophyta
	EPT001TT0701C020607	1	166	AAM66752	1.81417E-14	Odontella sinensis	Heterokontophyta
transketolase	EPT001TT0701C000175	5	2446	WP_017316342	0	Mastigocladopsis repens	Cyanobacteria
	EPT001TT0701C000263	5	2295	YP_720382	0	Trichodesmium erythraeum	Cyanobacteria
	EPT001TT0701C000308	5	2244	WP_009556088	0	Oscillatoriales cyanobacterium	Cyanobacteria
	EPT001TT0701C000558	5	2027	AHB88511	0	Thermosynechococcus sp.	Cyanobacteria
	EPT001TT0701C000746	5	1932	WP_017739732	0	Scytonema hofmanni	Cyanobacteria
	EPT001TT0701C000854	5	1876	WP_009456507	0	Fischerella	Fischerella
	EPT001TT0701C003762	5	1299	NP_896236	1.7401E-129	Synechococcus sp.	Cyanobacteria
	EPT001TT0701C003807	5	1293	AAW65685	1.5207E-109	Euglena gracilis	Euglenozoa
	EPT001TT0701C004409	5	1230	WP_006454760	4.3261E-151	Synechococcus sp.	Cyanobacteria
	EPT001TT0701C004779	4	1196	XP_001616126	1.19892E-41	Apicomplexa	Apicomplexa
	EPT001TT0701C006434	5	1055	AHB88511	1.9107E-85	Thermosynechococcus sp.	Cyanobacteria
	EPT001TT0701C007070	5	1021	ABP35605	7.0284E-122	Karlodinium veneficum	Dinophyta
	EPT001TT0701C007737	4	975	WP_017325228	2.212E-69	Synechococcus sp.	Cyanobacteria
	EPT001TT0701C008358	1	940	XP_002765174	5.55136E-62	Perkinsus marinus	Apicomplexa
	EPT001TT0701C012620	4	745	AAW65685	1.48734E-89	Euglena gracilis	Euglenozoa
	EPT001TT0701C013049	5	725	WP_009556088	2.81659E-37	Oscillatoriales cyanobacterium	Cyanobacteria
	EPT001TT0701C016882	5	557	WP_006042518	1.04051E-56	Synechococcus sp.	Cyanobacteria
	EPT001TT0701C017154	5	540	AHB88511	1.84899E-20	Thermosynechococcus sp.	Cyanobacteria
	EPT001TT0701C017387	5	524	NP_896236	1.51321E-53	Synechococcus sp.	Cyanobacteria
	EPT001TT0701C017931	3	468	XP_002503179	3.72784E-12	Micromonas sp.	Chlorophyta

<Continued>

Gene Name	Contig No.	No. Of Reads	Length (bp)	Genbank Accession No.	E-Value (Blastx)	Origin	Phylum
transketolase	EPT001TT0701C018126	3	444	XP_002503179	9.83175E-13	Micromonas sp.	Chlorophyta
	EPT001TT0701C019072	5	322	WP_019501710	9.6571E-48	Pseudanabaena sp.	Cyanobacteria
	EPT001TT0701C019328	5	294	WP_017662794	4.65401E-34	Geitlerinema sp.	Cyanobacteria
	EPT001TT0701C020887	5	138	WP_006678495	1.08603E-11	Paenibacillus dendritiformis	Firmicutes
RuBisCO	EPT001TT0701C001031	3	1806	AAO13032	0	Prorocentrum minimum	Dinophyta
	EPT001TT0701C001333	1	1694	XP_005535718	8.54381E-13	Cyanidioschyzon merolae	Rhodophyta
	EPT001TT0701C002139	4	1521	AAO13073	0	Prorocentrum minimum	Dinophyta
	EPT001TT0701C002223	3	1506	AAO13027	0	Prorocentrum minimum	Dinophyta
	EPT001TT0701C002262	3	1495	XP_005705388	2.24384E-22	Galdieria sulphuraria	Rhodophyta
	EPT001TT0701C002863	3	1409	Q42813	0	Paragymnodinium shiwhaense	Dinophyta
	EPT001TT0701C002918	1	1400	BAD28364	3.07654E-10	Oryza sativa	Tracheophyta
	EPT001TT0701C003343	3	1347	AAO13032	0	Prorocentrum minimum	Dinophyta
	EPT001TT0701C003367	3	1343	AAO13030	0	Prorocentrum minimum	Dinophyta
	EPT001TT0701C003436	3	1335	AAO13027	0	Prorocentrum minimum	Dinophyta
	EPT001TT0701C003806	3	1294	Q42813	0	Paragymnodinium shiwhaense	Dinophyta
	EPT001TT0701C004057	4	1264	AAO13030	5.4848E-165	Prorocentrum minimum	Dinophyta
	EPT001TT0701C005203	2	1161	AGW32491	5.753E-134	Prorocentrum donghaiense	Dinophyta
	EPT001TT0701C005231	3	1159	AAO13081	0	Prorocentrum minimum	Dinophyta
	EPT001TT0701C005310	3	1527	AGW32491	0	Prorocentrum donghaiense	Dinophyta
	EPT001TT0701C005619	3	1125	AGW32491	0	Prorocentrum donghaiense	Dinophyta
	EPT001TT0701C005809	3	1111	AAO13026	1.8492E-126	Prorocentrum minimum	Dinophyta
	EPT001TT0701C006221	3	1527	AGW32491	0	Prorocentrum donghaiense	Dinophyta
	EPT001TT0701C006376	3	1068	Q42813	6.7382E-179	Paragymnodinium shiwhaense	Dinophyta
	EPT001TT0701C007036	3	1024	Q42813	3.6942E-171	Paragymnodinium shiwhaense	Dinophyta
	EPT001TT0701C007892	5	968	AAO13030	2.6283E-107	Prorocentrum minimum	Dinophyta
	EPT001TT0701C008524	3	931	Q42813	2.0331E-154	Paragymnodinium shiwhaense	Dinophyta
	EPT001TT0701C009130	3	898	AAQ04822	7.4743E-90	Prorocentrum minimum	Dinophyta
	EPT001TT0701C009638	3	873	Q42813	1.1135E-143	Paragymnodinium shiwhaense	Dinophyta
	EPT001TT0701C009639	1	872	BAD28364	6.09982E-09	Oryza sativa	Tracheophyta
	EPT001TT0701C009688	3	872	AAO13030	4.6571E-134	Prorocentrum minimum	Dinophyta

<Continued>

Gene Name	Contig No.	No. Of Reads	Length (bp)	Genbank Accession No.	E-Value (Blastx)	Origin	Phylum
RuBisCO	EPT001TT0701C009919	3	858	Q42813	2.0142E-142	Paragymnodinium shiwhaense	Dinophyta
	EPT001TT0701C010097	2	850	XP_002185762	1.21673E-06	Phaeodactylum tricornutum	Heterokontophyta
	EPT001TT0701C010431	3	826	AAO13081	8.0106E-132	Prorocentrum minimum	Dinophyta
	EPT001TT0701C010733	4	822	AAO13088	1.3507E-132	Prorocentrum minimum	Dinophyta
	EPT001TT0701C010927	3	814	Q42813	2.1754E-135	Paragymnodinium shiwhaense	Dinophyta
	EPT001TT0701C011291	3	799	AGW32491	1.1483E-101	Prorocentrum donghaiense	Dinophyta
	EPT001TT0701C011745	3	779	AGW32491	1.9532E-98	Prorocentrum donghaiense	Dinophyta
	EPT001TT0701C011754	3	780	Q42813	6.38118E-73	Paragymnodinium shiwhaense	Dinophyta
	EPT001TT0701C011781	3	778	Q42813	1.6382E-129	Paragymnodinium shiwhaense	Dinophyta
	EPT001TT0701C011806	4	777	AAO13030	1.8583E-125	Prorocentrum minimum	Dinophyta
	EPT001TT0701C011817	3	776	Q42813	1.6808E-126	Paragymnodinium shiwhaense	Dinophyta
	EPT001TT0701C011852	3	776	Q42813	8.0796E-121	Paragymnodinium shiwhaense	Dinophyta
	EPT001TT0701C012174	4	764	AAO13027	1.3963E-69	Prorocentrum minimum	Dinophyta
	EPT001TT0701C012981	5	729	AGW32491	1.9564E-62	Prorocentrum donghaiense	Dinophyta
	EPT001TT0701C013009	4	728	AAQ04822	1.64852E-77	Prorocentrum minimum	Dinophyta
	EPT001TT0701C013100	4	726	Q42813	1.90373E-41	Paragymnodinium shiwhaense	Dinophyta
	EPT001TT0701C013652	4	702	AAO13027	2.48666E-64	Prorocentrum minimum	Dinophyta
	EPT001TT0701C013935	4	690	AAO13081	1.25527E-60	Prorocentrum minimum	Dinophyta
	EPT001TT0701C014163	4	680	AAQ04822	3.16386E-53	Prorocentrum minimum	Dinophyta
	EPT001TT0701C014489	4	668	AAO13030	1.8007E-106	Prorocentrum minimum	Dinophyta
	EPT001TT0701C014967	5	650	AAO13060	3.84665E-50	Prorocentrum minimum	Dinophyta
	EPT001TT0701C014994	4	649	Q42813	5.7945E-101	Paragymnodinium shiwhaense	Dinophyta
	EPT001TT0701C015458	3	628	AAG37859	3.5605E-103	Symbiodinium sp.	Dinophyta
	EPT001TT0701C015485	5	625	AAO13030	2.30676E-54	Prorocentrum minimum	Dinophyta
	EPT001TT0701C015603	5	622	AAO13048	5.99634E-47	Prorocentrum minimum	Dinophyta
	EPT001TT0701C016252	4	592	AGW32491	2.12219E-48	Prorocentrum donghaiense	Dinophyta
	EPT001TT0701C016254	4	592	Q42813	1.49984E-94	Paragymnodinium shiwhaense	Dinophyta
	EPT001TT0701C016541	4	578	Q42813	1.57849E-37	Paragymnodinium shiwhaense	Dinophyta

<Continued>

Gene Name	Contig No.	No. Of Reads	Length (bp)	Genbank Accession No.	E-Value (Blastx)	Origin	Phylum
RuBisCO	EPT001TT0701C016789	3	564	ABY20940	6.72073E-91	Symbiodinium sp. ex Stylophora pistillata	Dinophyta
	EPT001TT0701C017428	4	521	AAO13088	6.77635E-78	Prorocentrum minimum	Dinophyta
	EPT001TT0701C017524	4	512	AAO13081	1.17689E-74	Prorocentrum minimum	Dinophyta
	EPT001TT0701C017532	4	512	AAO13053	1.1532E-29	Prorocentrum minimum	Dinophyta
	EPT001TT0701C017540	3	511	Q42813	1.59061E-71	Paragymnodinium shiwhaense	Dinophyta
	EPT001TT0701C017824	3	480	ABY20940	1.1986E-74	Symbiodinium sp. ex Stylophora pistillata	Dinophyta
	EPT001TT0701C017932	4	468	ABY20940	1.26309E-76	Symbiodinium sp. ex Stylophora pistillata	Dinophyta
	EPT001TT0701C017959	3	465	Q42813	1.2234E-71	Paragymnodinium shiwhaense	Dinophyta
	EPT001TT0701C018178	3	439	Q42813	1.40848E-67	Paragymnodinium shiwhaense	Dinophyta
	EPT001TT0701C018362	4	414	AGW32477	6.5449E-65	Prorocentrum donghaiense	Dinophyta
	EPT001TT0701C018458	5	400	AGW32491	1.75924E-62	Prorocentrum donghaiense	Dinophyta
	EPT001TT0701C018853	4	349	ABY20940	1.35107E-54	Symbiodinium sp. ex Stylophora pistillata	Dinophyta
	EPT001TT0701C018868	4	347	AGW32491	1.54582E-50	Prorocentrum donghaiense	Dinophyta
	EPT001TT0701C019076	4	323	ABY20940	1.03177E-49	Symbiodinium sp. ex Stylophora pistillata	Dinophyta
	EPT001TT0701C019188	4	309	ACI63676	8.85115E-46	uncultured eukaryote	
	EPT001TT0701C019218	5	308	ACI63676	3.05296E-46	uncultured eukaryote	
	EPT001TT0701C019230	3	306	ABY20940	1.37041E-46	Symbiodinium sp. ex Stylophora pistillata	Dinophyta
	EPT001TT0701C019253	4	303	ABY20940	2.35421E-46	Symbiodinium sp. ex Stylophora pistillata	Dinophyta
	EPT001TT0701C019494	4	276	Q42813	2.76421E-39	Paragymnodinium shiwhaense	Dinophyta
	EPT001TT0701C019495	4	275	Q42813	4.01457E-30	Paragymnodinium shiwhaense	Dinophyta
	EPT001TT0701C019626	5	263	AGW32481	2.15297E-39	Prorocentrum donghaiense	Dinophyta
	EPT001TT0701C019725	3	253	ABY20940	1.27546E-36	Symbiodinium sp. ex Stylophora pistillata	Dinophyta
	EPT001TT0701C019780	4	247	AFR11414	5.58262E-32	Symbiodinium sp.	Dinophyta
	EPT001TT0701C020072	5	217	AFR11414	9.17242E-27	Symbiodinium sp.	Dinophyta

Gene Name	Contig No.	No. Of Reads	Length (bp)	Genbank Accession No.	E-Value (Blastx)	Origin	Phylum
RuBisCO	EPT001TT0701C020094	5	213	AGW32491	5.19635E-30	Prorocentrum donghaiense	Dinophyta
	EPT001TT0701C020127	3	209	ABY20940	2.3541E-26	Symbiodinium sp. ex Stylophora pistillata	Dinophyta
	EPT001TT0701C020164	4	208	AFR11414	1.47862E-24	Symbiodinium sp.	Dinophyta
	EPT001TT0701C020262	5	201	ACI63676	2.44504E-27	uncultured eukaryote	
	EPT001TT0701C020265	5	200	AGW32481	4.62589E-26	Prorocentrum donghaiense	Dinophyta
	EPT001TT0701C020268	5	200	ACI63672	1.438E-27	uncultured eukaryote	
	EPT001TT0701C020325	5	194	ACI63676	2.31043E-25	uncultured eukaryote	
	EPT001TT0701C020352	3	191	Q42813	2.09631E-26	Paragymnodinium shiwhaense	Dinophyta
	EPT001TT0701C020363	5	190	AGW32481	1.35879E-25	Prorocentrum donghaiense	Dinophyta
	EPT001TT0701C020381	5	188	AGW32481	1.61015E-26	Prorocentrum donghaiense	Dinophyta
	EPT001TT0701C020478	4	179	Q42813	7.75415E-26	Paragymnodinium shiwhaense	Dinophyta
	EPT001TT0701C020519	4	175	Q42813	8.07445E-23	Paragymnodinium shiwhaense	Dinophyta
	EPT001TT0701C020600	5	167	ACI63672	1.29711E-20	uncultured eukaryote	
	EPT001TT0701C020705	5	156	ACI63676	1.04045E-17	uncultured eukaryote	
	EPT001TT0701C020706	5	156	ACI63676	1.04045E-17	uncultured eukaryote	
	EPT001TT0701C020969	5	132	AFR11414	1.09257E-11	Symbiodinium sp.	Dinophyta
	EPT001TT0701C020975	4	132	AFR11417	2.35205E-14	Symbiodinium sp.	Dinophyta
	EPT001TT0701C021063	5	125	AGW32498	5.84534E-13	Prorocentrum donghaiense	Dinophyta
	EPT001TT0701C021095	5	122	AGW32481	5.48731E-11	Prorocentrum donghaiense	Dinophyta
	EPT001TT0701C021133	4	119	Q42813	5.88003E-13	Paragymnodinium shiwhaense	Dinophyta
	EPT001TT0701C021193	4	114	AFR11417	4.23878E-11	Symbiodinium sp.	Dinophyta
	EPT001TT0701C021279	5	106	ACI63720	4.72775E-10	uncultured eukaryote	
triosephosphate isomerase	EPT001TT0701C000583	4	1685	XP_005760841	2.57618E-94	Emiliania huxleyi	Haptophyta
	EPT001TT0701C002678	4	1439	XP_005760841	1.31169E-96	Emiliania huxleyi	Haptophyta
	EPT001TT0701C005908	2	1102	CCO18266	6.9976E-78	Bathycoccus prasinos	Chlorophyta
	EPT001TT0701C006309	4	1073	XP_005760841	6.5165E-97	Emiliania huxleyi	Haptophyta
	EPT001TT0701C006744	4	1043	XP_005760841	1.6336E-97	Emiliania huxleyi	Haptophyta
	EPT001TT0701C006807	3	1037	CCO18266	1.57381E-76	Bathycoccus prasinos	Chlorophyta

<Continued>

Gene Name	Contig No.	No. Of Reads	Length (bp)	Genbank Accession No.	E-Value (Blastx)	Origin	Phylum
triosephosphate isomerase	EPT001TT0701C007094	5	1020	XP_002785920	8.66716E-72	Perkinsus marinus	Apicomplexa
	EPT001TT0701C008506	1	933	CCO18266	3.45066E-77	Bathycoccus prasinos	Chlorophyta
	EPT001TT0701C008830	4	916	CDJ28937	4.26314E-64	Eimeria mitis	Apicomplexa
	EPT001TT0701C009871	3	862	XP_003080998	3.67338E-75	Ostreococcus tauri	Chlorophyta
	EPT001TT0701C010570	4	829	XP_005760841	3.00739E-71	Emiliania huxleyi	Haptophyta
	EPT001TT0701C011799	2	778	XP_003080998	2.48229E-77	Ostreococcus tauri	Chlorophyta
	EPT001TT0701C011830	5	775	AEF33397	5.37237E-32	Crassostrea ariakensis	Mollusca
	EPT001TT0701C013752	4	696	XP_005760841	2.29275E-38	Emiliania huxleyi	Haptophyta
	EPT001TT0701C015435	4	630	XP_005760841	2.04062E-66	Emiliania huxleyi	Haptophyta
	EPT001TT0701C016050	4	602	XP_005760841	1.25754E-67	Emiliania huxleyi	Haptophyta
	EPT001TT0701C016449	5	582	XP_005758706	7.44839E-43	Emiliania huxleyi	Haptophyta
	EPT001TT0701C016474	4	581	XP_005760841	9.66045E-67	Emiliania huxleyi	Haptophyta
	EPT001TT0701C017483	4	513	XP_005758706	1.3225E-17	Emiliania huxleyi	Haptophyta
	EPT001TT0701C018195	4	437	XP_005760841	2.27373E-41	Emiliania huxleyi	Haptophyta
	EPT001TT0701C020080	4	215	XP_005760841	8.05409E-15	Emiliania huxleyi	Haptophyta
phosphoribulokinase	EPT001TT0701C002663	5	1440	AAX13963	1.6855E-152	Pyrocystis lunula	Dinophyta
	EPT001TT0701C003015	5	1387	AAX13963	3.9252E-151	Pyrocystis lunula	Dinophyta
	EPT001TT0701C004102	5	1260	AAX13963	6.4614E-150	Pyrocystis lunula	Dinophyta
	EPT001TT0701C005664	5	1123	AAX13963	9.3205E-134	Pyrocystis lunula	Dinophyta
	EPT001TT0701C010536	5	830	AAX13963	1.7993E-116	Pyrocystis lunula	Dinophyta
	EPT001TT0701C014867	5	654	AAX13963	1.47728E-57	Pyrocystis lunula	Dinophyta
	EPT001TT0701C015861	5	607	AAX13963	2.96644E-40	Pyrocystis lunula	Dinophyta
	EPT001TT0701C015946	5	607	AAX13963	2.35477E-85	Pyrocystis lunula	Dinophyta
	EPT001TT0701C017811	5	482	AAX13963	1.117E-72	Pyrocystis lunula	Dinophyta
	EPT001TT0701C018286	5	425	AAX13963	2.40765E-19	Pyrocystis lunula	Dinophyta
	EPT001TT0701C018557	5	388	AAX13963	1.02897E-09	Pyrocystis lunula	Dinophyta
	EPT001TT0701C018564	5	386	AAX13963	3.06721E-54	Pyrocystis lunula	Dinophyta

<Continued>

Gene Name	Contig No.	No. Of Reads	Length (bp)	Genbank Accession No.	E-Value (Blastx)	Origin	Phylum
ribose-5-phosphate isomerase	EPT001TT0701C003582	1	1319	AAW79354	3.7112E-114	Heterocapsa triquetra	Dinophyta
	EPT001TT0701C010114	2	850	AAW79354	3.2457E-100	Heterocapsa triquetra	Dinophyta
ribulose 5 phosphate epimerase	EPT001TT0701C003993	2	1272	AEF79975	3.66522E-84	Dunaliella salina	Chlorophyta
	EPT001TT0701C006830	2	1037	AEF79975	2.26731E-83	Dunaliella salina	Chlorophyta
	EPT001TT0701C007735	1	976	WP_021696056	8.79987E-26	Brevundimonas abyssalis	Proteobacteria
	EPT001TT0701C014289	5	676	AEF79975	1.34983E-32	Dunaliella salina	Chlorophyta
	EPT001TT0701C016024	3	603	AEF79975	4.66083E-38	Dunaliella salina	Chlorophyta
	EPT001TT0701C017042	3	548	XP_003558725	1.73224E-37	Brachypodium distachyon	Tracheophyta
SBPase	EPT001TT0701C001958	2	1554	ABF68590	5.6032E-157	Lingulodinium polyedrum	Dinophyta
	EPT001TT0701C003222	3	1359	ABF68589	2.5748E-123	Prymnesium parvum	Haptophyta
	EPT001TT0701C011539	3	788	ABF68589	6.68433E-86	Prymnesium parvum	Haptophyta
	EPT001TT0701C013101	3	719	ABF68590	1.04647E-44	Lingulodinium polyedrum	Dinophyta
	EPT001TT0701C015984	3	605	ABF68590	7.28968E-47	Lingulodinium polyedrum	Dinophyta
Aldolase	EPT001TT0701C007735	2	976	WP_019460803	4.36733E-25	Roseomonas sp.	Proteobacteria
	EPT001TT0701C008118	1	955	YP_008599592	8.1351E-45	Ralstonia pickettii	
	EPT001TT0701C014068	1	685	WP_007867174	1.41739E-24	Clostridium citroniae	

Chapter 5. Real-time PCR based quantification of the red tide dinoflagellate *Cochlodinium polykrikoides* in South Sea of Korea in 2014

5.1. Introduction

Red tides, which refer to the discoloration of the sea surface due to plankton blooms, caused by dinoflagellates often leads to destruction of the balance in marine ecosystems, large-scale fish mortality, and a great loss in the aquaculture industry (Hallegraeff, 1993; Anderson, 1997; Jeong et al., 2000, 2010, 2013; Park et al., 2009a, 2013a, 2013b; Dyhrman et al., 2006; Moorthi et al., 2006; Kudela and Gobler, 2012; Lee et al., 2013). Thus, monitoring the dynamics of red tide dinoflagellate species and predicting the outbreak of the blooms are critical for minimizing losses due to red tides (Park et al., 2009a, 2013a, 2013b). For a long time, the abundance of dinoflagellates in natural water samples has been determined by the microscopic enumeration of cells (Coyne et al., 2005; Park et al., 2007). However, this method is time consuming and its accuracy is affected by the ability of each individual researcher (Coyne et al., 2005; Dyhrman et al., 2006; Moorthi et al., 2006; Park et al., 2007). From the late 1990's to the early 2000's, quantitative real-time PCR (qPCR) methods were developed to quantify the abundance of dinoflagellates. These methods have been widely used because they can analyze a larger amount of sample over a given time than other traditional cell enumeration methods (Bowers et al., 2000; Suzuki et al., 2000; Cullen et al., 2002; Fontaine and Guillot, 2002; Grey et al., 2003; Phister and Mills, 2003; Vaitomaa et al., 2003; Galluzzi et al., 2004; Skovhus et al., 2004; Coyne et al., 2005; Dyhrman

et al., 2006; Moorthi et al., 2006; Park et al., 2009a; Park & Park, 2010; Cary et al, 2014; Casabianca et al., 2014; Smith et al., 2014; Zhang et al., 2014).

The quantitative real-tim PCR (qPCR) methods quantify the dinoflagellate abundance by the following procedures: (1) detecting an increase in fluorescence during each PCR cycle, and (2) calculating the threshold cycle (Ct) of each reaction at a point where the fluorescence signal crosses a certain value (Cullen et al., 2002; Coyne et al., 2005; Fontaine and Guillot, 2002; Heid et al. 1996; Suzuki et al., 2000; Phister and Mills, 2003; Vaitomaa et al., 2003; Skovhus, 2004). Essentially, the qPCR method relies on the standard curves obtained by the serial dilution of DNA extracted from cultured target species (the DNA extraction and dilution method). However, this method can lead to unrealistic results compared to those measured by the microscopy based cell counting method since the amplification efficiencies of extracted DNA of cells obtained from laboratory cultures may not accurately represent the true amount of DNA of cells obtained from water samples collected from natural environments (Coyne et al., 2005). Furthermore, the extraction of DNA from cells obtained from field samples can be affected by unknown inhibitors, and thus, qPCR results can vary significantly in quantity and quality (Coyne et al., 2005). Therefore, improvement of this conventional method is needed.

The dinoflagellate *Cochlodinium polykrikoides* Margalef causes harmful red tides worldwide (Iwataki et al., 2008; Mikulski et al., 2008; Park et al., 2013a, 2014). Red tides caused by C. polykrikoides kill fish in aquaculture tanks within 2 hours by clogging fish gills when cell abundance exceeds approximately 1,000 cells mL^{-1} (Tang and Gobler, 2009; Lim et al., 2014). Thus, *C. polykrikoides* red tides have caused large economic losses in aquaculture industries in many countries (Park et al., 2013a). Detection of *C. polykrikoides* cells, accurate quantification

of their abundance, and early prediction of red tide outbreaks are some of the most critical steps in minimizing this economic loss. However, qualifying the abundance of *C. polykrikoides* using microscopy across great areas would require a large amount of time. Therefore, qPCR has been used to assess the abundance of *C. polykrikoides* in water samples. However, these methods sometimes provide results that do not reflect the actual abundance of these organisms and thus, improvement of this method is needed (Godhe et al., 2007; Blair et al., 2009; Erdner et al., 2010).

To improve method of quantifying abundance of *C. polykrikoides* using qPCR, the abundance of *C. polykrikoides* in natural water samples was measured using 4 different preparation methods to obtain the standard curve which is used to convert fluorescence to cell abundance. The four tested methods were: (1) extracting DNA from a dense culture of *C. polykrikoides* and then diluting the extracted DNA in serial (the CDD method), (2) extracting DNA from each of the serially diluted cultures with different concentrations of *C. polykrikoides* cultures (the CCD method), (3) extracting DNA from a dense field sample of *C. polykrikoides* collected from natural seawater and then diluting the extracted DNA in serial (the FDD method), and (4) extracting DNA from each of serially diluted field sample with different concentrations of *C. polykrikoides* (the FCD method). The result from each preparation was compared with those from direct cell enumeration by using dense *C. polykrikoides* samples obtained from patches collected from the waters off the coast of Tongyoung, Wando, and Yeosu-Namhae, South Sea, Korea during *C. polykrikoides* red tides in 2014 and 2015. The results of this study provide the basis for improving the accuracy of qPCR for quantifying the abundance of *C. polykrikoides* and possibly other dinoflagellates that are linked to red tides.

5.2. Material and Methods

5.2.1. Sample collection for standard curve generation and field sample test

For the quantitative real-time PCR (qPCR) amplification of field samples and standard curve conduction, the culture of *Cochlodinium polykrikoides* (CPTY0208) was used. The *C. polykrikoides* (CPTY0208) was originally isolated from Tongyoung, South Sea of Korea in 2002 (Table 4.1; Figs 5.1A, B). The strain was maintained 20 ℃ with continuous illumination at 10 μE m^{-2} s^{-1} with a cool white fluorescent light under a 14:10-h light-dark cycle and transferred to a new 2-L poly carbonate (PC) bottles containing F/2 medium approximately every 2-3 weeks. To determine cell abundance, a 10 mL aliquot of culture was fixed with 5% Lugol's solution and > 3,000 cells in triplicate 1-mL Sedgwick-Rafter counting (SRC) chambers were enumerated.

Futhermore, the water samples were collected from the surface of the coast of Wando, South Sea, Korea using a clean bucket in September 2015 during an intense *C. polykrikoides* red tide for the field sample test (Table 4.1.; Fig. 5.1A, B). The water samples were gently poured into 20 L PC bottles, after which 10 mL aliquots were taken from the bottles, fixed with 5% Lugol's solution, and examined under a compound microscope to determine cell abundances by enumerating cells in three 1 mL SRC chambers.
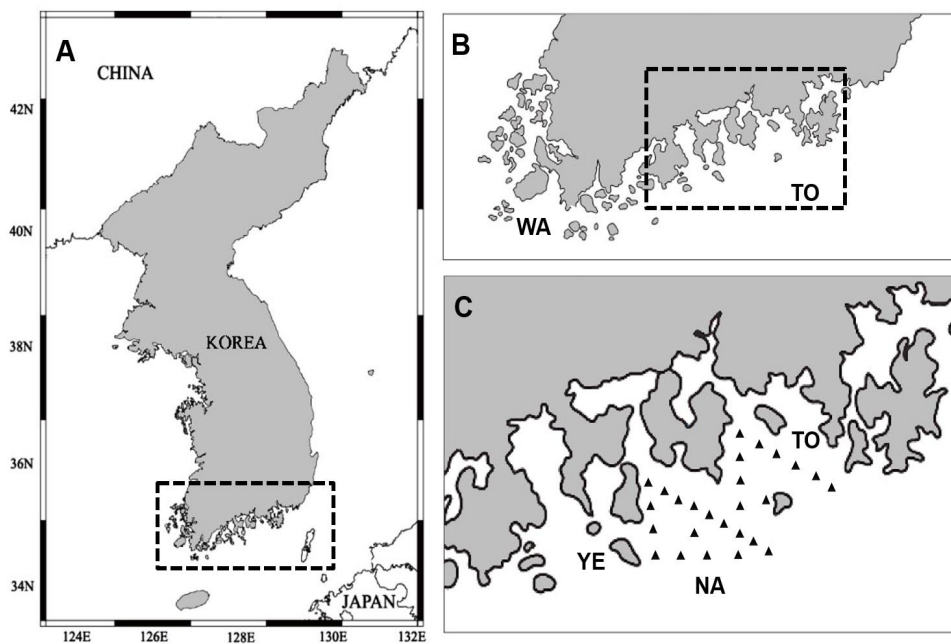
Fig. 5.1. Sampling locations of field samples used in this study. **A.** Map of Korea. **B.** Enlarged from (A). TO: Tongyoung. WA: Wando. **C.** Enlarged from (B). YE: Yeosu. NA: Namhae. Water samples were collected from 2 stations in WA and one station in TO in 2015 and from 26 stations (black triangle) in 2014.

Table 4.1. Four different preparation methods used to determine standard curves used in this study to determine the efficiency of real-time PCR in respect to the quantification of the red-tide dinoflagellate *Cochlodinium polykrikoides* and information on the origin of *C. polykrikoides.*

Method	Treatment	Type	Collection date	Collection area	Temp. (°C)	Salinity	Dilution of DNA (% of originally extracted DNA) or Actual cell concentration (cells ml^{-1})
CDD	DNA dilution first	Culture[*]	2002 08	Tongyoung, Korea	21.1	32.10	100%, 50%, 25%, 10%, 2%, 1%, 0.1%
CCD	Cell dilution first	Culture[*]	2002 08	Tongyoung, Korea	21.1	32.10	2.8, 14, 27, 139, 278, 695, 1390
FDD	DNA dilution first	Field sample[**]	2015 09	Wando, Korea	24.7	32.52	100%, 50%, 25%, 10%, 5%, 1%, 0.5%, 0.1%
FCD	Cell dilution first	Field sample[**]	2015 09	Wando, Korea	24.7	32.52	1.5, 7.3, 17, 85, 171, 427, 854, 1708

CDD. Standard curve determined with the dilution of DNA obtained directly from *C. polykrikoides* cultures; **CCD.** Standard curve determined with the cell dilution method using *C. polykrikoides* cultures; **FDD.** Standard curve determined with the DNA dilution method using field samples of *C. polykrikoides*; **FCD.** Standard curve determined with cell dilution methods using field samples of *C. polykrikoides*. [*]Cell concentration of the culture (2,780 cells ml^{-1}). [**]Cell concentration of the field sample (4,420 cells ml^{-1}).

5.2.2. Four different sample preparations utilized to determine standard curves

In this study, 4 different preparations of DNA materials for determining standard curves were tested (Fig. 5.2). In the first method, the DNA of cells from a dense *C. polykrikoides* culture was extracted and then the extracted DNA was serially diluted to obtain varying concentrations of DNA (i.e., cultured cells, DNA extraction & dilution, prepared using the CDD method). In the method utilized for cell harvesting, a 100 mL aliquot from a 2 L PC bottle containing a dense *C. polykrikoides* culture was filtered onto a 25 mm GF/C filter (Whatman Inc., Floreham Park, NJ). The filter was loosely rolled and placed into a 1.5 mL tube and stored at -20 °C in a freezer until the DNA extraction was conducted. The DNA from cells on the filter was extracted using the AccuPrep® Genomic DNA Extraction Kit (Bioneer Cooperation, Daejeon, Korea) under following condition. (1) 360 μL of Phosphate-Buffered Saline (PBS, Bioneer Cooperation, Daejeon, Korea) and Binding buffer 400 μl were added to the 1.5 ml tube with filter containing cells and 40 μl Protinase-K were also added to remove proteins from samples. (2) The mixtures were incubated in 60 °C for 10-30 min and further added 200 μL of isoprophanol for more accurate extraction of DNA from filter. (3) After 1 min of centrifuge in 13,000 rpm, upper solution were transferred to filter tube and maintained for 1 min. (4) After another 1 min of centrifuge in 13,000 rpm, wastes were removed and 500 μL of washing buffer were added. Step 4 were repeated 2 times. (5) To remove ethanol completely from sample, another 3 min of centrifuge in 13,000 rpm were performed. (6) Filters were transferred to new 1.5 ml tube and 50 μL of Elution buffer were added to obtain DNA from filter. (7) Obtained DNA were

stored at −20 °C in a freezer until following steps were performed.

With the extracted DNA, serial dilution were performed by adding predetermined volumes of deionized sterile water (DDW) (Bioneer, Daejeon, Korea) to the 1.5 mL tubes, to ultimately prepare 7 different DNA concentrations (100%, 50%, 20%, 10%, 2%, 1%, and 0.1%) (Table 4.1, Fig. 5.2A). This procedure was conducted in triplicate. Then samples were stored at −20 °C in the freezer until quantitative real-time PCR (qPCR) amplification was conducted.

In the second method tested, cells from the dense *C. polykrikoides* culture were serially diluted and then DNA from each concentration was extracted to obtain different quantities of DNA in each sample (i.e., cultured cells, cell dilution & DNA extraction, prepared using the CCD method). In this method, 7 different volumes from a 2 L PC bottle containing a dense *C. polykrikoides* culture were transferred into seven 800 mL PC bottles and then freshly filtered seawater were added to the bottles to make 7 different concentrations of *C. polykrikoides* cultures (100%, 50%, 20%, 10%, 2%, 1%, and 0.1%) (Table 4.1, Fig. 5.2B). A 100 mL aliquot was removed from each bottle and then cells were collected on a 25 mm GF/C filter. This procedure was conducted in triplicate. The extraction of DNA and the methods for elution and storage of the extracted DNA were the same as those utilized in the first method.

In the third method, the DNA of cells from a dense *C. polykrikoides* patch off Wando was extracted and then serially diluted to obtain different concentrations of DNA (i.e., field cells, DNA extraction & dilution, using the FDD method). In this method, to harvest cells, a 100 mL aliquot from a 20 L PC bottle containing a dense *C. polykrikoides* culture was filtered onto a 25 mm GF/C filter. This procedure was conducted in triplicate. The extraction of DNA and elution and storage

of the extracted DNA were the same as in the first method except that 8 different DNA concentrations were prepared (100%, 50%, 20%, 10%, 2%, 1%, 0.5%, and 0.1%) (Table 4.1, Fig. 5.2C).

In the fourth method, cells from the dense *C. polykrikoides* patch off Wando were serially diluted and then DNA from each concentration of cells was extracted to obtain different concentrations of DNA (i.e., field cells, cell dilution & DNA extraction, using the FCD method). In this method, 8 different volumes from a 20 L PC bottle containing the dense *C. polykrikoides* culture were transferred into eight 800 mL PC bottles and then freshly filtered seawater were added to the bottles to prepare 8 different concentrations of *C. polykrikoides* cells (100%, 50%, 20%, 10%, 2%, 1%, 0.5%, and 0.1%) (Table 4.1, Fig. 5.2D). A 100 mL aliquot was removed from each bottle and then cells were collected on a 25 mm GF/C filter. This procedure was conducted in triplicate. DNA extraction and elution and storage procedures for the extracted DNA were the same as those implemented in the second method.
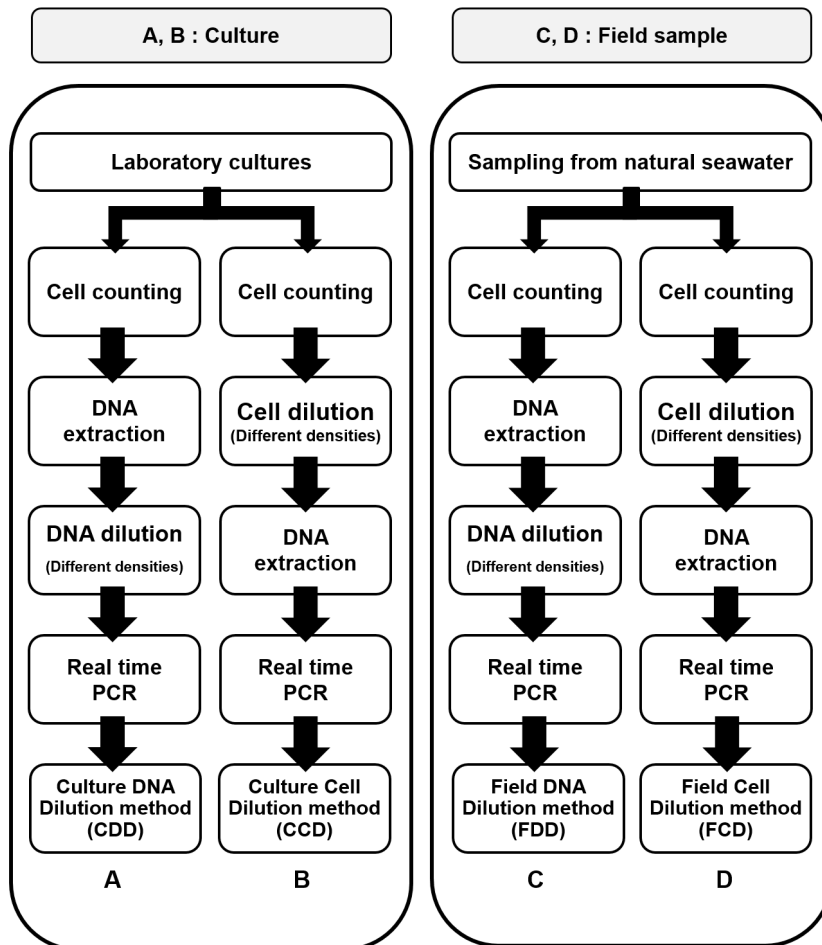
Fig. 5.2. Comparison of the processes used to prepare target DNA and cell concentrations in the 4 different methods. **A.** Standard curve determined with DNA dilution methods using *Cochlodinium polykrikoides* cultures (CDD). **B.** Standard curve determined with cell dilution methods using *C. polykrikoides* cultures (CCD). **C.** Standard curve determined with DNA dilution methods using field samples of *C. polykrikoides* (FDD). **D.** Standard curve determined with cell dilution methods using field samples of *C. polykrikoides* (FCD).

5.2.3. PCR amplification, sequencing, and phylogenetic analysis.

With extracted DNA of the cells from the cultured *C. polykrikoides* (CPTY0208), the large subunit ribosomal DNA (LSU rDNA) was amplified using D1RF (Scholin et al., 1994) as the forward primer and LSUB (Litaker et al., 2003) as the reverse primer (Table 4.2). For PCR amplification, SolgTM f-Taq DNA Polymerase[©] (SolGent Co., Daejeon, Korea) was used by following steps. (1) 1 μL of extracted DNA, 5 μL of 10x buffer, 1 μL of dNTP, 0.2 μM (final concentrations) of primers (forward and reverse), 0.25 μL of Taq polymerase and DDW was combined in a total final volume of 50 μL for each sample. The combined products were then amplified under following conditions: a 3 min initial denaturation at 94°C, followed by 38 cycles of 1 min at 95 °C, 1 min at 55 °C, and 3 min at 72 °C in series, and then one 5 min extension at 72 °C using GeneAmp PCR System 2700 (Perkin-Elmer, Boston, MA). Obtained PCR products were confirmed by loading on 1% agarose gel and stored in at −20 °C in a freezer until purification and sequencing analysis.

After amplification, the PCR products were purified using the AccuPrep[®] PCR purification kit (Bioneer Corp., Daejeon, Korea) according to the manufacturer's instructions. (1) 50 μL of PCR product were transferred to new 1.5 ml tube and combined with 250 μL of binding buffer. (2) Aquatic mixture were transferred to filter tube and centrifuged in 13,000 rpm for 1 min. (3) After removing disposal, 500 μL of Washing buffer were added and centrifuged in 13,000 rpm for 1 min. (4) Step 3 were repeated for 2 times. (5) To completely remove EtOH from filter, tubes were centrifuged again in 13,000 rpm for 3 min. (6) Filters were transferred to new 1.5 ml tube

and 30 μL of Elution buffer were added to obtain DNA from filter. (7) Sequence were obtained from purified DNA by using ABI PRISM 3730 DNA Analyzer (Applied Biosystems, Foster City, CA).

5.2.4. Design of TaqMan probe and primer set for detection.

In addition to the sequences of *C. polykrikoides* CPTY0208 obtained from PCR amplification, the available LSU rDNA sequences of *C. polykrikoides* and phylogenetically related dinoflagellate were obtained from GenBank (National Center for the Biotechnology Information, NCBI), and were aligned using MEGA v.4 (Tamura et al., 2007). Manual curation of the alignments was conducted to identify unique sequences and to develop a *C. polykrikoides* specific primer-probe set for the quantitative real-time PCR (qPCR) assay. The sequences for the primer-probe set were selected from the region that were conserved among *C. polykrikoides* strains, but allowed for discrimination from other dinoflagellates with coverage of 100-150 bp in length (Table 4.2). The primer and probe sequences of the target species were analyzed with Primer 3 (Whitehead Institute and Howard Hughes Medical Institute, MD) and Oligo Calc: Oligonucleotide Properties Calculator software (Kibbe, 2007), to determine the optimal melting temperature and secondary structure, and subsequently, the primers and probe were synthesized by Biosearch Technologies (CA, USA). The probe was dual-labeled with the fluorescent dyes FAM and BHQplus (Biosearch Technologies Inc., Novato, CA) at the 5' and 3' ends, respectively.

Table 4.2. Information on the primers and probes used in this study.

Type	Name	Sequence (5'-3')	Reference
Forward primer	D1RF	ACCCGGTGAATTTAAGCATA	Scholin et al., 1994
Reverse primer	LSUB	ACGAACGATTTGCACGTCAG	Litaker et al., 2003
Forward primer	CP4SF	AAGCGGATGGAACCAGTCC	This study
Reverse primer	CP4SR	CAAACGCGTTCACCCA	This study
Probe	CP4S	GTGGGGGTCATTGGTGATT	This study

5.2.5. Determination of cycle threshold (Ct) and standard curve conduction

The qPCR assays for determination of the standard curve obtained by each of the 4 different preparations were performed using the following steps: (1) 1 μL of DNA template, 0.2 μM (final concentrations) of primers (forward and reverse), 0.15 μM (final concentration) of probe and 5 μL of HiFast Probe Hi-Rox (Genepole, Gwangmyung, Korea) were combined in a total final volume of 10 μL, and DDW was added to each sample. The thermal cycling conditions for the qPCR assay were 2 min at 95 ℃, followed by 45 cycles of 10 s at 95 ℃, 45 s at 60 ℃, and 20 sec at 72 ℃ in series. The DNA of each sample was amplified 7-12 times to ensure accuracy of results and natural seawater samples without *C. polykrikoides* cells were used as the negative control.

For the comparison of the standard curves obtained by each of the 4 different preparations, the fluorescence of each reaction tube was quantified per cycle and the threshold for a positive reaction was automatically selected by using the default settings on the

accompanying qPCR instrument using Rotor-Gene Q Series Software (Qiagen, Hilden, Germany). Then, based on the result obtained, the threshold of all 4 standard curves was fixed at 0.0188, which was first automatically selected by the software, which showed most optimal florescence results. From the threshold, the threshold cycle (Ct) values, which were the intersection between the amplification curve and threshold line, were obtained.

The standard curve of each of the 4 different preparations was obtained by plotting Ct and log (cell abundance) determined by cell enumeration.

5.2.6. Determination of *Cochlodinium polykrikoides* cell abundance in field samples using the 4 different standard curves

To compare *C. polykrikoides* cell abundance in natural water samples as determined using the 4 different standard curves, the water samples collected from the surface of the coastal waters off of Tongyoung in August of 2015 (n = 24) and Wando in September of 2015 (n = 40) and from 3-5 depths at each of the 26 stations off Yeosu-Namhae, South Sea, Korea in September-October of 2014 (n = 505) during *C. polykrikoides* red tides were analyzed (Table 4.1; Fig. 5.1). The DNA extraction of *C. polykrikoides* cells from each sample and qPCR amplification were conducted as described above. Determination of cell abundance using microscopy was also conducted as described above.

5.3. Results

When the abundance of *C. polykrikoides* in the coastal waters off of Wando, September 2015 and in a laboratory clonal culture were 2–1700 cells mL^{-1}, the slopes of the regression lines of log (cell abundance determined by cell counting) as a function of threshold cycle (Ct) value and correlation coefficients (r^2) values obtained by using 4 different methods were each different (Fig. 5.3A–D). The r^2 values of two DNA dilution methods, the CDD (r^2 = 0.991) and FDD (r^2 = 0.984) methods (Fig. 5.3A, C) were slightly higher than that of two cell dilution methods, the CCD (r^2 = 0.951) and FCD (r^2 = 0.911) methods (Fig. 5.3B, D). The equations obtained by these results were applied to the qPCR results obtained from field samples collected during 2014 and 2015.

In the analyses of 505 field samples collected from 3–5 depths of 26 stations off Yeosu-Namhae in 2014, the slope of the regression line of *C. polykrikoides* cell abundance was calculated by cell counting as a function of the cell abundance determined by qPCR obtained using the CCD method was 0.929 (r^2 = 0.531, Fig. 5.4B), while the slope from the CDD method was 4.23 (r^2 = 0.441, Fig. 5.4A). The slope obtained using the FCD method was 1.16 (r^2 = 0.532, Fig. 5.4D), while from the FDD method, it was 1.52 (r^2 = 0.475, Fig. 5.4C).

In the analyses of the water samples collected from Tongyoung and Wando (n = 11) in 2015, the slope of the regression line of the cell abundance of *C. polykrikoides* assessed by cell enumeration as a function of the cell abundance determined by qPCR obtained using the CCD method was 1.03 (r^2=0.685, Fig. 5.5B), but that obtained using the CDD method was 3.92 (r^2=0.599, Fig. 5.5A). The slope calculated using the FCD method was 1.33 (r^2=0.687, Fig. 5.5D), while that from the FDD was 1.48 (r^2=0.629, Fig. 5.5C).
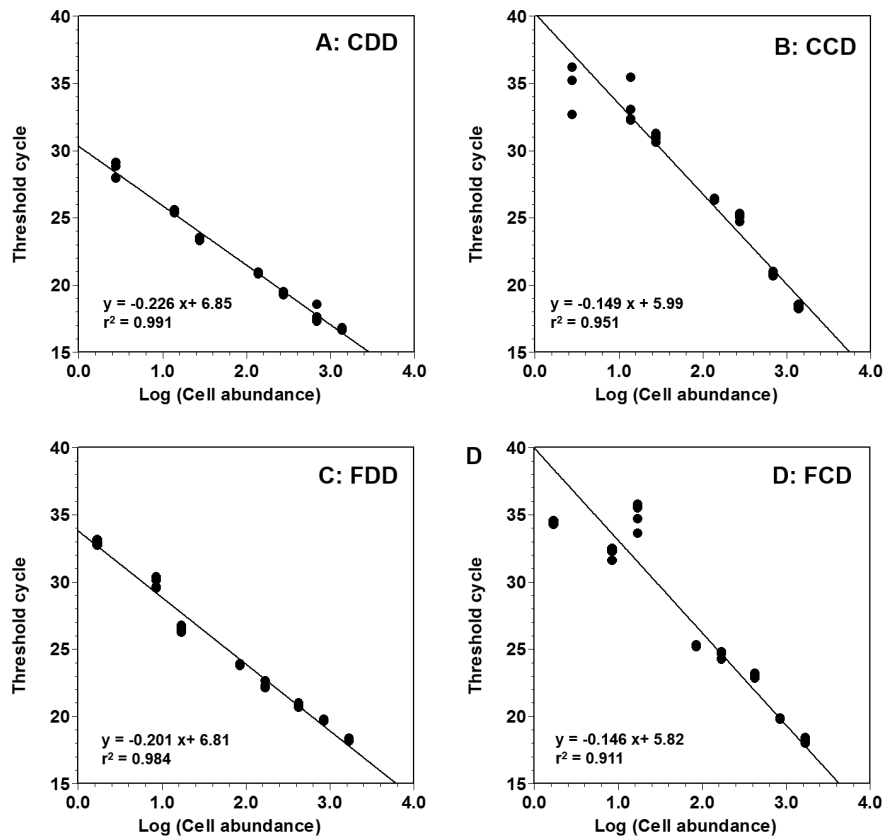
Fig. 5.3. The standard curves were determined by plotting log (cell abundance) as a function of the threshold cycle (Ct) in the DNA dilution (A and C) and the cell dilution (B and D) methods. **A.** Standard curve determined with serially diluted DNA of cultured *Cochlodinium polykrikoides* (CDD). **B.** Standard curve determined with serially diluted cell lysates of cultured *C. polykrikoides* (CCD). **C.** Standard curve determined with serially diluted DNA of *C. polykrikoides* collected from field water (FDD). **D.** Standard curve determined with serially diluted cell lysates of *C. polykrikoides* collected from field water (FCD).
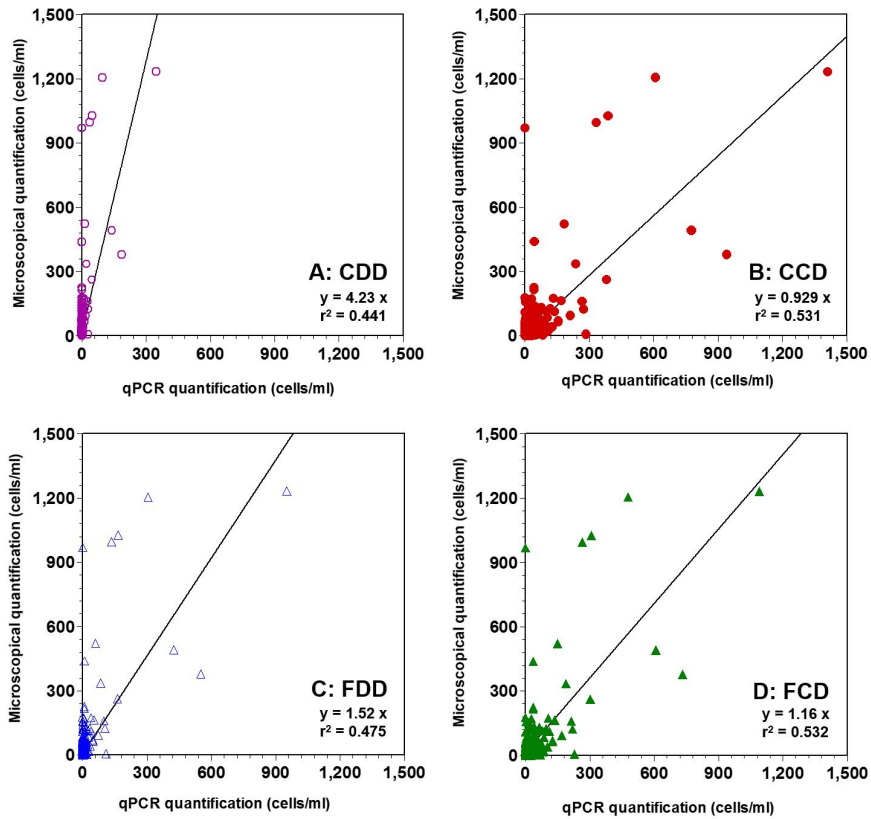
Fig. 5.4. Correlation between the cell abundance of *Cochlodinium polykrikoides* in the water samples collected from Yeosu-Namhae in 2014 obtained from qPCR (CAP, cells mL^{-1}) and cell enumeration (CAE, cells mL^{-1}) (n = 505). **A.** Correlation using the standard curve conducted with serially diluted DNA of cultured *C. polykrikoides* (CDD). **B.** Correlation using the standard curve conducted with serially diluted cell lysates of cultured *C. polykrikoides* (CCD). **C.** Correlation using the standard curve conducted with serially diluted DNA of *C. polykrikoides* collected from field water (FDD). **D.** Correlation using the standard curve conducted with serially diluted cell lysates of *C. polykrikoides* collected from field water (FCD). Symbols represent single treatment. The equations of the regression lines are as follows: (A) CAE = 4.23 (CAP), r^2 = 0.441; (B) CAE = 0.929 (CAP), r^2 = 0.531; (C) CAE = 1.52 (CAP), r^2 = 0.475; (D) CAE = 1.16 (CAP), r^2 = 0.532.

5.4. Discussion

Cochlodinium polykrikoides is one of the red tide species that have caused most serious damage in aquaculture industry in Korea and some other countries (Park et al., 2013). Due to its recurrent red tide events every year, Korea has spent tremendous amounts of annual budget. Thus, early detection of *C. polykrikoides* cells and quantifying its abundance are critical steps in reducing great loss due to its red tides. The conventional qPCR has been suggested to quantify the abundance of *C. polykrikoides* in large amounts of water samples in a short period and thus it was once developed. However, after analyzing several hundred samples, we realized that the conventional qPCR did not give the values similar to the real cell abundances of *C. polykrikoides*. This gives a task to improve this conventional method and conducted this study. The results of this study clearly showed that the cell abundance of *C. polykrikoides* obtained using the CCD method gave the values closest to the cell abundance determined by cell enumeration, while the CDD method, a conventional method, gave the values farthest from the cell abundance determined by cell enumeration. Thus, this improved method is suggested to use for quantifying the cell abundance of *C. polykrikoides*.
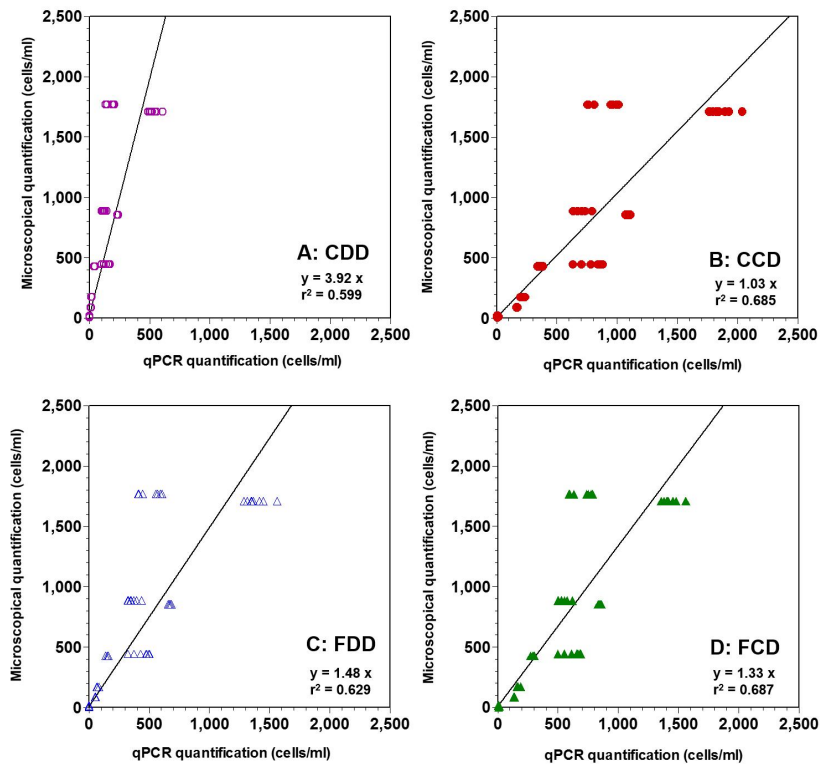
Fig. 5.5. Correlation between the cell abundance of *Cochlodinium polykrikoides* in water samples (n = 11) collected from Wando and Tongyoung in 2015 obtained from qPCR (CAP, cells ml⁻¹) and microscopic cell enumeration (CAE, cells ml⁻¹). **A.** Correlation using the standard curve determined with serially diluted DNA of cultured *C. polykrikoides* (CDD). **B.** Correlation using the standard curve conducted with serially diluted cell lysates of cultured *C. polykrikoides* (CCD). **C.** Correlation using the standard curve conducted with serially diluted DNA of *C. polykrikoides* collected from field water (FDD). **D.** Correlation using the standard curve conducted with serially diluted cell lysates of *C. polykrikoides* collected from field water (FCD). Symbols represent mean $\pm$ standard error. The equations for the regression lines areas follows : (A) CAE = 3.92 (CAP), r^2 = 0.599; (B) CAE = 1.03 (CAP), r^2 = 0.685; (C) CAE = 1.48 (CAP), r^2 = 0.629; (D) CAE = 1.33 (CAP), r^2 = 0.687.

In this study, a new specific primer and probe set for the detection of all 3 ribotypes of *C. polykrikoides* was developed. Thus, the new specific primer and probe set developed in this study can be used for detecting *C. polykrikoides* in waters where ≧ 2 ribotypes of *C. polykrikoides* co-exist as shown in Park et al. (2014).

When qPCR results were compared to the cell counting results under light microscopy, however, the abundances of these species in natural samples as revealed by qPCR have not matched well with those from the microscopic enumeration of cells. Some previous studies have also mentioned of this problem in other red tide species such as *Chattonella subsalsa*, *Heterosigma akakshiwo*, or *Alexandrium* species and offered dilution of field DNA samples to construct standard curve as substitutional method (Coyne et al., 2005; Galluzzi et al., 2010; Penna & Galluzzi, 2013). Thus, to improve accuracy of qPCR method of quantifying the abundance of these red tide species, it is worthwhile to compare the results from these 4 different preparation methods tested in this study.

Because standard curves obtained using fluorescence intensity and cell abundance are critical factors affecting variations in the abundances calculated, we compared conventional methods with modified methods that previous studies have proposed. This study is the first to compare the results from these 4 different methods, and results clearly showed that the 4 different methods yield different results.

For *C. polykrikoides,* which caused red tides in the South Sea of Korea in 2014-2015, the CCD was the most accurate method. In contrast, the result obtained using the conventional CDD method most dramatically varied from the abundance determined using cell enumerations. To the best of our knowledge, there have been no previous efforts to quantify the abundance of *C. polykrikoides* in

natural water samples using qPCR followed by a subsequent comparison of these results with the values obtained using traditional cell enumeration. Therefore, this study suggests that the CCD method should be utilized to quantify the abundance of *C. polykrikoides* in natural water samples. Moreover, the abundances of *C. polykrikoides* obtained using the CCD method were closer to the actual abundance than those determined using the CDD or FCD method than the FDD method. Therefore, the cell dilution methods (i.e., CCD and FCD) may be more accurate for the determination of the abundance of *C. polykrikoides* than the DNA dilution methods (i.e., CDD and FDD). On the contrary, the variation from the regression line of log (cell abundance) as a function of the threshold cycle (Ct) value, obtained by the CDD and FDD methods (i.e., higher r^2 value) were smaller than those found with the CCD and FCD (i.e., lower r^2 values). The DNA dilution methods are likely to ensure that the amount of DNA in the serial dilutionis closer to the target DNA concentration than that from the cell dilution methods (Fig. 5.6A). However, while the amount of DNA in each *C. polykrikoides* cell may be similar among cells, it may not be identical. Some studies reported that the amount and copy number of a certain portion of DNA in dinoflagellate cells even in a culture may vary (Gribble and Anderson, 2007; Park et al., 2007; Hou et al., 2010). Therefore, the concentration of DNA determined by qPCR by the CDD and FDD methods may not exactly match the cell numbers. The cell dilution methods are likely to ensure cell numbers in serial dilutions are closer to the target cell number than the DNA dilution methods (Fig. 5.6B). Therefore, the cell number determined by qPCR from DNA obtained using the CCD and FCD methods may match with the cell numbers more accurately than the DNA dilution methods.

Inhibitors in natural waters have been suggested to prevent the

amplification of DNA in PCR (Park et al., 2009b) reactions. However, the accuracy of the CCD method (slope = 0.929–1.03) is slightly higher than that from the FCD method (slope = 1.16–1.33). Therefore, the results of this study suggest that potential inhibitors in natural waters containing *C. polykrikoides* cells may not considerably inhibit the amplification of DNA in PCR reactions. Furthermore, using cultured *C. polykrikoides* cells for the qPCR methods may not be markedly different from using cells collected from sea samples.

Molecular techniques for detecting red tide cells and quantifying their abundance in natural water samples are rapidly improving. These techniques harbor select critical factors that can dramatically alter the final result. The results of this study suggest that the standard curve determined by the relationships between Ct and cell abundance is one of the most critical factors affecting accuracy in determining cell abundance in natural water samples.
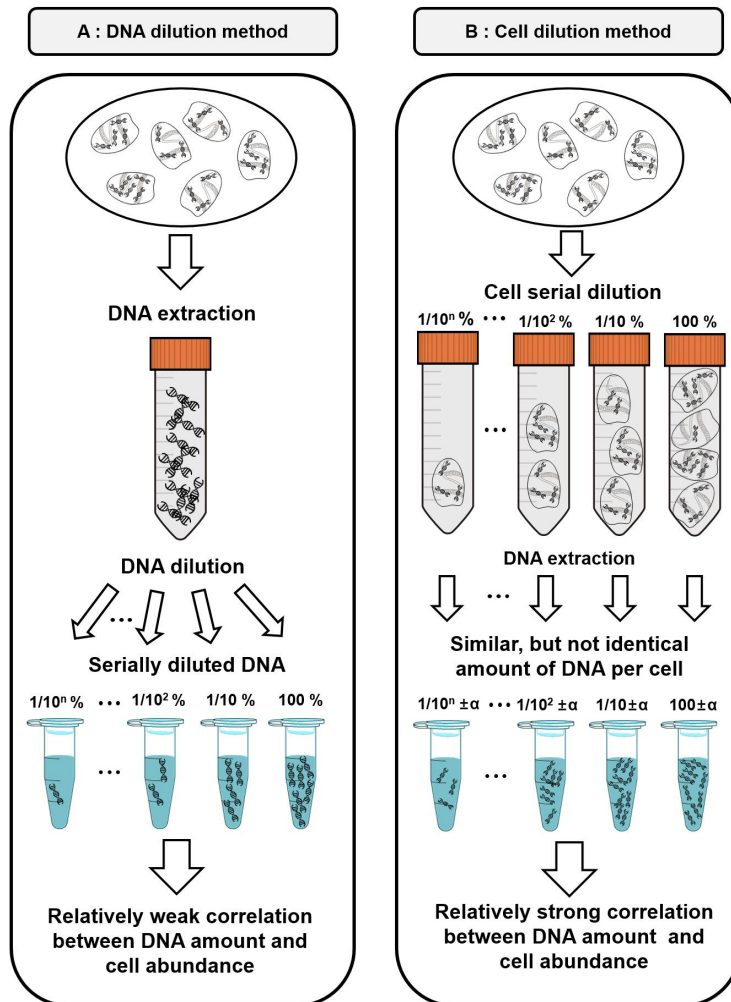
Fig. 5.6. Diagrams comparing of the quantity of DNA and cell number using the DNA dilution and cell dilution methods. **A.** DNA dilution method. The DNA concentration of each tube contains serially diluted DNA, and, therefore, correlation between DNA amount and cell abundance is relatively weak. **B.** Cell dilution method. Each tube contains serially diluted *Cochlodinium polykrikoides* cells and therefore correlation between DNA concentration and cell abundance is relatively strong.

Chapter 6. Overall Discussion

In this thesis, the overall methods for taxonomy, transcriptomic analysis, and quantification of cell concentrations of dinoflagellate species were improved and applied. Because dinoflagellate are one of the crucial components in marin food-web, understanding the ecological niches of these species are very important. Thus, to understand the ecological niches of dinoflagellate populations in the sea, morphology, phylogenetic relationships and genetic characteristics of dinoflagellate species are critical aspects to be exactly explored first. In this thesis, I reported new symbiotic dinoflagellate speices for the first time and worked further on the morphological and molecular characteristics of other sister species. Furthermore, to understand genetic relationship with trophic mode of dinoflagellates, *de novo* assembly of transcriptomes of the mixotrophic dinoflagellate and the heterotrophic dinoflagellates were compared. Finally, I modified the detection and quantification method to for a red tide dinoflagellate species.

The result of chapter 2 was examination of closely related phylogenetic lineages within symbiotic dinoflagellate genus *Symbiodinium* to find whether differences in morphology can be used together with genetic and ecological evidence to describe new species. Based on morphological and genetic comparisons, I recognized *Symbiodinium tridacnidorum* sp. nov., a new Indo-Pacific species. the new *Symbiodinium* species, *Sybiodinium tridacnidorum*, sp. nov. belonging to clade *A3* and reported its morphological and molecular characteristics for the first time. In addition, I found fixed differences in nuclear (internal transcribed spacer [ITS] and large subunit [LSU]) ribosomal DNA (rDNA), chloroplast (cp23S) and mitochondrial (cob) gene sequences from cultured and field-collected samples of *Symbiodinium*

microadriaticum (*sensu* Trench and Blank, 1987) and *Symbiodinium* sp. associated predominantly with giant clams and Pacific *Cassiopeia* jellyfish [comprising members of the ITS2 *A3* lineage, *sensu* LaJeunesse (2001)]. Furthermore, I additionally described the amphiesmal plate tabulations of original strain of *Symbiodinium microadriaticum* (CCMP2464) which was used by Trench and Blank, and based on this result, and amphiesmal plate tabulations of two strains of new *Symbiodinium speices* of clade *A3*, *Symbiodinium tridacnidorum* (CCMP832 and rt-272) cultured from Indo-Pacific giant clams in the subfamily Tridacninae. When these tabulations were compared to other reported *Symbiodinium* species including *S. voratum* (Clade E) and *S. natans* (clade A), the amount of morphological differentiation between species did not correspond to their degree of genetic divergence and this result represent that each *Symbiodinium* clade may consisted of several species. Thus, this chapter clearly showed that two genetically distinct strains of *S. tridacnidorum* obtained from different regions of the Pacific Ocean have stable morphology among individuals which differ from other species, while species belong to identical clades may have variations in size, shape, number and in arragement of their amphiesmal plates and can have variations due to the genetic and ecological differences. In addition, result of this chapter provides complete morphological standard for the *Symbiodinium* species.

The result of chapter 3 provided the morphological diagnose of recently established two clade B Symbiodinim species, *Symbiodinium minutum* and *Symbiodinium psygmorphilum* for the first time. In addition, these results were compared to morphology of currently reported *Symbiodinium* species including species beloning to clade A and E. Interestingly, the results obtained from this chapter showed that the plate formulae and plate shapes of *S. minutum* and *S. psygmophilum*

are morphologically distinct from other known species (between clades) and also had differences one another (within clade). Thus, we confirm the species status of *S. minutum* and *S. psygmophilum* based on morphological and genetic characters and report the detailed morphological characteristics of these two species. In addition, this study suggests that the species in the same clade may have somewhat different plate shapes due to its molecular differences such as clades, or ecological differences such as hosts or locations in the species. Therefore, both molecular genetic and morphological characterizations should be combined to fully describe a species in *Symbiodinium*.

The result of chapter 4 compared the *de novo* assembly of transcriptomes of the mixotrophic dinoflagellate *Paragymnodinium shiwhaense* and the heterotrophic dinoflagellate *Gyrodiniellum shiwhaense*. The expressed genes discovered by transcriptome analysis showed big dissimilarities, although there were many similar genes. Especially, among the 21,932 unigenes expressed in *P. shiwheaense*, 3615 unigenes (16.5%) were expressed in *G. shiwhaense*, while among the 10,805 unigenes expressed in *G. shiwhaense*, 3449 unigenes (31.9%) were expressed in *P. shiwheaense*. The numbers of the expressed unigenes of *P. shiwhaense* were approximately 35–50% greater than those of *G. shiwhaense*. In particular, *P. shiwhaense* had 12 and 13 genes in the photosystem I and II, respectively, while *G. shiwhaense* had 9 and 8 genes, respectively. Furthermore, *P. shiwhaense* had all 12 genes related to the Calvin cycle that can run all 7 complete pathways related to the regeneration process in the cycle, while *G. shiwhaense* did not have the ribulose-5 phosphate isomerase (Rpi) gene and Phosphoribulokinase (PRK) gene and thus cannot run any complete pathway. Based on the absence of the Rpi and PRK gene and uncapablity of running any of the Calvin cycle pathways, it is

suggested that *G. shiwhaense* is likely to be evolved from mixotrophic dinoflagellates with losing many genes, in particular genes related to photosynthesis and/or *P. shiwhaense* from heterotrophic dinoflagellates with acquiring genes related to photosynthesis.

The result of chapter 5 provides the modification of most effective method to detect the red-tide ichthyotoxic dinoflagellate *Cochlodinium polykrikoides* by developing new species-specific primer and probe set for detecting all 3 ribotypes of *C. polykrikoides* and comparatively evaluated the efficiencies of 4 different preparation methods used to determine standard curves. Each methods yielded different results and to confirm the accuracy of result, the abundance of *C. polykrikoides* in the samples collected from the coastal waters of South Sea, Korea, in 2014-2015, obtained using the standard curves determined by the CCD methods, the method using standard curve obtained by extraction of DNA from each of the serially diluted cultures with different concentrations of *C. polykrikoides* cultures, and the FCD methods, extracting DNA from each of serially diluted field sample with different concentrations of *C. polykrikoides* were the most similar (0.93-1.03 times) and the second closest (1.16-1.33 times) to the actual cell abundances obtained by enumeration of cells. Thus, our results suggest that the CCD method is a more effective tool to quantify the abundance of *C. polykrikoides* than the conventional method, which uses standard curves obtained by extraction of DNA from a dense culture of *C. polykrikoides* followed by serial dilution of the extracted DNA (CDD method).

To conclude, the result of this thesis will provide overall understanding of taxonomy of dinoflagellate species especially symbiotic dinoflagellates by providing complete morphological standard for the *Symbiodinium* species. Furthermore, the comparative transcriptome

analysis of dinoflagellates possessing different trophic modes will provide better understanding of genetic influence to the trophic mode of dinoflagellate species. Finally, the improved qPCR methods and devlopment of new specific primer and probe set reflecting the 2 recently discovered ribotypes of the most critical red-tide dinoflagellate species in Korean aquaculture industry, *C. polykrikoides*, will contribute to the advanced researches on red tide dynamics by *C. polykrikoide*.

References

Abramoff, M. D., Magalhaes, P. J., Ram, S. J. 2004. Image processing with Image. J. Biophotonics Int. 11:36-42.

Anderson, D.M., 1997. Turning back the harmful red tide. Nature 388, 513–514.

Baillie, B. K., Belda-Baillie, C. A., Maruyama, T., 2000. Conspecificity and Indo-Pacific distribution of *Symbiodinium* genotypes (Dinophyceae) from giant clams. J. Phycol., 36: 1153–61.

Barshis, D.J., Ladner, J.T., Oliver, T.A., Palumbi, S.R., 2014. Lineage-specific transcriptional profiles of *Symbiodinium* spp. unaltered by heat stress in a coral host. Mol. Biol. Evol. 31 (6): 1343-1352.

Baums, I. B., Devlin-Durante M. K., LaJeunesse, T. C., 2014. New insights into the dynamics between reef corals and their associated dinoflagellate endosymbionts from population genetic studies. Molecular Ecology, 23: 4203–4215.

Bayer, T., Aranda, M., Sunagawa, S., Yum, L. K., DeSalvo, M. K., Lindquist, E., Coffroth, M. A., Voolstra, C. R., Medina, M., 2012. *Symbiodinium* transcriptomes: genome insights into the dinoflagellate symbionts of reef-building corals. PloS

Blair, D., Momigliano, P., Garrard, S., Heimann, K., 2009. Review of genetic probe development for invasive marine species, with a focus on choice of target gene and on DNA amplification technology. In March Interim Report (Part 2) to the Marine and Tropical Sciences Research Facility (p. 33). Reef and Rainforest

Research Centre Limited Cairns.

Bowers, H. A., Tengs, T., Glasgow, H. B., Burkholder, J. M., Rublee, P. A., Oldach, D. W., 2000. Development of real-time PCR assays for rapid detection of *Pfiesteria piscicida* and related dinoflagellates. Appl. Environ. Microbiol. 66 (11), 4641-4648

Brandt, K, 1881. Ueber das Zusammenleben von Thieren und Algen. Verhandlungen der Physikalischen Gesellschaft zu Berlin, 1881-82: 22-26.

Carlos, A. A., Baillie, B. K., Brett, K., Kawaguchi, M., Maruyama T, 1999. Phylogenetic position of *Symbiodinium* (Dinophyceae) isolates from tridacnids (Bivalvia), cardiids (Bivalvia), a sponge (Porifera), a soft coral (Anthozoa), and a free-living strain. J. Phycol., 35: 1054-62.

Cary, S. C., Coyne, K. J., Rueckert, A., Wood, S. A., Kelly, S., Gemmill, C. E., Vieglais, C., Hicks, B. J., 2014. Development and validation of a quantitative PCR assay for the early detection and monitoring of the invasive diatom *Didymosphenia geminata*. Harmful Algae 36, 63-70.

Casabianca, S., Perini, F., Casabianca, A., Battocchi, C., Giussani, V., Chiantore, M., Penna, A., 2014. Monitoring toxic Ostreopsis cf. ovata in recreational waters using a qPCR based assay. Mar. Pollut. Bull. 88 (1), 102-109.

Coffroth, M. A., Santos, S. R. 2005. Genetic Diversity of Symbiotic Dinoflagellates in the Genus *Symbiodinium.* Protist 156:19-34.

Conesa, A., Götz, S., García-Gómez, J. M., Terol, J., Talón, M., Robles, M., 2005. Blast2GO: a universal tool for annotation, visualization

and analysis in functional genomics research. Bioinformatics, 21 (18): 3674-3676.

Coyne, K. J., Handy, S. M., Demir, E., Whereat, E. B., Hutchins, D. A., Portune, K. J., Doblin, M. A., Cary, S. C., 2005. Improved quantitative real-time PCR assays for enumeration of harmful algal species in field samples using an exogenous DNA reference standard. Limnol. Oceanogr.-Meth. 3 (9), 381-391.

Cullen, D. W., Lees, A. K., Toth, I. K., Duncan, J., 2002. Detection of *Colletotrichum coccodes* from soil and potato tubers by conventional and quantitative real-time PCR. Plant. Pathol. 51 (3), 281-292.

DeBoer, T. S., Baker, A. C., Erdmann, M. V., Ambariyanto, Jones, P. R., Barber, P. H, 2012. Patterns of *Symbiodinium* distribution in three giant clam species across the biodiverse Bird's Head region of Indonesia. Marine Ecology Progress Series, 444: 117-132.

Diekmann, O. E., Olsen, J. L., Stam, W. T., Bak, R. P. M. 2003. Genetic variation within *Symbiodinium* clade B from the coral genus Madracis in the Caribbean (Netherlands Antilles. Coral Reefs 22:29-33.

Dyhrman, S. T., Erdner, D., La Du, J., Galac, M., Anderson, D. M., 2006. Molecular quantification of toxic *Alexandrium fundyense* in the Gulf of Maine using real-time PCR. Harmful Algae 5 (3), 242-250.

Erdner, D. L., Anderson, D. M., 2006. Global transcriptional profiling of the toxic dinoflagellate *Alexandrium fundyense* using massively parallel signature sequencing. BMC genomics, 7: 88.

Erdner, D. L., Percy, L., Keafer, B., Lewis, J., Anderson, D. M., 2010. A quantitative real-time PCR assay for the identification and enumeration of Alexandrium cysts in marine sediments. Deep-Sea. Res. Pt. II. 57 (3), 279-287.

Fay, S. A., Weber, M. X., J. H., Lipps, J. H. 2009. The distribution of *Symbiodinium* diversity within individual host foraminifera. Coral Reefs 28:717-726.

Finney, J.C., Pettay, T., Sampayo, E.M., Warner, M.E., Oxenford, H. LaJeunesse, T.C, 2010. The relative significance of host-habitat, depth, and geography on the ecology, endemism and speciation of coral endosymbionts. Microbial Ecology, 60: 250–263.

Fitt, W. K, 1985. Effect of different strains of the zooxanthellae *Symbiodinium microadriaticum* on growth and survival of their coelenterate and molluscan hosts. Proc. 5th Int. Coral Reef Congr., 6: 131–136.

Fontaine, M., Guillot, E., 2002. Development of a TaqMan quantitative PCR assay specific for *Cryptosporidium parvum*. Fems. Microbiol. Lett. 214 (1): 13-17.

Freudenthal, H. D, 1962. *Symbiodinium* gen. nov. and *Symbiodinium microadriaticum* sp. nov., a zooxanthella: taxonomy, life cycle, and morphology. J. Protozool. 9: 45–52.

Galluzzi, L., Bertozzini, E., Penna, A., Perini, F., Garcés, E., Magnani, M., 2010. Analysis of rRNA gene content in the Mediterranean dinoflagellate *Alexandrium catenella* and *Alexandrium taylori*: implications for the quantitative real-time PCR-based monitoring methods. J. Appl. Phycol. 22 (1), 1-9.

Galluzzi, L., Penna, A., Bertozzini, E., Vila, M., Garcés, E., Magnani, M., 2004. Development of a real-time PCR assay for rapid detection and quantification of *Alexandrium minutum* (a dinoflagellate). Appl. Environ. Microbiol. 70 (2), 1199-1206.

Gavelis, G.S., White, R.A., Suttle, C.A., Keeling, P.J., Leander, B.S., 2015. Single-cell transcriptomics using spliced leader PCR: Evidence for multiple losses of photosynthesis in polykrikoid dinoflagellates. BMC genomics 16: 528.

Giovannoni, S. J., DeLong, E. F., Olsen, G. J., Pace, N. R, 1988. Phylogenetic group-specific oligodeoxynucleotide probes for identification of single microbial cells. J. Bacteriol., 170: 720–726.

Godhe, A., Cusack, C., Pedersen, J., Andersen, P., Anderson, D. M., Bresnan, E., Cembella, A., Dahl, E., Diercks, S., Elbrächter, M., Edler, L., Galluzzi, L., Gescher, C., Gladstone, K., Karlson, B., Kulis, D., LeGresley, M., Lindahl, O., Marin, R., McDermott, G., Medlin, L. K., Naustvoll, L., Penna, A., Töbe, K., 2007. Intercalibration of classical and molecular techniques for identification of *Alexandrium fundyense* (Dinophyceae) and estimation of cell densities. Harmful Algae 6 (1): 56-72.

Gómez, F. 2012. A quantitative review of the lifestyle, habitat and trophic diversity of dinoflagellates (Dinoflagellata, Alveolata. Syst. Biodivers. 10: 267-275.

Gou, W. L., Sun, J., Li, X. Q., Zhen, Y., Xin, Z., Yu, Z. G., Li, R. X. 2003. Phylogenetic analysis of a free-living strain of *Symbiodinium* isolated from Jiaozhou Bay, P.R. China. J. Exp. Mar. Biol. Ecol. 296:135-144.

Gray, M., Wawrik, B., Paul, J., Casper, E., 2003. Molecular detection

and quantitation of the red tide dinoflagellate *Karenia brevis* in the marine environment. Appl. Environ. Microbiol. 69 (9): 5726–5730.

Gribble, K. E., Anderson, D. M. 2007. High intraindividual, intraspecific, and interspecific variability in large-subunit ribosomal DNA in the heterotrophic dinoflagellates *Protoperidinium*, *Diplopsalis*, and *Preperidinium* (Dinophyceae. Phycologia, 46(3), 315–324.

Guillard, R. R. L., Hargraves, P. E, 1993. *Stichochrysis immobilis* is a diatom, not a chysophyte. Phycologia, 32: 234–236.

Guo, R., Wang, H., Suh, Y.S., Ki, J.S., 2016. Transcriptomic profiles reveal the genome-wide responses of the harmful dinoflagellate *Cochlodinium polykrikoides* when exposed to the algicide copper sulfate. BMC genomics 17 : 29.

Hallegraeff, G.M., 1993. A review of harmful algal blooms and their apparent global increase. Phycologia 32, 79–99.

Hansen, G., Daugbjerg, N. 2009. *Symbiodinium natans* sp. nov.: a free-living dinoflagellate from Tenerife (northeast-Atlantic Ocean. J. Phycol. 45:251–263.

Hansen, P.J. 1991. Quantitative importance and trophic role of heterotrophic dinoflagellates in a coastal pelagial food web. Mar. Ecol. Prog. Ser. 73:253–261.

Hartz, A. J., Sherr, B. F., Sherr, E. B., 2011. Photoresponse in the heterotrophic marine dinoflagellate *Oxyrrhis marina*. J. Eukaryot. Microbiol., 58: 171–177.

Heid, C. A., Stevens, J., Livak, K. J., Williams, P. M., 1996. Real time quantitative PCR. Genome. Res. 6 (10), 986–994.

Heisler, J., Glibert, P. M., Burkholder, J. M., Anderson, D. M., Cochlan, W., Dennison, W. C., Dortch, Q., Gobler, C. J., Heil, C. A., Humphries, E., Lewitus, A., Magnien, R., Marshall, H. G.,Sellner, K., Stockwell, D. A., Stoecker, D. K., Suddleson, M., 2008. Eutrophication and harmful algal blooms: a scientific consensus. Harmful algae, 8 (1): 3-13.

Hennige, S. J., Suggett, D. J., Warner, M. E., McDougall, K. E., Smith, D. J, 2009. Photobiology of *Symbiodinium* revisited: bio-physical and bio-optical signatures. Coral Reefs, 28: 179-95.

Hill, M., Allenby, A., Ramsby, B., Schonberg, C., Hill, A. 2011. *Symbiodinium* diversity among host clionaid sponges from Caribbean and Pacific reefs: Evidence of heteroplasmy and putative host-specific symbiont lineages. Mol. Phylogenet. Evol. 59:81-88.

Hirose, M., Reimer J. D., Hidaka M., Suda S, 2008. Phylogenetic analyses of potentially free-living *Symbiodinium* spp. isolated from coral reef sand in Okinawa, Japan. Marine Biology, 155: 105-112.

Holland S. B., Dawson, M. N., Crow G. L., Hofmann D. K, 2004. Global phylogeography of Cassiopea (Scyphozoa: Rhizostomeae): molecular evidence for cryptic species and multiple invations of the Hawaiian Islands. Marine Biology, 145: 1119-1128.

Hou, Y., Zhang, H., Miranda, L., Lin, S., 2010. Serious overestimation in quantitative PCR by circular (supercoiled) plasmid standard: microalgal *pcna*asthemodelgene.PLoSOne,5(3),e9545.

Huerta-Cepas, J., Szklarczyk, D., Forslund, K., Cook, H., Heller, D., Walter, M. C., Rattei, T., Mende, D. R., Sunagawa, S., Kuhn, M., Jensen, L. J., von Mering, C., Bork, P., 2015. eggNOG 4.5: a

hierarchical orthology framework with improved functional
annotations for eukaryotic, prokaryotic and viral sequences.
Nucleic Acids Res, 44 (D1): D286-D293.

Iglesias-Prieto, R., Matta, J. L., Robins, W. A., Trench, R. K. 1992.
Photosynthetic response to elevated temperature in the symbiotic
dinoflagellate *Symbiodinium microadriaticum* in culture
(bleaching/coral reefs). Proc. Natl. Acad. Sci. USA 89:
10302-10305.

Iwataki, M., Kawami, H., Mizushima, K., Mikulski, C. M., Doucette, G. J.,
Relox, J. R., Anton, A., Fukuyo, Y., Matsuoka, K., 2008.
Phylogenetic relationships in the harmful dinoflagellate
Cochlodinium polykrikoides (Gymnodiniales, Dinophyceae) inferred
from LSU rDNA sequences. Harmful Algae 7 (3): 271-277.

Jeong, H. J. 1999. The ecological roles of heterotrophic dinoflagellates
in marine planktonic community. J. Eukaryot. Microbiol.
46:390-396.

Jeong, H. J., Park, J.K., Choi, H.Y., Yang, J.S., Shim, J.H., Shin, Y.K.,
Yih, W.H., Kim, H.S., Cho, K.J., 2000. The outbreak of red tides
in the coastal waters off Kohung, Chonnam, Korea. 2. The
temporal and spatial waters variations in the phytoplanktonic
community in 1997. J. Kor. Soc. Oceanogr. 5: 27-36 (written in
Korean with English abstract).

Jeong, H. J., Yoo, Y. D., Kim, J. S., Seong, K. A., Kang, N. S., Kim, T.
H., 2010. Growth, feeding and ecological roles of the mixotrophic
and heterotrophic dinoflagellates in marine planktonic food webs.
Ocean Sci, 45 (2): 65-91.

Jeong, H. J., Lee, K. H., Yoo, Y. D., Kang, N. S., Lee, K., 2011.

Feeding by the Newly Described, Nematocyst-Bearing Heterotrophic Dinoflagellate *Gyrodiniellum shiwhaense*. J Eukaryot Microbiol, 58 (6): 511-524.

Jeong, H. J., Yoo, Y. D., Kang, N. S., Lim, A. S., Seong, K. A., Lee, S. Y., Lee, M. J., Lee, K. H., Kim, H. S., Shin, W. G., Nam, S.W., Yih, W. H., Lee, K. 2012. Heterotrophic feeding as a newly identified survival strategy of the dinoflagellate *Symbiodinium*. Proc. Natl. Acad. Sci. USA. 109: 12604-12609.

Jeong, H. J., Yoo, Y. D., Lee, K. H., Kim, T. H., Seong, K. A., Kang, N. S., Lee, S. Y., Kim, J. S., Kim, S., Yih, W. H. 2013. Red tides in Masan Bay, Korea in 2004-2005: I. Daily vari- ations in the abundance of red-tide organisms and environmental factors. Harmful Algae 30 (Suppl. 1): S75-S88.

Jeong, H. J., Lee, S. Y., Kang, N. S., Yoo, Y. D., Lim, A. S., Lee, M. J., Kim, H. S., Yih, W. H., Lajeunesse, T. C. 2014a. Genetics and morphology characterize the dinoflagellate *Symbiodinium voratum*, n. sp., (Dinophyceae) as the sole representative of *Symbiodinium* clade E. J. Eukaryot. Microbiol. 61: 75-94.

Jeong, H. J., Lim, A. S., Yoo, Y. D., Lee, M. J., Lee, K. H., Jang, T.Y., Lee, K. 2014b. Feeding by heterotrophic dinoflagellates and ciliates on the free-living dinoflagellate *Symbiodinium* sp, Clade E. J. Eukaryot. Microbiol. 61: 27-41

Jeong, H. J., Lim, A. S., Franks, P. J., Lee, K. H., Kim, J. H., Kang, N. S., Lee, M. J., Jang, S. H., Lee, S. Y., Yoon, E. Y., Park, J. Y., Yoo, Y. D., Seong, K.A., Kwon, J.E., Jang, T.Y., 2015. A hierarchy of conceptual models of red-tide generation: nutrition, behavior, and biological interactions. Harmful Algae, 47, 97-115.

Jiang, Y. P., Cheng, F., Zhou, Y. H., Xia, X. J., Shi, K., Yu, J. Q., 2012. Interactive effects of CO 2 enrichment and brassinosteroid on CO 2 assimilation and photosynthetic electron transport in *Cucumis sativus*. Environ Exp Bot 75:98-106.

Kang, N. S., Jeong, H. J., Moestrup, Ø., Shin, W., Nam, S. W., Park, J. Y., de Salas, M. F., Kim K. W., Noh, J. H., 2010. Description of a new planktonic mixotrophic dinoflagellate *Paragymnodinium shiwhaense* n. gen., n. sp. from the coastal waters off western Korea: morphology, pigments, and ribosomal DNA gene sequence. J Eukaryot Microbiol, 57 (2): 121-144.

Kang, N. S., Jeong, H. J., Moestrup, Ø., Park, T. G., 2011. *Gyrodiniellum shiwhaense* n. gen., n. sp., a new planktonic heterotrophic dinoflagellate from the coastal waters of western Korea: morphology and ribosomal DNA gene sequence. J Eukaryot Microbiol, 58 (4): 284-309.

Kang, N. S., Lee, K. H., Jeong, H. J., Yoo, Y. D., Seong, K. A., Potvin, É., Hwang, Y. J., Yoon, E. Y. 2013. Red tides in Shiwha Bay, western Korea: a huge dike and tidal power plant established in a semi-enclosed embayment system. Harmful Algae, 30 (Suppl. 1): S114-S130.

Keeling, P.J., Burki, F., Wilcox, H.M., Allam, B., Allen, E.E., Amaral-Zettler, L.A., Armbrust, E.V., Archibald, J.M., Bharti, A.K., Bell, C.J., Beszteri, B., Bidle, K.D., Cameron, C.T., Campbell, L., Caron, D.A., Cattolico, R.A., Collier, J.L., Coyne, K., Davy, S.K., Deschamps, P., Dyhrman, S.T., Edvardsen, B., Gates, R.D., Gobler, C.J., Greenwood, S.J., Guida, S.M., Jacobi, J.L., Jakobsen, K.S., James, E.R., Jenkins, B., John, U., Johnson, M.D., Juhl, A.R., Kamp, A., Katz, L.A., Kiene, R., Kudryavtsev, A., Leander, B.S.,

Lin, S., Lovejoy, C., Lynn, D., Marchetti, A., McManus, G., Nedelcu, A.M., Menden-Deuer, S., Miceli, C., Mock, T., Montresor, M., Moran, M.A., Murray, S.A., Nadathur, G., Nagai, S., Ngam, P.B., Palenik, B., Pawlowski, J., Petroni, G., Piganeau, G., Posewitz, M.C., Rengefors, K., Romano, G., Rumpho, M.E., Rynearson, T., Schilling, K.B., Schroeder, D.C., Simpson, A.G.B., Slamovits, C.H., Smith, D.R., Smith, G.J., Smith, S.R., Sosik, H.M., Stief, P., Theriot, E., Twary, S.N., Umale, P.E., Vaulot, D., Wawrik, B., Wheeler, G.L., Wilson,W.H., Xu, Y., Zingone, A.,Worden, A.Z., 2014. The Marine Microbial Eukaryote Transcriptome Sequencing Project (MMETSP): illuminating the functional diversity of eukaryotic life in the oceans through transcriptome sequencing. PLoS Biol. 12 (6), e1001889.

Kevin, J. M., Hall, T. W., McLaughlin, J. J. A., Zahl, P. A. 1969. *Symbiodinium microadriaticum* Freudenthal, a revised taxonomic description, ultrastructure. J. Phycol. 5:341–350.

Kibbe, W. A., 2007. OligoCalc: an online oligonucleotide properties calculator. Nucleic. Acids. Res. 35 (suppl 2), W43-W46.

Kim, G. H., Jeong, H. J., Yoo, Y. D., Kim, S., Han, J. H., Han, J. W., Zuccarello, G. C., 2013a. Still acting green: Continued expression of photosynthetic genes in the heterotrophic dinoflagellate *Pfiesteria piscicida* (Peridiniales, Alveolata. PloS one, 8 (7): e68232.

Kim, J. S., Jeong, H. J., Yoo, Y. D., Kang, N. S., Kim, S. K., Song, J. Y., Lee, M. J., Kim, S. T., Kang, J. H., Seong, K. A., Yih, W. H. 2013b. Red tides in Masan Bay, Korea, in 2004-2005: III. Daily variation in the abundance of mesozooplankton and their grazing impacts on red-tide organisms. Harmful Algae 30S: S102-S113.

Kleffmann, T., Russenberger, D., von Zychlinski, A., Christopher, W., Sjölander, K., Gruissem, W., Baginsky, S., 2004. The *Arabidopsis thaliana* chloroplast proteome reveals pathway abundance and novel protein functions. Curr Biol, 14: 354-362.

Kudela, R. M. Gobler, C. J, 2012. Harmful dinoflagellate blooms caused by *Cochlodinium* sp.: Global expansion and ecological strategies facilitating bloom formation. Harmful Algae, 14: 71-86.

LaJeunesse, T. C, 2001. Investigating the biodiversity, ecology, and phylogeny of endosymbiotic dinoflagellates in the genus *Symbiodinium* using the internal transcribed spacer region: in search of a "species" level marker. J. Phycol., 37: 866-880.

LaJeunesse, T. C. 2002. Diversity and community structure of symbiotic dinoflagellates from Caribbean coral reefs. Mar. Biol. 141:387-400.

LaJeunesse, T. C., Thornhill, D. J., Cox, E., Stanton, F., Fitt, W. K., Schmidt, G. W, 2004a. High diversity and host specificity observed among symbiotic dinoflagellates in reef coral communities from Hawaii. Coral Reefs, 23: 596-603.

LaJeunesse, T. C., Bhagooli, R., Hidaka, M., DeVantier, L., Done, T., Schmidt, G. W., Fitt, W. K., Hoegh-Guldberg, O, 2004b. Closely related *Symbiodinium* spp. differ in relative dominance in coral reef host communities across environmental, latitudinal and biogeographic gradients. Mar. Ecol. Prog. Ser., 284: 147-161.

LaJeunesse, T. C., Loh, W., Trench, R. K, 2009. Do Introduced endosymbiotic dinoflagellates 'take' to new hosts? Biological Invasions, 11: 995-1003.

LaJeunesse T. C., Pettay, T., Sampayo, E. M., Phongsuwan, N., Brown,

B., Obura, D., Hoegh-Guldberg, O. Fitt, W. K, 2010. Long-standing environmental conditions, geographic isolation and host-symbiont specificity influence the relative ecological dominance and genetic diversification of coral endosymbionts in the genus *Symbiodinium.* J. Biogeogr., 37: 785–800.

LaJeunesse, T. C., Thornhill, D. J, 2011. Improved resolution of reef-coral endosymbiont (*Symbiodinium*) species diversity, ecology, and evolution through psbA non-coding region genotyping. PloS ONE, 6: e29013.

LaJeunesse, T. C., Parkinson, J. E., Reimer, J. D. 2012. A genetics-based description of *Symbiodinium minutum* sp. nov. and *S. psygmophilum* sp. nov, Dinophyceae), two dinoflagellates symbiotic with Cnidaria. J. Phycol., 48:1380–1391.

LaJeunesse, T. C., Wham, D. C., Pettay, D. T., Parkinson, J. E., Keshavmurthy, S., Chen, C. A., 2014. Ecologically differentiated stress tolerant endosymbionts in the dinoflagellate genus *Symbiodinium* Clade D are different species. Phycologia, 53: 305–319.

LaJeunesse, T. C., Lee, S. Y., Gil-Agudelo, D. L., Knowlton, N., Jeong, H. J., 2015. *Symbiodinium necroappetens* sp. nov. (Dinophyceae): an opportunist 'zooxanthella' found in bleached and diseased tissues of Caribbean reef corals. European J. Phycol, 50 (2): 223-238.

Larkin, M. A., Blackshields, G., Brown, N. P., Chenna, R., McGettigan, P. A., McWilliam, H., Valentin, F., Wallace, I. M., Wilm, A., Lopez, R., Thompson, J. D., Gibson, T. J., Higgins, D.G, 2007. Clustal w and clustal x version 2.0. Bioinformatics, 23: 2947–2948.

Lee, C., Park, T., Park, Y., Lim, W., 2013. Monitoring and trends in harmful algal blooms and red tides in Korean coastal waters, with emphasis on *Cochlodinium polykrikoides*. Harmful Algae, 30S: S3–S14.

Lee, K. H., Jeong, H. J., Jang, T. Y., Lim, A. S., Kang, N. S., Kim, J. H., Kim, K. Y., Park, K-. T., Lee, K. 2014a. Feeding by the newly described mixotrophic dinoflagellate *Gymnodinium smaydae*: feeding mechanism, prey species, and effect of prey concentration. J. Exp. Mar. Biol. Ecol. 459:114–125.

Lee, R., Lai, H., Malik, S. B., Saldarriaga, J. F., Keeling, P. J., Slamovits, C. H., 2014b. Analysis of EST data of the marine protist *Oxyrrhis marina*, an emerging model for alveolate biology and evolution. BMC genomics, 15 (1): 15–122.

Lee, S. K., Jeong, H. J., Jang, S. H., Lee, K. H., Kang, N. S., Lee, M. J., Potvin, É., 2014c. Mixotrophy in the newly described dinoflagellate *Ansanella granifera*: feeding mechanism, prey species, and effect of prey concentration. Algae, 29: 137–152.

Lee, S. Y., Jeong, H. J., Kang, N. S., Jang, T. Y., Jang, S. H., Lim, A. S., 2014d. Morphological characterization of *Symbiodinium minutum* and *S. psygmophilum* belonging to clade B. Algae, 29: 299–310.

Lee, M. J., Jeong, H. J., Lee, K. H., Jang, S. H., Kim, J. H., Kim, K. Y., 2015a. Mixotrophy in the nematocyst-taeniocyst complex-bearing phototrophic dinoflagellate *Polykrikos hartmannii*. Harmful Algae, 49: 124–134.

Lee, S. Y., Jeong, H. J., Kang, N. S., Jang, T. Y., Jang, S. H., Lajeunesse, T. C., 2015b. *Symbiodinium tridacnidorum* sp. nov., a dinoflagellate common to Indo-Pacific giant clams, and a revised

morphological description of *Symbiodinium microadriaticum* Freudenthal, emended Trench & Blank. Eur J Phycol, 50 (2): 155-172.

Lewis, C. L., Coffroth, M. A. 2004. The acquisition of exogenous algal symbionts by an octocoral after bleaching. Science 304:1490-1492.

Lim, A. S., Jeong, H. J., Jang, T. Y., Jang, S. H., Franks, P. J. S. 2014. Inhibition of growth rate and swimming speed of the harmful dinoflagellate *Cochlodinium polykrikoides* by diatoms: Implications for red tide formation. Harmful Algae 37:53-61.

Lin, S., Cheng, S., Song, B., Zhong, X., Lin, X., Li, W., Cai, M., Li, L., Zhang, Y., Zhang, H., Ji, Z., Cai M., Zhuang, Y., Shi, X., Lin, L., Wang, L., Wang, Z., Liu, X., Yu, S,, Zeng, P., Hao, H., Zou Q., Chen C., Li Y., Wang, Y., Xu, C., Meng, S., Xu, X., Wang, J., Yang, H., Campbell, D. A., Sturm, N. R., Dagenais-Bellefeuille, S., Morse, D., 2015. The *Symbiodinium kawagutii* genome illuminates dinoflagellate gene expression and coral symbiosis. Science, 350: 691-694.

Litaker, R. W., Vandersea, M. W., Kibler, S. R., Reece, K. S., Stokes, N. A., Steidinger, K. A., Millie, D. F., Bendis, B. J., Pigg, R. J., Tester, P. A., 2003. Identification of *Pfiesteria piscicida* (Dinophyceae) and Pfiesteria-Like organisms using internal transcribed spacer-specific PCR assays. J. Phycol., 39 (4): 754-761.

Lobban C. S., Schefter, M. Simpson, A. G. B., Pochon, X., Pawlowski, J. Foissner, W, 2002. Maristentor dinoferus n. gen., n. sp. a giant heterotrich ciliate (Spirotrichea: Heterotrichida) with zooxanthellae, from coral reefs on Guam, Mariana Islands. Marine Biology, 140: 411-423.

Loeblich, A. R. III., Sherley, J. L. 1979. Observations on the theca of the mobile phase of free-living and symbiotic isolates of Zooxanthella microadriaticum (Freudenthal) comb.nov. J. Mar. Biol. Assoc. U. K.. 59:195-205.

Lowe, C. D., Mello, L. V., Samatar, N., Martin, L. E., Montagnes, D. J., Watts, P. C., 2011. The transcriptome of the novel dinoflagellate *Oxyrrhis marina* (Alveolata: Dinophyceae): response to salinity examined by 454 sequencing. BMC genomics, 12: 519.

McLaughlin, J. J., Zahl, P. A, 1966. Endozoic algae. In Symbiosis volume 1 (Henry, S. M, editor), 257-297. Academic Press Incorporation, New York.

Mikulski, C. M., Park, Y. T., Jones, K. L., Lee, C. K., Lim, W. A., Lee, Y., Scholin, C. A., Doucette, G. J., 2008. Development and field application of rRNA-targeted probes for the detection of *Cochlodinium polykrikoides* Margalef in Korean coastal waters using whole cell and sandwich hybridization formats. Harmful Algae 7 (3), 347-359.

Moestrup, Ø., Hansen, G., Daugbjerg, N., Lundholm, N., Overton, J., Vestergård, M., Steenfeldt, S.J., Calado, A.J., Hansen, P.J., 2014. The dinoflagellates *Pfiesteria shumwayae* and *Luciella masanensis* cause fish kills in recirculation fish farms in Denmark. Harmful Algae, 32:33–39.

Moorthi, S. D., Countway, P. D., Stauffer, B. A., Caron, D. A., 2006. Use of quantitative real-time PCR to investigate the dynamics of the red tide dinoflagellate *Lingulodinium polyedrum*. Microbial. Ecol. 52 (1): 136-150.

Morey, J. S., Monroe, E. A., Kinney, A. L., Beal, M., Johnson, J. G.,

Hitchcock, G. L., Van Dolah, F. M., 2011. Transcriptomic response of the red tide dinoflagellate, *Karenia brevis,* to nitrogen and phosphorus depletion and addition. BMC genomics, 12: 346.

Murray, S. A., Suggett, D. J., Doblin, M. A., Kohli, G. S., Seymour, J. R., Fabris, M., Ralph, P. J., 2016. Unravelling the functional genetics of dinoflagellates: a review of approaches and opportunities. PiP, 37-52.

Norton J. H., Shepherd M. A., Long H. M. Fitt W. K, 1992. The zooxanthellal tubular system in the giant clam. The Biological Bulletin, 183: 503-506.

Park, T. G., de Salas, M. F., Bolch, C. J., Hallegraeff, G. M., 2007. Development of a real-time PCR probe for quantification of the heterotrophic dinoflagellate *Cryptoperidiniopsis brodyi* (Dinophyceae) in environmental samples. Appl. Environ. Microbiol. 73 (8), 2552-2560.

Park, T. G., Park, G. H., Park, Y. T., Kang, Y. S., Bae, H. M., Kim, C. H., Jeong, H. J., Lee, Y. 2009a. Identification of the dinoflagellate community during *Cochlodinium polykrikoides* (Dinophyceae) blooms using amplified rDNA melting curve analysis and real-time PCR probes. Harmful Algae 8 (3), 430-440.

Park, T. G., Park, Y. T., Lee, Y., 2009b. Development of a SYTO9 based real-time PCR probe for detection and quantification of toxic dinoflagellate *Karlodinium veneficum* (Dinophyceae) in environmental samples. Phycologia 48 (1), 32-43.

Park, T. G., Park, Y. T., 2010. Detection of *Cochlodinium polykrikoides* and *Gymnodinium impudicum* (Dinophyceae) in sediment samples from Korea using real-time PCR. Harmful Algae 9 (1), 59-65.

Park, J., Jeong, H. J., Yoo, Y.D., Yoon, E.Y., 2013a. Mixotrophic dinoflagellate red tides in Korean waters: distribution and ecophysiology. Harmful Algae 30S, S28–S40.

Park, M. G., Kim, S., Shin, E-. Y., Yih, W., Coats, D. W. 2013b. Parasitism of harmful dinoflagellates in Korean coastal waters. Harmful Algae 30S:S62–S74.

Park, B. S., Wang, P., Kim, J. H., Kim, J. H., Gobler, C. J., Han, M. S., 2014. Resolving the intra-specific succession within *Cochlodinium polykrikoides* populations in southern Korean coastal waters via use of quantitative PCR assays. Harmful Algae, 37: 133-141.

Penna, A., Galluzzi, L., 2013. The quantitative real-time PCR applications in the monitoring of marine harmful algal bloom (HAB) species. Environ. Sci. Pollut. R. 20(10), 6851-6862.

Phister, T. G., Mills, D. A., 2003. Real-time PCR assay for detection and enumeration of *Dekkera bruxellensis* in wine. Appl. Environ. Microbiol. 69 (12): 7430-7434.

Pinzón, J. H., 2011. Phylogenetics, population genetics and ecology to understand the evolution of coral-algal mutualisms. Dissertation Penn State, pp. 153

Pinzón, J. H., Devlin-Durante M. K., Weber, X. M., Baums, I. B. LaJeunesse, T. C, 2011. Microsatellite loci for *Symbiodinium* A3 (*S. fitti*) a common algal symbiont among Caribbean Acropora (stony corals) and Indo-Pacific giant clams (Tridacna. Conservation Genetics Resources, 3: 45–47.

Pochon, X., Garcia-Cuestos, L., Baker, A. C., Castella, E., Pawlowski, J. 2007. One-year survey of a single Micronesian reef reveals

extraordinarily rich diversity of *Symbiodinium* types in sorited foraminifera. Coral Reefs, 26: 867–882

Pochon, X., Gates, R. D. 2010. A new *Symbiodinium* clade (Dinophyceae) from soritid foraminifera in Hawai´i. Mol. Phylogenet. Evol. 56:492–497.

Pochon, X., Putnam, H. M., Burki, F., Gates, R. D, 2012. Identifying and characterizing alternative molecular markers for the symbiotic and free-living dinoflagellate genus *Symbiodinium.* PloS ONE, 7: e29816.

Porter, K. G, 1988. Phagotrophic phytoflagellates in microbial food webs. Hydrobiologia, 159 (1): 89–97.

Porto, I., Granados, C., Restrepo, J. C., Sanchez, J. A, 2008. Macroalgal-associated dinoflagellates belonging to the genus *Symbiodinium* in Caribbean reefs. PloS ONE, 3: e2160.

Pozdnyakov, I.A., Skarlato, S.O., 2015. Analysis of the dinoflagellate *Prorocentrum minimum* transcriptome: Identifying the members of the voltage-gated cation channel superfamily. Cell Tissue Biol. 9 (6): 483–492.

Probert, I., Siano, R., Poirier, C., Decelle, J., Biard, T., Tuji, A., Suzuki, N., Not, F, 2014. *Brandtodinium* gen. nov. and *B. nutricula* comb. nov. (Dinophyceae), a dinoflagellate commonly found in symbiosis with polycystine radiolarians. J. Phycol., 50: 388–399.

Raines, C. A, 2003. The Calvin cycle revisited. Photosynthesis research, 75(1): 1–10.

Richardson, E., Dorrell, R. G., Howe, C. J., 2014. Genome-wide transcript profiling reveals the coevolution of plastid gene

sequences and transcript processing pathways in the fucoxanthin dinoflagellate *Karlodinium veneficum*. Mol. Biol. Evol. 31 (9): 2376-2386.

Rio, D. C., Ares, M., Hannon, G. J., Nilsen, T. W., 2010. Purification of RNA using TRIzol (TRI reagent. Cold Spring Harb Protoc, 2010 (6): pdb-prot5439.

Rodriguez-Lanetty, M., Chang, S. J., Song, J. I. 2003. Specificity of two temperate dinoflagellate-anthozoan associations from the north-western Pacific Ocean. Mar. Biol. 143:1193-1199.

Rogers, Y. H., Venter, J. C., 2005. Genomics: massively parallel sequencing. Nature, 437 (7057): 326-327.

Ronquist, F., Huelsenbeck, J. P, 2003. MRBAYES 3: Bayesian phylogenetic inference under mixed models. Bioinformatics, 19: 1572–1574.

Rowan, R., Powers, D. A, 1991. A molecular genetic classification of zooxanthellae and the evolution of animal-algal symbiosis. Science, 251: 1348–1351.

Rowan, R., Knowlton, N. 1995. Intraspecific diversity and ecological zonation in coral-algal symbiosis. Proc. Natl. Acad. Sci. USA. 92:2850-2853.

Rowan, R., Whitney, S. M., Fowler, A. Yellowlees, D, 1996. Rubisco in marine symbiotic dinoflagellates: Form II enzymes in eukaryotic oxygenic phototrophs encoded by a nuclear multigene family. Plant Cell, 8: 539–553.

Ryan, D. E., Pepper, A. E., Campbell, L., 2014. *De novo* assembly and characterization of the transcriptome of the toxic dinoflagellate

Karenia brevis. BMC genomics 15 (1): 1.

Salcedo, T., Upadhyay, R. J., Nagasaki, K., Bhattacharya, D., 2012. Dozens of toxin-related genes are expressed in a nontoxic strain of the dinoflagellate *Heterocapsa circularisquama*. Mol. Biol. Evol., 29: 1503-1506.

Salvucci, M. E., Portis, A. R., Ogren, W. L, 1986. Light and CO2 response of ribulose-1, 5-bisphosphate carboxylase/oxygenase activation in *Arabidopsis* leaves. Plant physiology, 80 (3): 655-659.

Sampayo, E., Dove, S., LaJeunesse, T. C. 2009. Cohesive molecular genetic data delineate species diversity in the dinoflagellate genus *Symbiodinium.* Molecular Ecology, 18: 500–519.

Sanchez-Puerta, M. V., Lippmeier, J. C., Apt, K. E., Delwiche, C. F., 2007. Plastid genes in a non-photosynthetic dinoflagellate. Protist, 158: 105-117.

Santos, S. R. Taylor, D. J., Coffroth M. A, 2001. Genetic comparisons of freshly isolated vs. cultured symbiotic dinoflagellates: implications for extrapolating to the intact symbiosis. J. Phycol., 37: 900–912.

Santos, S.R., Kinzie III, R.A., Sakai, K., Coffroth, M.A. 2003. Molecular characterization of nuclear small subunit (18S)-rDNA pseudogenes in a symbiotic dinoflagellate (Symbiodinium, Dinophyta). J. Eukaryot. Microbiol. 50:417-421.

Scholin, C. A., Herzog, M., Sogin, M., Anderson, D. M., 1994. Identification of group-and strain-specific genetic markers for globally distributed *Alexandrium* (Dinophyceae). II. Sequence analysis of a fragment of the LSU rRNA gene. J. Phycol. 30 (6), 999-1011.

Secord, D., Kareiva, P, 1996. Perils and pitfalls in the host specificity paradigm. BioScience, 46: 448–453.

Seong, K. A., Jeong, H. J. 2013. Interactions between marine bacteria and red tide organisms in Korean waters. Algae 28:297–305.

Sherr, E.B., Sherr, B.F., 2007. Heterotrophic dinoflagellates: a significant component of microzooplankton biomass and major grazers of diatoms in the sea. Mar. Ecol. Prog. Ser. 352, 187–197.

Shoguchi, E., Shinzato, C., Kawashima, T., Gyoja, F., Mungpakdee, S., Koyanagi, R., Takeuchi, T., Hisata, K., Tanaka, M., Fujiwara, M., Hamada, M., Seidi, A., Fujie, M., Usami, T., Goto, H., Yamasaki, S., Arakaki, N., Suzuki, Y., Sugano, S., Toyoda, A., Kuroki, Y., Fujiyama, A., Medina, M., Coffroth, M.A., Bhattacharya, D., Satoh, N., 2013. Draft assembly of the *Symbiodinium minutum* nuclear genome reveals dinoflagellate gene structure. Curr. Biol. 23 (15): 1399–1408.

Skovhus, T. L., Ramsing, N. B., Holmström, C., Kjelleberg, S., Dahllöf, I., 2004. Real-time quantitative PCR for assessment of abundance of *Pseudoalteromonas* species in marine samples. Appl. Environ. Microbiol. 70 (4), 2373–2382.

Slamovits, C. H., Keeling, P. J., 2008. Plastid-derived genes in the nonphotosynthetic Alveolate *Oxyrrhis marina*. Mol Biol Evol, 25: 1297–1306.

Slamovits, C. H., Keeling, P. J., 2010. Contributions of *Oxyrrhis marina* to molecular biology, genomics and organelle evolution of dinoflagellates. J Plankton Res, 33: 591–602.

Smith, K. F., de Salas, M., Adamson, J., Rhodes, L. L., 2014. Rapid and

accurate identification by real-time PCR of biotoxin-producing dinoflagellates from the family *Gymnodiniaceae*. Marine drugs, 12 (3): 1361-1376.

Spurr, A. R. 1969. A low viscosity epoxy resin embedding medium for electron microscopy. J. Ultrastruct. Res. 26:31-42.

Stamatakis, A., 2006. RAxML-VI-HPC: maximum likelihood-based phylogenetic analyses with thousands of taxa and mixed models. Bioinformatics 22: 2688-2690.

Stanley Jr, G. D. 2006. Photosymbiosis and the evolution of modern coral reefs. Science312:857-858.

Stat, M., Bird C. E., Pochon X., Chasqui L. Chauka, L. J., Concepcion, G. T., Logan, D., Takabayashi, M., Toonen, R. J. Gates, R. D, 2011. Variation in *Symbiodinium* ITS2 sequence assemblages among coral colonies. PloS ONE, 6: e15854

Stat, M., Carter, D., Hoegh-Guldberg, O. 2006. The evolutionary history of *Symbiodinium* and scleractinian hosts – Symbiosis, diversity, and the effect of climate change. Perspect. Plant Ecol. Evol. Syst. 8:23-43.

Stoecker, D.K., 1999. Mixotrophy among dinoflagellates. J. Eukaryot. Microbiol. 46 (4): 397-401.

Streusand, V. J., Portis, A. R, 1987. Rubisco activase mediates ATP-dependent activation of ribulose bisphosphate carboxylase. Plant Physiology, 85(1): 152-154.

Suzuki, M. T., Taylor, L. T., DeLong, E. F., 2000. Quantitative analysis of small-subunit rRNA genes in mixed microbial populations via 5'-nuclease assays. Appl. Environ. Microbiol. 66 (11): 4605-4614.

Tamura, K., Dudley, J., Nei, M., Kumar, S., 2007. MEGA4: molecular evolutionary genetics analysis (MEGA) software version 4.0. Mol. Biol. Evol. 24 (8), 1596–1599.

Tang, Y., Gobler, C.J., 2009. Characterization of the toxicity of *Cochlodinium polykrikoides* isolates from Northeast US estuaries to finfish and shellfish. Harmful Algae, 8: 454–462.

Taylor, D. L, 1974. Symbiotic marine algae; taxonomy and biological fitness. In Symbiosis in the Sea (Vernberg, W. B., editor), 245–262. University of South Carolina Press, Columbia.

Teich, R., Zauner, S., Baurain, D., Brinkmann, H., Petersen, J., 2007. Origin and distribution of Calvin cycle fructose and sedoheptulose bisphosphatases in plantae and complex algae: a single secondary origin of complex red plastids and subsequent propagation via tertiary endosymbioses. Protist, 158: 263–276.

Thornhill, D. J., Lewis, A., Wham, D.C., LaJeunesse, T. C, 2014. Host-specialist lineages dominate the adaptive radiation of reef coral endosymbionts. Evolution, 68: 352–267.

Trench, R. K., Blank, R. J, 1987. *Symbiodinium microadriaticum* Freudenthal, *S. goreauii* sp. nov., *S. kawagutii* sp. nov., and *S. pilosum* sp. nov.: Gymnodinioid dinoflagellate symbionts of marine invertebrates. J. Phycol., 23: 469–481.

Trench, R. K, 1993. Microalgal-invertebrate symbioses: A review. Endocytobiosis Cell Research, 9: 135–175.

Trench, R. K, 2000. Validation of some currently used invalid names of dinoflagellates. J. Phycol., 36: 972.

Vaitomaa, J., Rantala, A., Halinen, K., Rouhiainen, L., Tallberg, P.,

Mokelke, L., Sivonen, K., 2003. Quantitative real-time PCR for determination of microcystin synthetase E copy numbers for *Microcystis* and *Anabaena* in lakes. Appl. Environ. Microbiol. 69 (12): 7289-7297.

Wang, D. Z., Zhang, H., Zhang, Y., Zhang, S. F., 2014. Marine dinoflagellate proteomics: Current status and future perspectives. J. Proteomics., 105: 121-132.

Weber, M. X, 2009. The Biogeography and Evolution of *Symbiodinium* in Giant Clams (Tridacnidae. PhD Dissertation, 119, University of California, Berkeley.

Wilson, A. T., Calvin, M, 1955. The photosynthetic cycle. CO2 dependent transients. Journal of the American Chemical Society, 77(22): 5948-5957.

Yamashita, H., Koike, K, 2013. The genetic identity of free-living *Symbiodinium* obtained over a broad latitudinal range in the Japanese coast. Phycological Research, 61: 68-80.

Yang, I., Beszteri, S., Tillmann, U., Cembella, A., John, U. 2011. Growth-and nutrient-dependent gene expression in the toxigenic marine dinoflagellate *Alexandrium minutum*. Harmful Algae, 12: 55-69.

Yoo, Y. D., Jeong, H. J., Kang, N. S., Song, J. Y., Kim, K. Y., Lee, G., Kim, J., 2010. Feeding by the newly described mixotrophic dinoflagellate *Paragymnodinium shiwhaense*: feeding mechanism, prey species, and effect of prey concentration. J. Eukaryot. Microbiol., 57: 145-158.

Yoo, Y. D., Jeong, H. J., Kim, J. S., Kim, T. H., Kim, J. H., Seong, K. A., Lee, S. H., Kang, N. S., Park, J. W., Park, J., Yoon, E. Y., Yih, W. H. 2013. Red tides in Masan Bay, Korea in 2004-2005: II.

Daily variations in the abundance of het- erotrophic protists and their grazing impact on red-tide organisms. Harmful Algae 30S: S89-S101.

Zardoya, R., Costas. E., Lopez-Rodas, V., Garrido-Pertierra, A. Bautista, J.M, 1995. Revised dinoflagellate phylogeny inferred from molecular analysis of large subunit ribosomal RNA gene sequences. Journal of Molecular Evolution, 41: 637-645.

Zhang, Z., Green, B. R., Cavalier-Smith, T, 2000. Phylogeny of ultra-rapidly evolving dinoflagellate chloroplast genes: A possible common origin for sporozoan and dinoflagellate plastids. J. Mol. Evol., 51: 26-41.

Zhang, H., Bhattacharya, D., Lin, S., 2005. Phylogeny of dinoflagellates based on mitochondrial cytochrome b and nuclear small subunit rDNA sequence comparisons. J. Phycol., 41: 411-420.

Zhang, F., Shi, Y., Jiang, K., Song, W., Ma, C., Xu, Z., Ma, L., 2014. Rapid detection and quantification of *Prorocentrum minimum* by loop-mediated isothermal amplification and real-time fluorescence quantitative PCR. J. Appl. Phycol., 26 (3): 1379-1388.

Zhang, S., Sui, Z., Chang, L., Kang, K., Ma, J., Kong, F., Zhou, W., Wang, J., Guo, L., Geng, H., Zhong, J., Ma, Q., 2014. Transcriptome de novo assembly sequencing and analysis of the toxic dinoflagellate *Alexandrium catenella* using the Illumina platform. Gene 537 (2): 285-293.

국문초록

　와편모조류는 해양생태계에서 가장 우점하는 생물군이자 다양한 방식으로 생존을 유지하는 원생생물이다. 이들은 적조를 유발하여 해양생태계에 피해를 주는 것으로 잘 알려져 있지만 그 외에도 이들은 해양생태계에서 먹이, 포식자, 공생자 그리고 기생자로써 다양한 역할을 수행한다. 그러나 일부 와편모조류의 경우 그 분류학적 특징이나 생태 및 생리적 특성과 연관된 유전적 특징의 연구, 또는 자연환경에서의 정량 및 분포 등을 규명하기가 극히 어려운 상태에 있다. 이에 본 논문은 1) 유전적, 형태적 분류를 통하여 공생성 와편모조류의 신종 발굴 및 분류 기준 확립과, 2) 유전체 분석을 통해 와편모류의 섭식양상과 광합성에 대한 유전체 발현 양상간의 비교분석, 그리고 3) 적조를 유발하여 피해를 주는 와편모조류 종의 빠르고 정확한 탐지 및 정량측정 방법의 개발에 관해 연구를 수행하였다.

　와편모조류 중, 대표적인 공생성 와편모조류인 심바이오디니움은 산호, 해파리, 말미잘 뿐 아니라 대형 조개류 등 다양한 생물과 공생을 유지하는 것으로 잘 알려져 있다. 특히 이들은 산호의 생존에 필수불가결한 존재로써 열대해역의 산호초 형성에 크게 기여한다. 그러나 이들 종이 해양생태계에 중요한 역할을 수행함에도 불구하고, 심바이오디니움의 분류학적 수준은 아직 미흡한 단계에 있는데, 이는 심바이오디니움과 같은 소형 와편모조류의 경우, 그 크기가 작고 세포의 표면이 약해 형태적 분석이 매우 어렵기 때문이다. 이로 인해 현재까지 보고된 대부분의 심바이오디니움에 대한 대부분의 분류 연구에서 형태학적 분류가 없거나 미흡하며, 특히 심바이오디니움 속의 형태적, 유전적 기준이 되는 모식종마저도 그 형태적 특성이 미완성인 상태로 보고되어 있다. 이처럼 미흡한 분류학적 수준으로 인해 현재 심바이오디니움은 동일한 종에 대해서도 복수의 종명이 존재하는 경우가 많다. 이에 본 연구에서는 심바이오디니움의　분류학적　기준이　되는　모식종인　*Symbiodinium*

*microadriaticum*의 형태적 특징을 처음으로 완성하였으며, 이를 기준으로 대형 조개류에 공생하는 신종 심바이오디니움인 *Symbiodinium tridacnidorum*을 보고하게 되었다. 나아가 본 연구에서는 기존에 유전적으로만 분류되어있던 clade B 심바이오디니움에 속하는 두 종인 *Symbiodinium minutum* 및 *Symbiodinium psygmorphilum*에 대한 형태적 분석을 완료하여 본 공생생물종의 형태적 분류 기준을 확립하였다.

와편모조류는 자가영양성, 종속영양성, 그리고 혼합영양성의 세 가지 영양 방식을 띄며, 이는 해양생태계의 먹이망에서 와편모조류가 먹이 뿐 아니라 포식자로서의 역할을 수행하도록 한다. 그러나 지금까지의 연구에서 와편모류 종의 혼합영양성이나 종속영양성과 같은 섭식 방식의 차별성이 유전적 특성의 차이라는 관점에서 연구가 수행된 경우가 없어 이를 조사하고 이해해야 할 필요가 있다. 본 연구에서는 형태적, 유전적으로 유사하며 섭식하는 먹이종도 유사하지만 섭식 방법에 있어 차이를 보이는 혼합영양성 와편모류인 *Paragymnodinium shiwhaense*와 종속영양성 와편모류인 *Gyrodiniellum shiwhaense*의 유전체를 분석하여 발현된 유전자의 양상을 비교하였다. 또한 발현된 유전자가 섭식방법의 차이에 주는 영향을 비교분석하고, 그 중에서도 광합성 유전자의 발현에 대해 집중 분석하였다. 그 결과, 혼합영양성 와편모류는 광합성과 섭식영양을 동시해 수행하기 때문에 섭식으로만 영양분을 얻는 종속영양성 와편모류에 비해 유전자의 발현양이 더 많고 다양한 기능을 수행하는 더 많은 유전자가 발현될 것이라는 가설을 본 연구 결과를 통해 검증할 수 있었다.

매년 여름 한국은 유해한 적조생물인 코클로디니움 폴리크리코이데스의 과다증식으로 인한 적조로 인해 큰 피해를 보고 있다. 이에 해당 종의 출현을 감지하고, 적조를 예측하기 위해서 현장시료로부터 이들 코클로디니움 종을 정확하고 빠르게 정량할 필요가 있다. 그러나 유해한 적조생물인 코클로디니움을 현장 시료로부터 직접 계측할 경우, 다른 근연 종들과의 형태적 유사성으로 인해 정확한 종별 정량 계수에 어려움이 있다. 뿐만 아니라 코클로디니움의 정량분석을 위해 종종 사용하는 qPCR 방법의 경우도 세포 당 유전자 함량의 차이로 인한 오차요인의 문제가

있다. 이에 본 연구에서는 유해성 와편모류인 코클로디니움 폴리크리코이데스의 3가지 리보타입 모두를 포괄적으로 탐지할 수 있는 새로운 종특이 분자마커를 제작하였다. 또한 기존의 qPCR 정량, 정성방법을 더 개량하기 위하여 4가지 방식의 전처리 방법을 고안하고, 이를 통한 표준곡선들을 비교분석하였다. 이후 이 방법들의 정확성을 입증하기 위하여, 2014년부터 2015년에 이르기까지 한국연안으로부터 채집한 500개 이상의 현장시료를 대상으로 시험을 실시하였다. 시험 결과, 배양된 실험실 종으로부터 각 농도별로 유전자를 추출하여 제작한 표준곡선을 이용한 방법이 가장 정확하고, 현장시료로부터 각 농도별로 세포를 수집하여 유전자를 추출한 뒤 제작한 표준곡선을 이용한 방법이 그 다음으로 정확하다는 것을 확인할 수 있었다. 이로써, 현장시료로부터 더 정확하게 특정 와편모조류를 감지하여 정량할 수 있는 방법을 개선하게 되었다.

본 연구는 소형 와편모류의 정확한 분류, 섭식 방식의 다양성에 대한 유전적 차별성 관점의 이해, qPCR 방식의 개선 등을 위해 다양한 와편모류 종의 배양체를 이용한 실험 및 연구를 수행하였으며 그 결과, 본 연구를 통해 공생성 와편모류종을 분류함에 있어 포괄적인 방법과 기준을 제시하게 되었다. 나아가 본 연구를 통해 섭식기작과 유전자 발현간의 상관관계를 파악함으로써 와편모조류의 기반연구에 기여하였으며, 한국 연안에서 매해 큰 피해를 입히는 적조생물인 코클로디니움을 정확하게 탐지하고 정량할 수 있는 종특이 분자마커와 정량방법을 제시하여 해당 종으로 인한 적조연구를 위한 개선된 수단으로 기여하게 될것으로 기대하는 바이다.

Keywords: 심바이오디니움, 코클로디니움, 분류, 혼합영양, 섭식기작, 유전체, qPCR 정량분석